MODELS AND MECHANISMS OF GLIOMA CELL INVASION

Pavlo Grytsenko

MODELS AND MECHANISMS OF GLIOMA CELL INVASION

Proefschrift

ter verkrijging van de graad van doctor
aan de Radboud Universiteit Nijmegen
op gezag van de rector magnificus prof. dr. J.H.J.M. van Krieken,
volgens besluit van het college van decanen
in het openbaar te verdedigen op donderdag 14 december 2017
om 10.30 uur precies

door

Pavlo Grytsenko
geboren op 13 mei 1977
Kiev, Oekraïne

The research presented in this thesis was performed at the Department of Cell Biology, Radboud Institute for Molecular Life Sciences, Radboud University Nijmegen Medical Centre, Nijmegen, the Netherlands.

The work was supported by NWO-VICI (918.11.626), Pieken in the Delta Oost Nederland and the Cancer Genomics Center, The Netherlands.

Cover design: Pavlo Grytsenko and Olga Ilina.

Cover image: patient derived E-468 glioma cells (nestin, red) form networks intertwining with astrocytes (GFAP, blue) and myelinated axons (MBP, yellow) in mouse brain cortex.

ISBN: 978-94-6182-850-7

Layout and printing: Off Page, Amsterdam, the Netherlands

PROMOTOREN

Prof. dr. Peter Friedl
Prof. dr. Pieter Wesseling

MANUSCRIPTCOMMISSIE

Prof. dr. Richard van Wezel
Dr. Mark ter Laan
Prof. dr. Frank Winkler (Universität Heidelberg, Duitsland)

MODELS AND MECHANISMS OF GLIOMA CELL INVASION

Doctoral Thesis

to obtain the degree of doctor
from Radboud University Nijmegen
on the authority of the Rector Magnificus prof. dr. J.H.J.M. van Krieken,
according to the decision of the Council of Deans
to be defended in public on Thursday, December 14, 2017
at 10.30 hours

by

Pavlo Grytsenko
Born on May 13, 1977
in Kiev, Ukraine

SUPERVISORS

Prof. dr. Peter Friedl
Prof. dr. Pieter Wesseling

DOCTORAL THESIS COMMITTEE

Prof. dr. Richard van Wezel
Dr. Mark ter Laan
Prof. dr. Frank Winkler (Universität Heidelberg, Germany)

"Nothing in nature is by chance...
Something appears to be chance only because of our lack of knowledge."
Baruch Spinoza

"We are just waves in time and space, changing continuously, and the illusion of individuality is produced through the concatenation of the rapidly succeeding phases of existence. What we define as likeness is merely the result of the symmetrical arrangement of molecules which compose our body."
Nikola Tesla

TABLE OF CONTENTS

CHAPTER 1

GENERAL INTRODUCTION

Gliomas are a heterogeneous group of primary brain tumors originating from transformed brain cell progenitors which abnormally reproduce brain development programs[1–3]. Dependent on the cell of origin and genetical background gliomas can be divided in astrocytomas, oligodendrogliomas and epindenomas with different cancer progression stages[4]. The stage IV of astrocytomas, primary glioblastoma, is the most aggressive form of gliomas and one of the deadliest cancer in humans. The median survival time of glioblastoma patients is between 14.5 and 16.6 months, despite radio- and chemo-therapy treatments[5,6]. The high lethality of glioblastoma patients results from diffuse glioma cell dissemination in the brain[7]. After surgical resection of the primary lesion, glioma cells which have invaded into surrounding tissue give rise to recurrence of the tumor within months. Glioma cells disseminate into the brain stroma along the intertwining cell networks formed by astrocytes, neurons, myelinated axons and blood vessels[7,8]. However, due to anatomic and molecular complexity, the mechanisms of glioma cell invasion in the brain parenchyma is neither resolved mechanistically nor therapeutically exploited.

The aims of this thesis are: (1) to design three-dimensional (3D) invasion assays recapitulating glioma cell dissemination in different anatomical environments of the brain – along blood vessels and in neuronal/astrocytic networks; (2) to perform three-dimensional (3D) reconstruction of glioma lesions and characterize glioma invasion patterns in patient brain samples; (3) to identify cell-cell and cell-matrix adhesion molecules driving glioma cell invasion in the brain.

In **Chapter 2** we describe the brain tissue architecture at cellular and molecular levels and recapitulates the main anatomical structures which guide glioma cell invasion in the brain. Myelinated axons, astrocyte processes and blood vessels create a complex system of microchannels utilized by glioma cells for their disseminations. The extracellular space in the brain parenchyma is filled primarily with a soft matrix composed by hyaluronan-lectican-tenascin molecular complexes, unlike connective tissue where collagen bundles are predominant in extracellular matrix.

2D and 3D assays developed to study glioma cell invasion in vitro neither reproduce a complex anatomical and molecular structure of the brain tissue, nor a major mechanism of glioma cell dissemination in the brain - multicellular network expansion[8–10]. The majority of the assays devoid brain cellular components like astrocytes and myelinated axons, which are utilized by glioma cells for their invasion. We developed a set of 3D assays recapitulating different anatomical and molecular routes of glioma cell invasion in the brain tissue (**Chapter 3**). To mimic cohesive perivascular invasion of glioma cells, a hyaluronan-reconstituted basement membrane interface and organotypic brain slice assays were designed. As model for diffuse migration into the astrocyte-rich brain parenchyma, a 3D astrocyte scaffold assay was developed which supports both individual-cell and glioma multicellular network invasion. Each assay serves for both, high-resolution functional analysis of molecular mechanisms underlying glioma invasion, as well as high-throughput screening of clinically relevant treatments to inhibit glioma cell invasion and proliferation in distinct brain compartments (**Chapter 3**).

Cancer cells can invade peritumoral tissue either individually without cell-cell interaction to neighboring cells or collectively, as cohesive groups maintaining cell-cell junctions to their neighbor cells and moving as a coordinated group[11,12]. The concept that glioma cells infiltrate brain parenchyma exclusively as single cells has dominated the glioma field for decades, however is currently challenged based on recent data[10]. By 3D reconstruction of glioma lesions from patient samples and glioma models in mouse brain, we described the identification of moving multicellular networks with dendrite-like protrusions connecting glioma cells as an important yet unappreciated invasion strategy[10] (**Chapter 4**). Multicellular glioma networks thus adopt a specialized mode of collective invasion, which enables cell-cell interaction between glioma cells while moving through complex-shaped brain stroma. As central mechanism of glioma network formation and maintenance, we show that filament connections between glioma cells are stabilized by adherens junctions with p120 catenin as indispensable for glioma network migration and tumor growth in the mouse brain (**Chapter 4**).

Perivascular glioma cell invasion is driven mainly by basement membranes ensheathing capillaries and bigger blood vessels in the brain[7,8,13]. Therefore basement membrane proteins are potential candidates and mediators for glioma cell invasion and growth signalling in the brain[8,14]. Using the 3D astrocyte scaffold invasion assay we identified laminin 511 as a major extracellular matrix component driving glioma cell invasion (**Chapter 5**). Interference with different integrin subunits showed that β1 integrins are the predominant receptors mediating glioma cell migration along laminin 511. However, since interference with adhesion systems using antibody targeting and RNA interference, alone or in combination, was incomplete in inhibiting glioma invasion, the data further suggest the presence of integrin-independent, additional cell-matrix interaction strategies[15]. This further indicates potential limitations of anti-integrin therapies to combat perivascular glioma cell dissemination and growth (**Chapter 5**).

In conclusion, using novel 3D culture approaches and 3D reconstruction of glioma lesions in mouse brain and patient samples, we suggest new concepts of glioma cell dissemination in the brain parenchyma: diffuse multicellular network invasion ensured by p120 catenin and perivascular glioma cell invasion driven by β1 integrin - laminin 511 interactions.

REFERENCES

1. Brat, D. J. *et al.* Comprehensive, Integrative Genomic Analysis of Diffuse Lower-Grade Gliomas. *N. Engl. J. Med.* **372,** 2481–2498 (2015).
2. Ilkanizadeh, S. *et al.* Glial progenitors as targets for transformation in glioma. *Adv. Cancer Res.* **121,** 1–65 (2014).
3. Patel, A. P. *et al.* Single-cell RNA-seq highlights intratumoral heterogeneity in primary glioblastoma. **344,** 1396–1401 (2014).
4. Louis, D. N. *et al.* The 2016 World Health Organization Classification of Tumors of the Central Nervous System: a summary. *Acta Neuropathol.* **131,** 803–820 (2016).
5. Gilbert, M. R. *et al.* Dose-dense temozolomide for newly diagnosed glioblastoma: a randomized phase III clinical trial. *J. Clin. Oncol.* **31,** 4085–4091 (2013).
6. Stupp, R. *et al.* Effects of radiotherapy with concomitant and adjuvant temozolomide versus radiotherapy alone on survival in glioblastoma in a randomised phase III study: 5-year analysis of the EORTC-NCIC trial. *Lancet. Oncol.* **10,** 459–466 (2009).
7. Cuddapah, V. A., Robel, S., Watkins, S. & Sontheimer, H. A neurocentric perspective on glioma invasion. *Nat. Rev. Neurosci.* **15,** 455–465 (2014).
8. Gritsenko, P. G., Ilina, O. & Friedl, P. Interstitial guidance of cancer invasion. *J. Pathol.* **226,** 185–199 (2012).
9. Rape, A., Ananthanarayanan, B. & Kumar, S. Engineering strategies to mimic the glioblastoma microenvironment. *Adv. Drug Deliv. Rev.* **79–80,** 172–183 (2014).
10. Osswald, M. *et al.* Brain tumour cells interconnect to a functional and resistant network. *Nature* **528,** 93–98 (2015).
11. Te Boekhorst, V., Preziosi, L. & Friedl, P. Plasticity of Cell Migration In Vivo and In Silico. *Annu. Rev. Cell Dev. Biol.* **32,** 491–526 (2016).
12. Friedl, P., Locker, J., Sahai, E. & Segall, J. E. Classifying collective cancer cell invasion. *Nat. Cell Biol.* **14,** 777–783 (2012).
13. Farin, A. *et al.* Transplanted glioma cells migrate and proliferate on host brain vasculature: a dynamic analysis. *Glia* **53,** 799–808 (2006).
14. Yurchenco, P. D. Basement membranes: cell scaffoldings and signaling platforms. *Cold Spring Harb. Perspect. Biol.* **3,** (2011).
15. Schmidt, S. & Friedl, P. Interstitial cell migration: integrin-dependent and alternative adhesion mechanisms. *Cell Tissue Res* **339,** 83–92 (2010).

CHAPTER 2

INTERSTITIAL GUIDANCE OF CANCER INVASION

Pavel Gritsenko[1], Olga Ilina[1] and Peter Friedl[1,2]

[1] Microscopical Imaging of the Cell, Department of Cell Biology
Radboud Institute for Molecular Life Sciences ,
Radboud University Nijmegen Medical Centre
[2] David H Koch Center for Applied Research of Genitourinary Cancers,
Department of Genitourinary Medical Oncology, The University of
Texas, MD Anderson Cancer Center, Houston, Texas, USA

Journal of Pathology (2012); 226: 185–199

ABSTRACT

Cancer cell invasion into healthy tissues develops preferentially along pre-existing tracks of least resistance, followed by secondary tissue remodelling and destruction. The tissue scaffolds supporting or preventing guidance of invasion vary in structure and molecular composition between organs. In the brain, the guidance is provided by myelinated axons, astrocyte processes, and blood vessels which are used as invasion routes by glioma cells. In the human breast, containing interstitial collagen-rich connective tissue, disseminating breast cancer cells preferentially invade along bundled collagen fibrils and the surface of adipocytes. In both invasion types, physical guidance prompted by interfaces and space is complemented by molecular guidance. Generic mechanisms shared by most, if not all, tissues include (i) guidance by integrins towards fibrillar interstitial collagen and/or laminins and type IV collagen in basement membranes decorating vessels and adipocytes, and, likely, CD44 engaging with hyaluronan; (ii) haptotactic guidance by chemokines and growth factors; and likely (iii) physical pushing mechanisms. Tissue-specific, resticted guidance cues include ECM proteins with restricted expression (tenascins, lecticans), cell–cell interfaces, and newly secreted matrix molecules decorating ECM fibres (laminin-332, thrombospondin-1, osteopontin, periostin). We here review physical and molecular guidance mechanisms in interstitial tissue and brain parenchyma and explore shared principles and organ-specific differences, and their implications for experimental model design and therapeutic targeting of tumour cell invasion.

INTRODUCTION

Cancer cell invasion results from actomyosin dependent movement of the cellular body through or along tissue structures. After metastasis to secondary organs, local invasion by cancer cells may lead to secondary organ infiltration, thereby engaging with a tissue environment that differs from the primary organ [1]. At any invasion stage, cancer cells are confronted with non-neoplastic tissue composed of cells and cell-derived extracellular matrix (ECM). Cancer cells constitutively express adhesion receptors that bind to ECM as well as to resident stromal cells which not only activate the actomyosin machinery to generate traction forces needed to migrate, but also deliver important signals for their growth and survival [2]. Initially cancer invasion is largely non-destructive, but over time leads to substantial tissue remodelling, local destruction with ulceration, vessel disruption, and, ultimately, loss of function of invaded organs [3].

Two principal types of interstitial tissues are transmigrated by tumour cells: (i) collagen-rich interstitial connective tissue present in most parenchymatous organs of the body and (ii) the interstitium of the brain. Both share significant similarities but also show important anatomic and molecular differences that impact upon the invasion process. The understanding of how physical and molecular guidance mechanisms converge, and how these principles apply to different tissues and organ systems, is important for developing experimental *in vitro* models of cancer invasion; it is further important for addressing and interpreting cell invasion patterns and routes *in vivo* by histopathological analysis. Using brain parenchyma and breast stroma as prototypic models for nervous and peripheral connective tissue invasion, respectively, we here review key tissue structures and their molecular properties that enable and guide cancer invasion and discuss the implications for designing experimental models and molecular anti-invasion therapy.

CELL–CELL AND CELL–MATRIX RECEPTORS

During cell–tissue interaction and migration in most tumours, integrin and non-integrin cell surface receptors simultaneously engage with locally available ECM and cell surface ligands (Table 1).

INTEGRINS

Integrins are heterodimeric transmembrane glycoproteins consisting of non-covalently linked α and β chains, which both determine ligand binding strength and specificity. Eight distinct α and 18 β chains combine to form 24 different heterodimers with distinct ligand specificity for ECM proteins (eg collagens, laminins, fibronectin, vitronectin, tenascins, thrombospondin, and fibrin) and cell surface receptors (eg ICAM-1, VCAM-1, and L1-CAM) [4,5]. By these means, each cell type maintains a selective and activation-dependent integrin repertoire and thus ligand preference. The cytoplasmic integrin domains connect, via cytosolic adaptor and signalling proteins, to the actin cytoskeleton and mediate intracellular mechanocoupling and signal transduction [6]. Consequently,

integrins are important mediators for cell adhesion and migration. They further contribute to cell–cell contacts via direct interactions with counterpart cell receptors or indirectly, by bridging intercellular ECM molecules, including fibronectin or vitronectin [7].

SYNDECANS

Syndecans are a family of transmembrane heparan sulphate proteoglycans with four members, syndecans 1 to 4. Syndecans function mainly as co-receptors by binding to their ECM ligands in conjunction with other receptors, notably integrins [8]. Through their heparan sulphate side chains, syndecans may further engage directly in ligand binding [9].

DYSTROGLYCANS

Dystroglycans are heterodimeric complexes consisting of non-covalently associated α and β subunits with extracellular ligand-binding and transmembrane functions, respectively [10]. Dystroglycans are a part of the larger dystrophin-associated protein (DAP) complex that connects basement membranes to the cytoskeleton, particularly via α2 laminins and perlecan [10].

IMMUNOGLOBULIN (Ig) SUPERFAMILY CELL ADHESION PROTEINS

Ig superfamily members consist of immunoglobulin-like and fibronectin type III domains involved in homophilic and heterophilic cell–cell adhesion [11]. The superfamily includes a variety of cell adhesion molecules (CAMs) with distinct ligand-binding specificities, including ICAM (intercellular), NCAM (neural), Ep-CAM (epithelial), L1-CAM, VCAM (vascular), ALCAM (activated leukocyte), and JAM (junctional adhesion molecule), among others [11].

CADHERINS

Cadherins are transmembrane proteins consisting of several tandemly repeated cadherin domains that mediate calcium-dependent homophilic cell–cell contacts [12,13]. The cadherin superfamily comprises a total of more than 100 different members [14], with E- (epithelial) and N-cadherin (neural) most widely expressed in epithelial and neural tissues, respectively.

LINK MODULE SUPERFAMILY OF HA-BINDING PROTEINS (HYALADHERINS)

CD44 is the main HA receptor expressed by all nucleated cells in vertebrates [15]. Besides the standard form (CD44s), multiple splice variants encoded by variable exons v1–10 (CD44v1–10) can be expressed depending on the cell differentiation and activation state [16]. Interactions of CD44 with multiple other molecules, including collagens, laminins, and fibronectin, have been shown *in vitro*; however, the relevance of these interactions to processes *in vivo* is not clear.

Table 1. Cell–matrix and cell–cell adhesion molecules expressed in glioma and carcinoma cells compared with normal brain and breast tissue

Cell receptor	ECM/cell ligand	Glioma cells*	Carcinoma cells*	Ref
Integrin				
$\alpha_1\beta_1$	Type I and IV collagens, laminin	–	↓	[43,152]
$\alpha_2\beta_1$	Type I and IV collagens	↔	↓	[43,152,153]
$\alpha_3\beta_1$	Laminins including laminin-332, type IV collagen	↑	↓	[42,43,136,152]
$\alpha_6\beta_1$	Laminins	↔	↓	[42,43,152,158]
$\alpha_6\beta_4$	Laminins	↑	↓	[153–158]
$\alpha_9\beta_1$	Tenascins, fibronectin	↑	↔	[53,159]
$\alpha_5\beta_1$	Fibronectin	↔/–	↓	[42,43,152,153,160]
$\alpha_V\beta_3$	Vitronectin, laminin, thrombospondin, tenascins, type IV collagen, osteopontin, periostin, tropoelastin	↑	↑	[42,43,141,161]
$\alpha_V\beta_5$	Vitronectin, laminin, thrombospondin, tenascins, type IV collagen, osteopontin, periostin	↑	–	[161]
Syndecans (1 – 4)	Laminin, type I collagen, tenascins, fibronectin, thrombospondin, vitronectin	↔	↔	[44,162]
α- and β-dystroglycans	Laminin, perlecan	↓	↓	[45,163,164]
CD44	Hyaluronan, type IV collagen	↑	↑	[42,52,165,166]
ICAM-1	Hyaluronan, LFA-1	↑	↔	[42,167,168]
NCAM	NCAM, L1-CAM, neurocan	↓	–	[169–171]
L1-CAM	L1-CAM, NCAM	↑	↑	[172–175]
N-cadherin	N-cadherin	↓	↑	[176–178]
E-cadherin	E-cadherin	–	↓↔(D)/–(L)	[91,177,179]

*Expression in histopathological samples compared with normal human tissue: ↔, not altered; –, not expressed; ↑, up-regulation; ↓, down-regulation. D = ductal breast carcinoma; L = lobular breast carcinoma. References often show trends, with divergent expression regulation in patient subgroups.

These receptors mediate tissue recognition and mechanical coupling and, with their expression levels and tissue context, whether cells remain immobile, migrate slowly or rapidly; and they further determine whether migration occurs individually with cell–cell junctions absent or collectively, as multicellular groups with cell–cell junctions present [2,17].

GUIDANCE STRUCTURES OF BRAIN TISSUE

Brain tissue harbours both primary tumours of neural origin and secondary metastases originating from other tissues. The structures that guide invasion into brain tissue are cell processes of neuronal and astrocytic origin, blood vessels, and tissue gaps present along vessels and brain surfaces.

BRAIN CELLS AND VESSELS

The grey matter of the brain cortex consists of a dense network of neurons, including their dendrites and myelinated axons, together with astrocytes (Figure 1A). The top layer

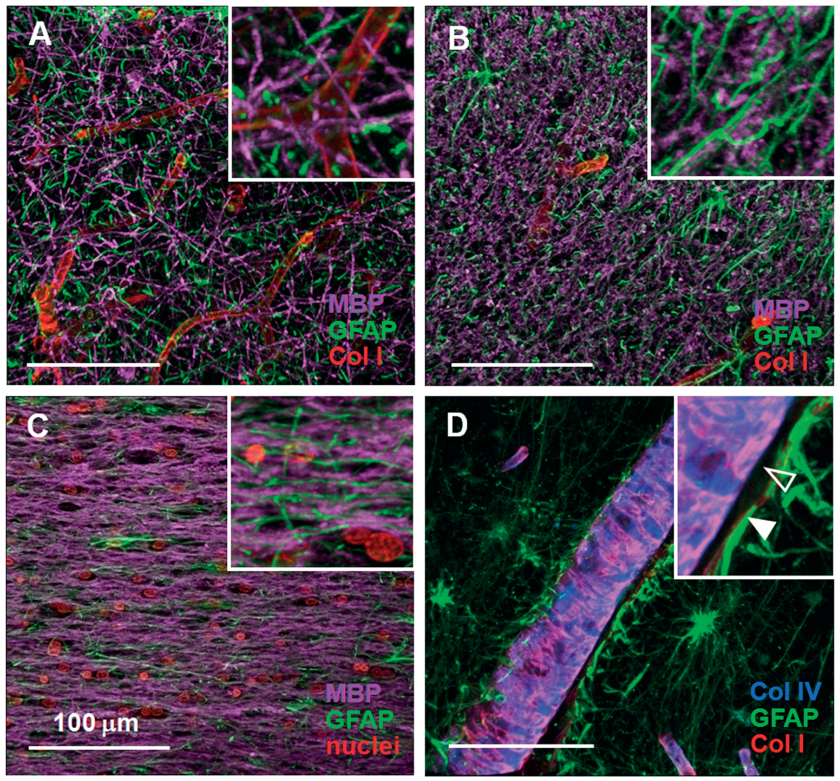

Figure 1. Three-dimensional reconstruction of human brain structures. Images represent 3D projections from 200-µm-thick sections of formalin-fixed post-mortem human brain, including cortex (A, D), white matter (B), and corpus callosum (C). Staining was performed using the following primary antibodies: rabbit anti-type I collagen (Col I) polyclonal Ab (pAb; Abcam); chicken anti-glial fibrillary acidic protein (GFAP) pAb (Abcam); rat anti-myelin basic protein (MBP) mAb (clone 12, Abcam); mouse anti-collagen IV mAb (clone Col-94, Sigma); and DAPI. Astrocyte processes and myelinated axons form interconnected networks in the cortex and aligned tracks in the white matter. (D) Blood vessel surrounded by glia limitans (filled arrowhead) bordering perivascular space (open arrowhead). Scale bars = 100 µm.

of the cortex, termed glia limitans superficialis, is formed by astrocyte processes which interact tightly with the pia mater, consisting of a basement membrane and an outward monolayer of mesothelial cells (Figure 2A). Besides contributing to the outer meninges, both pia mater and glia limitans also extend into the brain parenchyma, where they cover and ensheath arteries, arterioles, and larger veins [18]. Glia limitans with its basement membrane, but without pia mater, further surrounds small venules and capillaries [18]. Thus, all larger blood vessels in the brain differ from vessels in other organs by their dual-layer microanatomy with a continuous perivascular space bordered by pia mater and glia limitans (Figure 1D) [19]. Through this connection, the perivascular space conducts interstitial fluid and passenger leukocytes towards the subarachnoid space and ventricular cavities, thus fulfilling a draining function, which is similar to that of lymphatic vessels that are absent in the brain (Figure 2A) [20]. As an exception, in capillaries, the basement membranes of glia limitans and endothelial cells are fused to a singular layer and obliterate the perivascular space [20].

Adjacent to the cortex, the white matter consists of myelinated axon tracks with adjacent oligodendrocytes providing axonal myelin sheaths and astrocytes providing an interstitial stroma by their interconnected processes, but lacks neuronal cell bodies (Figures 1B and 1C). Myelinated fibres thus form elongated tracks with interspersed astrocyte processes and a gap-like interstitium filled with ECM (Figures 1B and 1C). The brain anatomy thus consists of cell-fibre and perivascular space-track systems, which both provide constitutive trails of least resistance to moving cells.

MOLECULAR COMPOSITION OF BRAIN ECM AND BASEMENT MEMBRANES

The brain ECM is mainly deposited by astrocytes and oligodendrocytes and comprises an estimated 20% of the brain volume in adults [21]. The main ECM components are hyaluronic acid (HA), tenascin R, and lecticans, which interconnect with each other non-covalently and form molecular networks filling the intercellular space [22].

HA is a non-sulphated, linear, high-molecular-weight glycosaminoglycan which, due to its water-binding capacity, controls the high water content of the brain interstitium [23]. Besides tenascins and lecticans, HA binds to cell surface receptors including CD44 and ICAM-1, which together contribute to both ECM organization and cell–matrix interaction. Tenascin R, a brain-specific member of the tenascin family comprising also tenascins C, X, and W, is a homotrimer with both lectican and integrin binding sites forming an adhesion bridge between the ECM and cells [24]. Lecticans comprise a family of chondroitin sulphate proteoglycans with four members (brevican, versican, neurocan, and aggrecan), whereby brevican and neurocan are brain-specific [25]. Lecticans contain HA and tenascin R binding sites and thus act as link molecules in protein–proteoglycan–glycosaminoglycan networks [26]. Compared with peripheral interstitial tissues, a distinctive feature of the brain ECM is the absence of fibrillar collagen networks, which results in a low stiffness of the brain

parenchyma [18]. In a restricted expression pattern, fibrillar collagens I and III are, however, deposited by leptomeningeal cells, pericytes, and smooth muscle cells in blood vessels and the brain meninges, including the pia mater [18, 27, 28] (Figure 1).

Basement membranes are dense sheet-like meshworks of 50–100 nm thickness, which are particularly permissive for guiding cell migration [29]. Basement membranes consist of interconnected collagen IV, laminins, heparan sulphate proteoglycans (perlecan), and nidogen/entactin [29]. Collagen IV is a heterotrimer composed of three α-polypeptide chains [30], which interconnect with laminins, also heterotrimeric molecules, consisting of α, β, and γ chains [31].

GUIDANCE OF GLIOMA CELLS

Gliomas are the most common primary brain tumours in adults. Gliomas presumably originate from transformed glial progenitors and, depending on their differentiation state, several subtypes exist, including astrocytomas, oligodendrogliomas, and ependymomas [32,33]. Glioma cells can form tumours in any brain region and infiltrate adjacent parenchyma diffusely, thereby, arguably, recapitulating the migration of glial progenitor cells during brain development [32,34,35]. Glioma cell invasion into brain tissue occurs along pre-existing brain structures, with notable preference for myelinated fibres and blood vessels (Figure 2) [36, 37]. Ultimately, through the perivascular space, glioma cells can reach and populate the subarachnoid space [37, 38]. As a consequence of such extended tissue invasion, surgical resection of gliomas is usually non-curative and followed by cell survival and regrowth from invasion zones beyond the resection margins [35]. For as yet unknown reasons, glioma cells usually do not invade vessel lumens; thus, unlike most other malignancies, systemic dissemination and metastasis in non-neuronal organs are a rarity in brain neoplasia [39].

GUIDANCE BY BLOOD VESSELS

Glioma cells migrate along blood vessels using two biomechanically distinct routes: (i) the glia limitans along the outward vessel–parenchyma interface (Figure 2B) and (ii) inside the lumen of the perivascular space (Figures 2C). For the interstitial-type migration along the glia limitans, glioma cells may displace astrocytes bordering the blood vessels and employ the basement membrane as a substrate [40,41], whereas the role of simultaneous glioma cell–astrocyte interactions is unclear. Glioma cells further penetrate through the glia limitans and its basement membrane to reach the barrier-free lumen of the perivascular space and migrate along the inner basement membranes of vessels [40,41] (Figure 2C).

In vivo, glioma cells express and/or up-regulate a range of receptors binding to laminins and collagen IV, including integrins (α2β1, α3β1, α6β1, α6β4, αvβ3, αvβ5), dystroglycans, and syndecans [42–45] (Table 1). Consequently, laminins and collagen IV are the main ligands supporting glioma cell invasion along basement membranes, with α3β1 integrin as the major laminin receptor and laminins 332 and 511 as the matching

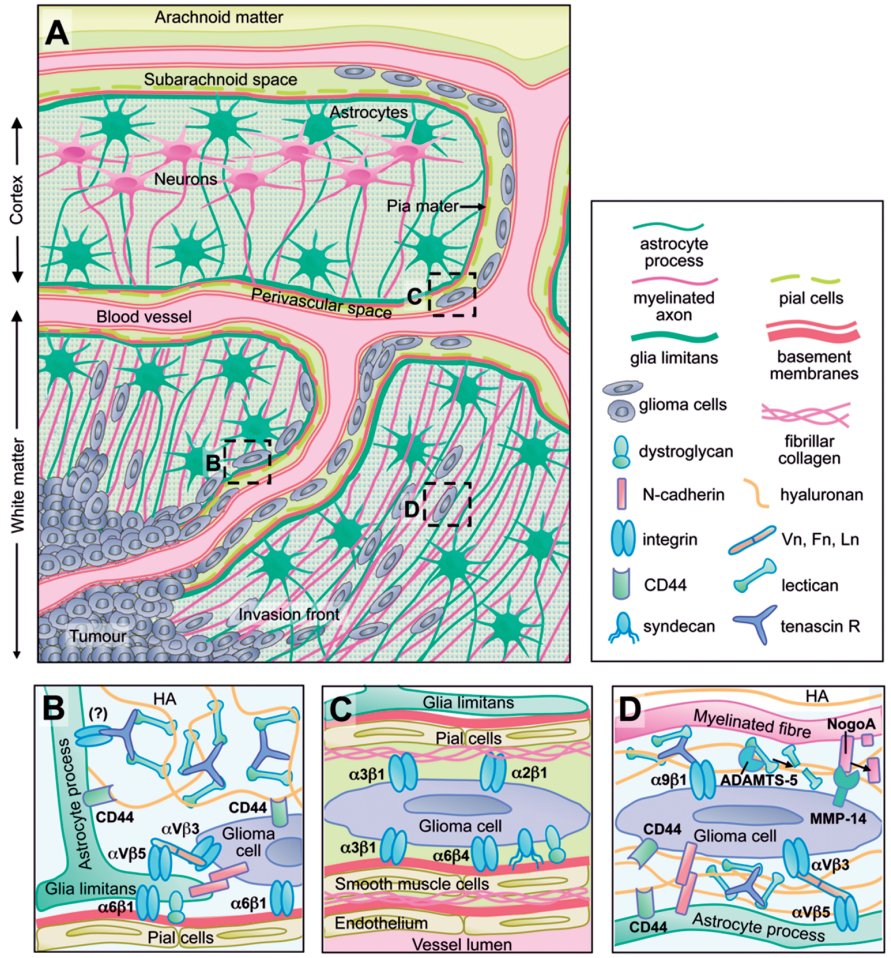

Figure 2. Anatomic and molecular guidance of glioma cell invasion. (A) Guidance along the glia limitans and perivascular space, as well as by neuronal and astrocyte tracks. (B) Extravascular guidance along the vessel–stroma interface. (C) Guidance by the perivascular space. (D) Glioma cell migration along white matter tracks. HA = hyaluronan; Vn = vitronectin; Fn = fibronectin; Ln = laminin

ligands [43,46]. Candidate cell–cell adhesions for the invasion route along the glia limitans comprise integrins connecting to cell surface-associated fibronectin and vitronectin, together with homophilic engagement of N-cadherin, L1-CAM, and NCAM (Figure 2B). Thus, whereas molecular guidance by the basement membrane appears to predominate in perivascular invasion, the role of glioma–astrocyte interactions remains to be clarified.

GUIDANCE BY NERVE TRACKS

The mechanisms of glioma cell invasion along myelinated fibres are likely multifactorial, whereby each relative contribution remains to be elucidated (Figure 2D).

Myelin sheaths formed by oligodendrocyte processes are considered as non-permissive substrates for cell migration, because they lack commonly known pro-migratory ECM proteins (eg laminins, collagens) and cell surface receptors that can bind these molecules [47]. In addition, myelin sheaths express repelling receptors, including Nogo-A, myelin-associated glycoprotein, and oligodendrocyte myelin glycoprotein, which together inhibit axonal growth and cell migration [48, 49]. Glioma cells, due to their altered protease expression profile, including increased MMP-14/MT1-MMP and MMP-2 levels [50], are, however, able to proteolytically cleave inhibitory molecules from the myelin surface using MMP-14 and thereby remove otherwise dominant anti-migration signals [51]. Thus, an anti-migratory brain scaffold is conditioned by ECM remodelling and processing of cell surface receptors towards a migration-enhancing tissue environment.

Due to their high water content and non-covalent intermolecular linkages, the ECM networks between myelinated fibres formed by HA, tenascin R, and lecticans are likely soft and deformable, compared with collagen-rich peripheral tissues. It is not known whether and how glioma cells use this HA-based matrix as a migration substrate; however, the consistent up-regulation of the HA receptors CD44 and ICAM-1, and of the tenascin R receptor α9β1 integrin in glioma cells, is suggestive of a pro-invasive cell–ECM interaction [42,52,53]. Glioma cells further up-regulate ADAMTS-5 (a disintegrin and metalloproteinase with thrombospondin motifs), which is secreted, cleaves brevican, and thereby likely disrupts ECM networks and lowers the physical interfibre resistance [26,54,55]. The distance between myelinated fibres in white matter tracks is less than 1 μm; thus, glioma cells have to expand the inter-fibre space and deform their nuclei, which are the largest and most rigid organelle in cells [56]. Consequently, glioma cell invasion along myelinated fibres in a rat brain model also depends on cell squeezing in a myosin II-dependent manner [57].

Simultaneously with myelinated fibres themselves, astrocyte processes localizing ubiquitously in all brain regions may contribute to glioma cell guidance (Figure 1). The border of gliomas shows an increased number of reactive astrocytes, which together with glioma cells secrete various pro-migratory molecules, including laminins, vitronectin, fibronectin, and thrombospondin [46, 58–61]. Because of their polyvalency (ie one molecule comprises more than one receptor-binding site), they adsorb to and decorate cell surfaces and provide a multimeric ECM meshwork available for counterpart cell surface receptor engagement (Figures 2B and 2D) [7]. Thus, glioma cells employing myelinated fibres and astrocyte processes as a substrate for migration engage multiple receptor–ligand systems for polarization and generating actomyosin-mediated traction forces, together with pericellular proteolysis.

GUIDANCE OF METASTATIC TUMOUR CELLS IN BRAIN TISSUE

Besides glioma cells, circulating tumour cells of other organs (mainly carcinoma and melanoma cells) may penetrate through blood vessels, establish metastatic brain lesions, and invade the brain. Similar to glioma cell invasion, metastatic brain invasion occurs preferentially along the blood vessels but spares white matter tracks and thus commonly lacks diffuse infiltration [62, 63]. The vascular basement membranes are considered the most important structures for initial growth and migration of carcinoma and melanoma cells metastasizing in the brain [64, 65]. It is likely that the lack of glioma cell-specific capabilities to remove anti-migratory activity of white matter tracks confines metastatic cell movement to the perivascular space, reminiscent of retained structural and molecular cues present in the connective tissue environment that they originate from.

CELL AND TISSUE STRUCTURES OF THE MAMMARY GLAND

The mammary gland is a prototypic peripheral organ consisting of the epithelium with an underlying basement membrane that forms the milk-producing alveoli and connecting ducts, and surrounding collagen-rich connective tissue including blood and lymph vessels and nerve tracks, as well as an adjacent layer of fat tissue (Figure 3A). In contrast to most other peripheral tissues, the postnatal mammary gland is structurally dynamic and undergoes glandular growth and sprouting during puberty and pregnancy, a process that is recapitulated in a pathological manner during breast cancer.

MAMMARY EPITHELIUM

The basic structural units of the mammary gland are alveoli joined together to form a lobule. Each lobule has its own lactiferous duct converging with other ducts to form a tree-like branching network towards the nipple. Both alveoli and ducts consist of

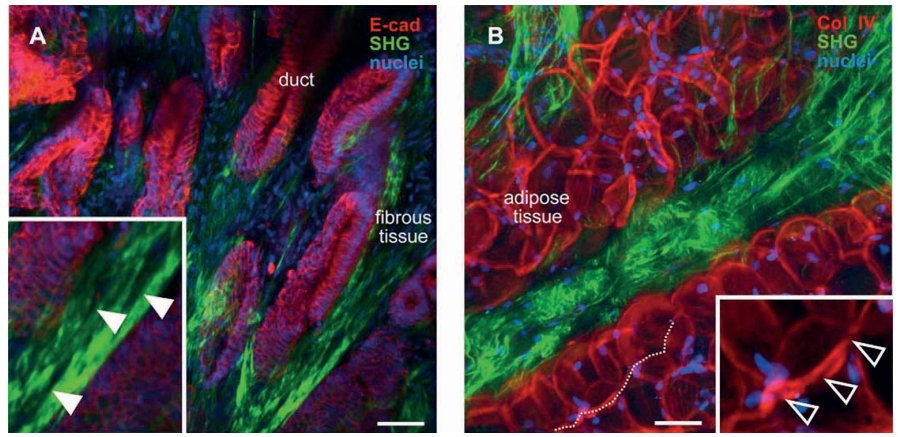

Figure 3. Three-dimensional reconstruction of human mammary gland tissue. Images represent 3D projections from 200-μm-thick sections of formalin-fixed breast carcinoma samples and show normal, non-invaded tissue regions. (A) Ducts surrounded by non-desmoplastic fibrous tissue. (B) Adipose tissue. Samples were labelled by mouse anti-collagen IV mAb (clone Col-94; Sigma), mouse anti-E-cadherin mAb (clone SHE78-7; Calbiochem), and DAPI. Fibrillar collagen was detected by second harmonic generation (SHG), revealing structural discontinuities and clefts (arrowheads). Dashed line in B, inter-adipocyte track part of which is highlighted in inset. Scale bars = 100 μm.

a bilayered epithelium, inner luminal cells surrounding the cavities, and outer myoepithelial cells engaging with the surrounding epithelial basement membrane [66]. Mammary ducts remain quiescent until puberty, when hormone-induced elongation and secondary branching occur by sprouting-type movement of the terminal end bud (TEB), a specialized region at the end of each primary duct. During pregnancy, through a similar sprouting mechanism, additional lateral branching occurs and luminal epithelial cells differentiate in the secretory alveoli [67].

ECM OF THE MAMMARY GLAND

The interstitial tissue of the mammary gland contains fibrillar type I collagen as a main structural component and interconnected glycoproteins [67, 68]. After extracellular deposition by fibroblasts, the propeptides of the triple-helical type I procollagen molecule are proteolytically cleaved by the endopeptidases ADAMTS-2, 3, and BMP-1 (bone morphogenetic protein-1), resulting in monomeric tropocollagen, which spontaneously polymerizes to multimeric fibrils [69–72]. The fibrous connective tissue of the normal breast stroma is heterogeneous in physical organization and density, with collagen fibrils measuring approximately 70 nm in diameter organized laterally into wavy fibre bundles (Figure 3) [73]. Thereby, regions of dense collagen bundles intersperse with loosely organized networks and inter-fibre clefts of variable widths, ranging from 3 to 30 μm [74] (O Ilina, unpublished data). This spatial structure of interstitial collagen, including physical and molecular signalling properties, are strongly modulated by collagen cross-linking and the presence of regulatory proteins. Collagen fibrils are cross-linked covalently by lysyl oxidases released by fibroblasts, stably bridging neighbouring collagen monomers and increasing fibril stiffness [75, 76]. The kinetics of fibril formation, their physical properties, and function towards cells are further modulated by type I collagen-binding ECM constituents, including fibrillar type III [77] and V collagens [78], fibronectin [79], decorin [80], and biglycan [81]. Fibronectin is an abundant fibrillar constituent of the ECM, with multi-adaptor functions, coupling cells and matrix via α5β1 integrin and providing binding sites for collagen type I and heparan sulphate proteoglycans [82]. Collagen-interacting molecules that modify its function further include proteoglycans (heparan sulphate, chondroitin sulphate) and hyaluronan, which together form a viscous, gel-like filling of inter-fibrillar spaces and provide binding sites for growth factors and cytokines. Heparan-sulphate proteoglycans bind growth factors, such as FGF1, FGF2, and HGF; chemokines incuding SDF-1α; and collagen-associated glycoproteins, including periostin [83]. HA non-covalently binds to proteoglycans and ECM proteins, including osteopontin, tenascin C, and versican [84, 85].

The adipose tissue of the mammary gland comprises groups of adipocytes with a cell surface-associated basement membrane composed of collagen type IV, laminins, and perlecan [86]. The interstitial ECM supporting adipocytes is composed of type I collagen fibres [87], interconnected with collagen types III, V, and VI, fibronectin, and proteoglycans [88], which form a loose reticular network with interstitial clefts [89] and interspersed cell- and vessel-rich fibrous septa (Figure 3B).

In human quiescent breast epithelium, α1β1, α2β1, α3β1, and α6β4 integrins are expressed by myoepithelial cells and are involved in the stable adhesion to ECM and thus cell anchoring to the matrix [90]. The quiescent state of normal breast epithelium is further maintained by desmocollin-2 (Dsc-2) and desmoglein-2 (Dsg-2), which form hemidesmosomal junctions between luminal epithelial and myoepithelial cells and E-cadherin connecting luminal epithelial cells laterally [91]. Thus, in the quiescent mammary gland, the structure of the ECM is mainly anti-migratory, stabilized by integrin- and cadherin-based cell–matrix and cell–cell adhesion.

GUIDANCE OF BREAST CARCINOMA INVASION

The majority of breast carcinomas originate from dedifferentiated luminal epithelial cells, histopathologically classified as ductal or lobular lesions depending on their original location [92]. Thereby, invading breast cancer cells appear to recapitulate the process of duct elongation occurring during development, although in a spatially and timely deregulated form. During gland formation, the terminal end buds invade the mammary stroma collectively as multicellular ducts with cell–cell junctions intact [93]. Similarly, ductal carcinomas form multicellular invasion strands consisting of cancer cells with cell–cell junctions retained, which with decreasing differentiation lose apicobasal polarity and the lumen [92]. During collective invasion, ductal carcinoma cells remain physically and functionally connected, with expressed cadherins (E-cadherin and P-cadherin), tight (JAM-A, claudin-3, and -4), and immunoglobulin-based junctions (ALCAM and L1-CAM) [2, 94–96]. Unlike ductal carcinoma, most of these cell–cell junction proteins are down-regulated in invading lobular carcinoma cells, with the loss of E-cadherin as a parameter for the diagnostic differentiation between ductal and lobular carcinoma [92]. Nonetheless, most invasive lobular carcinomas invade collectively as thin multicellular sheets and strands (Indian file pattern) parallel to collagen bundles, histologically with notable cell–cell contact retained or as detached individual cells with cell–cell junctions lost [97]. Candidate adhesion mechanisms for multicellular cohesion within Indian files that lack E-cadherin include N-cadherin and other cadherins, yet their mechanical and signalling contribution remains to be defined. Irrespective of the type of invasion, and in contrast to TEB sprouting which occurs with a basement membrane largely intact, the transition to invasive carcinoma is initiated by the disappearance of the basement membrane which allows for initial tumour cell contact to and migration along fibrillar collagen [98].

In response to the direct tumour cell–stroma interaction, both tumour cell- and stromal cell-derived changes in intracellular signalling and reactive cytokine and growth factor release induce substantial molecular and physical reorganization of the ECM molecular and physical reorganization, enhancing pro-migratory cancer cell activation and guidance [99]. The main structural and molecular guiding principles within the mammary gland are the ducts themselves, the surrounding bundled type I collagen fibres, their secondary

decoration with pro-migratory ECM molecules, and intercellular spaces between the basement membranes of adipocytes.

INTRADUCTAL GUIDANCE

As a not yet invasive precursor, carcinoma in situ is an intraluminal ductal or lobular accumulation of epithelial cells with disordered, multilayered epithelial organization, partially or completely obliterated lumen, but intact cell–cell junctions and basement membrane (Figures 4A and 4B). As a first in situ invasion route with basement membranes and stromal tissues intact, neoplastic epithelial cells proliferate within and likely move along the lumen of the duct, which leads to the expansive growth of tumour foci and outward pushing of the surrounding ECM but not interstitial invasion or metastatic dissemination [100].

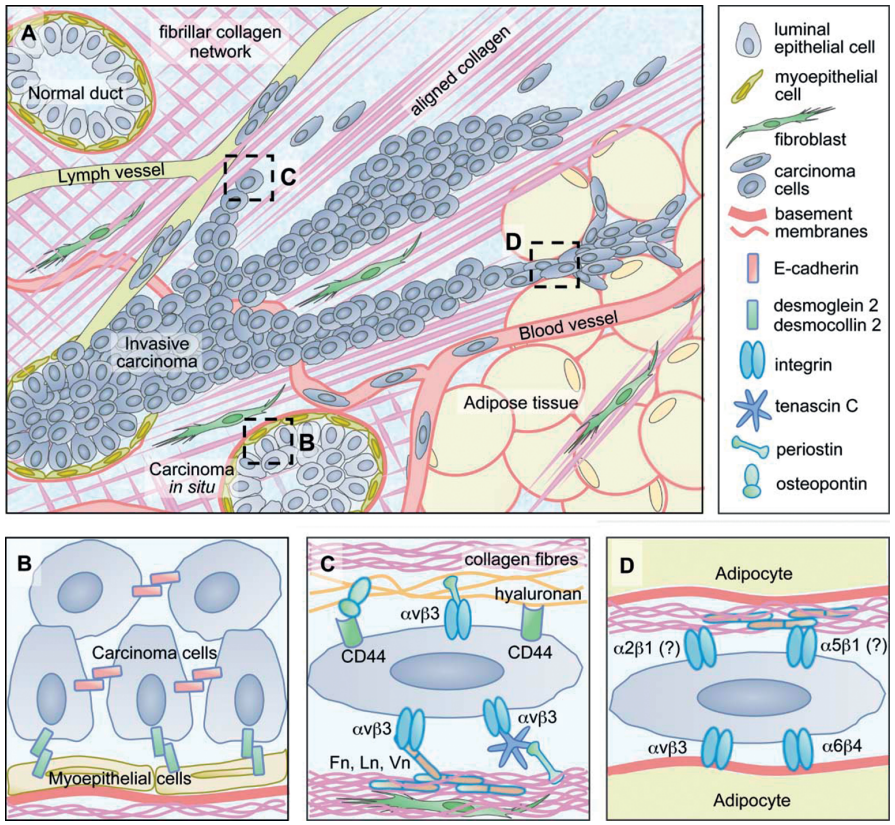

Figure 4. Anatomic and molecular guidance of breast cancer invasion. (A) Overview of guidance structures in the mammary gland. (B) Intraductal guidance in breast carcinoma *in situ*. (C) Guidance by fibrous tissue. (D) Carcinoma cell invasion in adipose tissue. HA = hyaluronan; Vn = vitronectin; Fn = fibronectin; Ln = laminin

HAPTOTATIC GUIDANCE

The ECM surrounding invading breast tumours undergoes substantial changes in density, composition, and structural organization, termed a desmoplastic reaction [101,102], including the accumulation of fibrillar collagen and other matrix components, which enhance neoplastic invasion and disease progression. With increased collagen I deposition, the fibres become aligned and bundled, and cross-linking is increased, resulting in elevated stiffness of peritumoural ECM [103]. As mechanisms, elevated activity of lysyl oxidases and tissue transglutaminases in stromal cells mediate covalent collagen cross-linking [104] and thereby enhance carcinoma cell invasion [105]. Adhesion-promoting additional ECM constituents, including laminin-332 [106], non-basement membrane collagen IV [107], fibronectin [108], and elastin [102], are jointly synthesized by carcinoma cells themselves and stroma cells, and reinforce migration-promoting activities, as suggested by their chemotaxis- and haptotaxis-enhancing effects *in vitro* [109]. Likewise, the composition of core proteins and glycosaminoglycan chains is altered in the ECM surrounding breast carcinoma. Versican, the major chondroitin sulphate proteoglycan present in the peritumoural stroma [110], forms non-covalent cross-links to different matrix molecules, including HA, tenascins, and fibronectin, and is recognized by the cell surface molecules β1 integrin and CD44 [111]. Similarly, the expression of HA is strongly up-regulated in the peritumoural stroma and carcinoma cells themselves [112,113], together with its receptor CD44 [114], thus creating additional options for cell–ECM interactions.

Besides structural ECM components, numerous matricellular proteins are de novo deposited nearby the front of invading tumours, including thrombospondin-1 [115], tenascin C [116], SPARC (osteonectin) [117], osteopontin [118], and periostin [119], all of which exert structural, growth factor binding and signalling functions towards tumour and stromal cells. Matricellular proteins, including osteopontin and thrombospondin-1, favour cell invasion *in vitro* in haptokinetic and 3D migration assays [120–122], and further support the growth and spontaneous metastasis of breast carcinoma cells in mouse models *in vivo* [123].

As mechanisms, matricellular proteins likely support motility and metastasis by complexing with and interconnecting between ECM structures, including fibrillar collagen type I, fibronectin, and heparin, thus modulating tissue porosity and stiffness, and providing additional functional ligands for cell surface receptors. As examples, periostin and osteopontin display binding sites towards cell surface αvβ1, αvβ5 and αvβ5 integrins and CD44 [120, 123, 124]. Tenascins C and X bind to collagen type I and fibronectin fibres via periostin [125] and/or the leucine-rich proteoglycan decorin [126], which provides bridging and possibly bundling of ECM, and additional ligand sites for cell guidance. Thus, interactions of various de novo deposited ECM proteins and proteoglycans with the collagen-based scaffold lead to its decoration and ‘functionalization’, which adds a migration-promoting layer, often together with signals for growth and survival.

PHYSICAL GUIDANCE BY COLLAGEN SCAFFOLDS

The molecular modifications of the peritumoural ECM microanatomy further lead to marked physical alterations, resulting in lateral association and bundling of collagen fibrils, and increased overall ECM stiffness. The curly normal structure of collagen fibres oriented parallel to ducts becomes straightened and realigned perpendicular to the tumour boundary, and fibre bundles are thickened with marked inter-bundle gaps and spaces [127]. Despite the elevated collagen density, inter-fibre clefts present in desmoplastic regions of invading tumours likely represent a network of microchannels suited to provide contact guidance to invading cells (O Ilina, unpublished data).

As part of the underlying process of anatomic restructuring, carcinoma-associated fibroblasts mechanically remodel the collagen network by adhesion, compaction and contraction [128], and/or proteolytic cleavage and re-alignment in parallel order [129]. Aligned collagen bundles are a strong pro-migratory stimulus for cell invasion and further correlated with enhanced metastasis *in vivo* [128], arguably by providing unhindered tracks of least resistance [130] and contact guidance [131]. Similar guidance is recapitulated by experimental microtracks in 3D collagen lattices enhancing breast cancer cell invasion *in vitro* [132]. As a consequence of entering narrow tracks, carcinoma cells adjust their calibre by first deforming themselves followed by lateral pushing, thereby accommodating the ECM geometry to the space required for invasion by a physical mechanism [132].

GUIDANCE BY ADIPOSE TISSUE

Following penetration of the stromal layer, breast carcinoma cells reach the adipose tissue, as an indication of particularly aggressive forms of invasive carcinomas [133]. Ductal breast cancer cells invade as solid strands between adipocytes, followed by adipocyte inclusion and destruction by the tumour mass [133]. Lobular carcinoma cells invade adipose tissue preferentially along collagen fibres between adipocytes as multicellular Indian files or as individual cells [134]. These different routes likely depend on adhesion or chemokine receptors differentially expressed by breast cancer cells and available counterpart ligands in the adipose tissue. Molecular guidance mechanisms of differential adipose tissue invasion are unknown, yet candidate pathways include integrins interacting with basement membrane components (ie α3β1, α6β4, and αvβ3, fibronectin (α5β1), and collagen type I (α2β1) [134,135] (Figure 4D). Carcinoma cells may further utilize barrier-free clefts formed by loosely organized ECM between adipocytes for unhindered invasion and expansive growth, thus adjusting the space by outward pushing of the fibrillar ECM network. Thus, peritumoural ECM provides a complex environment with distinct invasion-promoting molecular zones together with spaces of least resistance.

ADHESION RECEPTORS IN BREAST CARCINOMA INVASION

Together with migration-promoting ECM modifications, expression modulation of the adhesion receptor repertoire in breast carcinoma cells coincides with the acquisition of a mobile state. Numerous *in vitro* models implicate β1, β3, and β4 integrins as the major receptors for cell–matrix coupling and mechanotransduction in breast cancer cells, the blocking of which attenuates migration and invasion in 2D and 3D models [136, 137] (O Ilina, unpublished data). Histopathological data from human breast cancer lesions show marked down-regulation of most integrin subunits in tumour cells at the invasion front (Table 1 and references cited therein). Conversely, αvβ3 integrin, which is not expressed by normal breast epithelium, becomes up-regulated, which coincides with the increased stromal deposition of ECM ligands for αvβ3 integrin, including periostin, osteopontin, and tenascin C [138, 139]. Because of their pro-adhesive functions, the down-regulation of many integrins at the tumour invasive edge might allow cancer cells to turn over stable contacts to basement membrane or other ECM components, and transit to a mobile state through alternative integrins engaging with neo-ligands of the reactive stroma. *In vitro*, tenascin C, thrombospondin-1, and osteonectin modulate otherwise stable integrin-dependent attachment, which favours the turn-over of adhesion sites and enhances cell migration [140]; thus, lowering strong adhesion to ECM ligands may support invasiveness in a context-dependent manner. Consistently, β3 integrin supports the haptotactic migration of breast carcinoma cells towards osteopontin *in vitro* and enhances bone-specific spontaneous metastasis *in vivo* [141]. Likewise, integrins α6β4 and α3β1 mediate migration along or invasion into model basement membrane *in vitro* and furthermore are associated with enhanced systemic metastasis [135, 142], suggesting a role in promoting both cell migration and metastatic dissemination. In summary, the integrin profile in invading breast cancer cells likely matches and engages with an altered ligand repertoire in the reactive tumour stroma, which results in dynamic interactions with ECM and enhanced invasion.

In morphogenesis, the multicellular sprouting of breast epithelium during mammary gland development is not affected by the knockout of individual integrin subunits, including α2, α3, α4, and β4 [143–145], with reduced epithelial branching caused by α2 integrin deficiency [144] and mild defects of gland polarity and anchoring to the basement membrane after the loss of β1 integrin [145]. This mild phenotype suggests the function of as yet unknown compensatory adhesion systems to mediate normal duct elongation and sprouting morphogenesis, with unclear implications for the redundancy of pro-invasive adhesion systems in breast cancer.

Besides their contribution to cell migration and metastasis, integrins mediate stroma-derived growth and survival signals in tumour cells [137]. Consequently, the cellular mechanisms by which certain integrin subsets control poor outcome in breast carcinoma *in vivo*, ie their role in promoting invasion versus metastasis versus growth and survival, remain unclear.

INTRAVASATION AND METASTASIS OF CARCINOMA CELLS

Whereas in other tumour types blood and lymph vessels serve as pro-invasive structures [37, 130] perivascular invasion is not a prominent feature of invading breast

carcinoma in human lesions (O Ilina, unpublished data). However, similar to most metastasizing tumour types, breast cancer cells eventually reach the lumen of blood and lymph vessels. Tumour-associated blood vessels are less organized, with incomplete basement membrane, only loosely associated pericytes, and leaky cell–cell junctions [146], and thereby likely facilitate the vessel wall penetration and intravasation by tumour cells. In lymph vessels, carcinoma cells were shown to form tissue-like multicellular cords, 'emboli', and intravascular growing tumour foci, which eventually spread further and reach distant organs [147, 148]. A range of invasion-promoting factors locally up-regulated in the tumour stroma, including periostin [123], osteopontin [149], and tenascin C [116], strongly support distant breast cancer metastasis in mouse models *in vivo*, whereby their local and systemic effects [150] likely converge to enhance both local invasion and metastatic seeding at a distant site (eg by generating a 'pre-metastatic niche').

TUMOUR CELL INVASION IN BRAIN AND MAMMARY GLAND – SIMILARITIES AND DIFFERENCES

Despite their distinct invasion routes and molecular mechanisms, the invasion of glioma and carcinoma cells into the brain and mammary gland, respectively, shares the principle of guidance by the tissue scaffold, likely by a combination of molecular and physical mechanisms guiding cells along interfaces through pre-existing trails of least resistance. In the brain interstitium, which lacks fibrillar collagen, major invasion routes are basement membranes and intercellular tracks provided by myelinated axons and astrocyte processes. Basement membranes guide via laminin- and collagen-IV-mediated integrin engagement, whereas white matter tracks guide by cell–cell contacts and as yet unknown adhesion and force generation mechanisms. In the mammary gland, guided invasion follows gaps between bundled collagen fibres and interstitial spaces bordered by adipocyte-associated basement membrane, and likely depends on restricted integrin-mediated mechanocoupling. However, in both cases, it remains unclear how physical and molecular guidance principles are coordinated, how both principles synergize, and where they negatively impact each other.

Mechanically, migration through a porous interstitial space, along a viscoelastic protein polymer such as collagen bundles or basement membranes or along cell surfaces such as myelinated axons, represents a near barrier-free migration type with little or no enzymatic tissue modification required. Interface-mediated guidance is recapitulated *in vitro* by 2D culture in which cells move along a functionalized surface or by engineered 3D ECM-based models guiding cell invasion along tissue gaps and trails [17, 132]. In diffuse brain infiltration, the inter-scaffold substrate is soft ECM dominated by HA non-covalently linked to scaffold proteins; thus, the mechanical resistance is likely low and allows glioma cells to squeeze through the gaps and push the gel-like interstitial matrix aside. In the reactive stroma of breast tumours, the ECM content between collagen bundles is poorly contrasted by immunohistochemistry or non-linear (multi-photon) microscopy; thus, their composition

and mechanical properties in native state are unknown. Whereas the dimensions and function of the inter-fibre gaps *in vivo* likely provide space for invasion by cell squeezing, pulling, and pushing in collagen-based *in vitro* models [132], their guidance function in desmoplastic stroma remains to be shown. Histologically, invading cancer cells seem to 'respect' cell and ECM boundaries, resulting in proteolytic tissue destruction as a late consequence rather than as a prerequisite of invasion.

As a further shared event between brain and connective tissue invasion, tumour cells themselves, or the reactive tumour stroma, provide pro-migratory tissue conditioning. In breast carcinoma, the invasion-promoting properties of fibrillar collagen are increased by pro-migratory proteins deposited into the existing scaffold. In glioma, the proteolytic removal of otherwise anti-migratory activity is required for white matter infiltration, and it is not known whether similar mechanisms are involved in the invasion of peripheral connective tissue.

IMPLICATIONS

Despite extensive *in vitro* and *in vivo* investigations, for most invasion routes the combined molecular and physical mechanisms are not clear, and likely several complementary mechanisms converge to influence invasion outcome. Whereas molecular pathways have been studied extensively, the physical guidance mechanisms, including mandatory surface receptors and proteases required for contact guidance, remain poorly addressed. Thus, a mechanistic understanding of guidance, including its central signalling or mechanocoupling nodes that could be targeted, is required to design effective inhibition approaches, besides the targeting of integrins and other adhesion systems. It is likely that, even with integrins inhibited, major invasion pathways are still active in cancer cells, similar to leukocytes [151]; therefore, models are needed to identify additive effects and compensation in order to establish rational targeting of tissue invasion.

Structural and molecular insight into tissue invasion by cancer cells is further mandatory for the development of experimental *in vitro* and *in vivo* models exploring the mechanisms of cancer invasion. Whereas for breast cancer invasion, protein-scaffold-based collagen, basement membrane, and interconnecting accessory protein-containing ECM models appear sufficient as they reflect the natural main routes and ligands, glioma invasion is likely more complex and requires the simultaneous presence of cell and ECM scaffolds in an interconnected manner. The design of an appropriate cell environment comprising the main tissue components critical for each cancer cell invasion route *in vivo* will improve the clinically relevant identification of key molecules that guide cancer cell invasion, and dissect the relative contribution of physical versus molecular guidance.

ACKNOWLEDGEMENTS

We thank Pieter Wesseling, Peter Bult, and Han van Krieken for providing human brain and mammary gland samples and for helpful discussion. This work was supported by Pieken in the Delta Oest Nederlad (PID082022) and the European Union, FP7 European Tissue Transmigration Training Network (T3Net 237946).

AUTHOR CONTRIBUTION STATEMENT

PG and OI performed the experiments. All the authors wrote the manuscript.

REFERENCES

1. Langley RR, Fidler IJ. The seed and soil hypothesis revisited—the role of tumor–stroma interactions in metastasis to different organs. Int J Cancer 2011; 128: 2527–2535.
2. Ilina O, Friedl P. Mechanisms of collective cell migration at a glance. J Cell Sci 2009; 122: 3203–3208.
3. Coleman RE. Clinical features of metastatic bone disease and risk of skeletal morbidity. Clin Cancer Res 2006; 12: 6243s–6249s.
4. Humphries JD, Byron A, Humphries MJ. Integrin ligands at a glance. J Cell Sci 2006; 119: 3901–3903.
5. Schmidt S, Friedl P. Interstitial cell migration: integrin-dependent and alternative adhesion mechanisms. Cell Tissue Res 2010; 339: 83–92.
6. Anthis NJ, Campbell ID. The tail of integrin activation. Trends Biochem Sci 2011; 36: 191–198.
7. Robinson EE, Zazzali KM, Corbett SA, et al. Alpha5beta1 integrin mediates strong tissue cohesion. J Cell Sci 2003; 116: 377–386.
8. Morgan MR, Humphries MJ, Bass MD. Synergistic control of cell adhesion by integrins and syndecans. Nature Rev Mol Cell Biol 2007; 8: 957–969.
9. Xian X, Gopal S, Couchman JR. Syndecans as receptors and organizers of the extracellular matrix. Cell Tissue Res 2010; 339: 31–46.
10. Bozzi M, Morlacchi S, Bigotti MG, et al. Functional diversity of dystroglycan. Matrix Biol 2009; 28: 179–187.
11. Rougon G, Hobert O. New insights into the diversity and function of neuronal immunoglobulin superfamily molecules. Annu Rev Neurosci 2003; 26: 207–238.
12. Shapiro L, Weis WI. Structure and biochemistry of cadherins and catenins. Cold Spring Harbor Perspect Biol 2009; 1: a003053.
13. Shapiro L, Love J, Colman DR. Adhesion molecules in the nervous system: structural insights into function and diversity. Annu Rev Neurosci 2007; 30: 451–474.
14. Nollet F, Kools P, van Roy F. Phylogenetic analysis of the cadherin superfamily allows identification of six major subfamilies besides several solitary members. J Mol Biol 2000; 299: 551–572.
15. Ponta H, Sherman L, Herrlich PA. CD44: from adhesion molecules to signalling regulators. Nature Rev Mol Cell Biol 2003; 4: 33–45.
16. Naor D, Wallach-Dayan SB, Zahalka MA, et al. Involvement of CD44, a molecule with a thousand faces, in cancer dissemination. Semin Cancer Biol 2008; 18: 260–267.
17. Friedl P, Wolf K. Plasticity of cell migration: a multiscale tuning model. J Cell Biol 2010; 188: 11–19.
18. Zhang ET, Inman CB, Weller RO. Interrelationships of the pia mater and the perivascular (Virchow–Robin) spaces in the human cerebrum. J Anat 1990; 170: 111–123.
19. Krueger M, Bechmann I. CNS pericytes: concepts, misconceptions, and a way out. Glia 2010; 58: 1–10.
20. Owens T, Bechmann I, Engelhardt B. Perivascular spaces and the two steps to neuroinflammation. J Neuropathol Exp Neurol 2008; 67: 1113–1121.
21. Sykova E, Nicholson C. Diffusion in brain extracellular space. Physiol Rev 2008; 88: 1277–1340.
22. Zimmermann DR, Dours-Zimmermann MT. Extracellular matrix of the central nervous system: from neglect to challenge. Histochem Cell Biol 2008; 130: 635–653.
23. Itano N. Simple primary structure, complex turnover regulation and multiple roles of hyaluronan. J Biochem 2008; 144: 131–137.
24. Joester A, Faissner A. The structure and function of tenascins in the nervous system. Matrix Biol 2001; 20: 13–22.
25. Viapiano MS, Matthews RT. From barriers to bridges: chondroitin sulfate proteoglycans in neuropathology. Trends Mol Med 2006; 12: 488–496.
26. Yamaguchi Y. Lecticans: organizers of the brain extracellular matrix. Cell Mol Life Sci 2000; 57: 276–289.
27. Mohan H, Krumbholz M, Sharma R, et al. Extracellular matrix in multiple sclerosis lesions:

fibrillar collagens, biglycan and decorin are upregulated and associated with infiltrating immune cells. Brain Pathol 2010; 20: 966–975.
28. Reina MA, De Leon Casasola Ode L, Villanueva MC, et al. Ultrastructural findings in human spinal pia mater in relation to subarachnoid anesthesia. Anesth Analg 2004; 98: 1479–1485, table of contents.
29. Kalluri R. Basement membranes: structure, assembly and role in tumour angiogenesis. Nature Rev Cancer 2003; 3: 422–433.
30. Khoshnoodi J, Pedchenko V, Hudson BG. Mammalian collagen IV. Microsc Res Tech 2008; 71: 357–370.
31. Durbeej M. Laminins. Cell Tissue Res 2010; 339: 259–268.
32. Canoll P, Goldman JE. The interface between glial progenitors and gliomas. Acta Neuropathol 2008; 116: 465–477.
33. Riemenschneider MJ, Jeuken JW, Wesseling P, et al. Molecular diagnostics of gliomas: state of the art. Acta Neuropathol 2010; 120: 567–584.
34. Claes A, Idema AJ, Wesseling P. Diffuse glioma growth: a guerilla war. Acta Neuropathol 2007; 114: 443–458.
35. Taylor LP. Diagnosis, treatment, and prognosis of glioma: five new things. Neurology 2010; 75: S28–S32.
36. Giese A, Bjerkvig R, Berens ME, et al. Cost of migration: invasion of malignant gliomas and implications for treatment. J Clin Oncol 2003; 21: 1624–1636.
37. Giese A, Westphal M. Glioma invasion in the central nervous system. Neurosurgery 1996; 39: 235–250; discussion 250-232.
38. Arita N, Taneda M, Hayakawa T. Leptomeningeal dissemination of malignant gliomas. Incidence, diagnosis and outcome. Acta Neurochir (Wien) 1994; 126: 84–92.
39. Schweitzer T, Vince GH, Herbold C, et al. Extraneural metastases of primary brain tumors. J Neurooncol 2001; 53: 107–114.
40. Paulus W, Roggendorf W, Schuppan D. Immunohistochemical investigation of collagen subtypes in human glioblastomas. Virchows Arch A Pathol Anat Histopathol 1988; 413: 325–332.
41. Farin A, Suzuki SO, Weiker M, et al. Transplanted glioma cells migrate and proliferate on host brain vasculature: a dynamic analysis. Glia 2006; 53: 799–808.
42. Gingras MC, Roussel E, Bruner JM, et al. Comparison of cell adhesion molecule expression between glioblastoma multiforme and autologous normal brain tissue. J Neuroimmunol 1995; 57: 143–153.
43. Paulus W, Baur I, Schuppan D, et al. Characterization of integrin receptors in normal and neoplastic human brain. Am J Pathol 1993; 143: 154–163.
44. Watanabe A, Mabuchi T, Satoh E, et al. Expression of syndecans, a heparan sulfate proteoglycan, in malignant gliomas: participation of nuclear factor-kappaB in upregulation of syndecan-1 expression. J Neurooncol 2006; 77: 25–32.
45. Calogero A, Pavoni E, Gramaglia T, et al. Altered expression of alpha-dystroglycan subunit in human gliomas. Cancer Biol Ther 2006; 5: 441–448.
46. Kawataki T, Yamane T, Naganuma H, et al. Laminin isoforms and their integrin receptors in glioma cell migration and invasiveness: evidence for a role of alpha5-laminin(s) and alpha3beta1 integrin. Exp Cell Res 2007; 313: 3819–3831.
47. Jahn O, Tenzer S, Werner HB. Myelin proteomics: molecular anatomy of an insulating sheath. Mol Neurobiol 2009; 40: 55–72.
48. Giger RJ, Venkatesh K, Chivatakarn O, et al. Mechanisms of CNS myelin inhibition: evidence for distinct and neuronal cell type specific receptor systems. Restor Neurol Neurosci 2008; 26: 97–115.
49. Buss A, Sellhaus B, Wolmsley A, et al. Expression pattern of NOGO-A protein in the human nervous system. Acta Neuropathol 2005; 110: 113–119.
50. Nakada M, Kita D, Futami K, et al. Roles of membrane type 1 matrix metalloproteinase and tissue inhibitor of metalloproteinases 2 in invasion and dissemination of human malignant glioma. J Neurosurg 2001; 94: 464–473.
51. Belien AT, Paganetti PA, Schwab ME. Membrane-type 1 matrix metalloprotease (MT1-MMP) enables invasive migration of glioma cells in central nervous system white matter. J Cell Biol 1999; 144: 373–384.

52. Kuppner MC, Van Meir E, Gauthier T, et al. Differential expression of the CD44 molecule in human brain tumours. Int J Cancer 1992; 50: 572–577.
53. Brown MC, Staniszewska I, Lazarovici P, et al. Regulatory effect of nerve growth factor in alpha9beta1 integrin-dependent progression of glioblastoma. Neuro Oncol 2008; 10: 968–980.
54. Nakada M, Miyamori H, Kita D, et al. Human glioblastomas overexpress ADAMTS-5 that degrades brevican. Acta Neuropathol 2005; 110: 239–246.
55. Matthews RT, Gary SC, Zerillo C, et al. Brain-enriched hyaluronan binding (BEHAB)/brevican cleavage in a glioma cell line is mediated by a disintegrin and metalloproteinase with thrombospondin motifs (ADAMTS) family member. J Biol Chem 2000; 275: 22695–22703.
56. Friedl P, Wolf K, Lammerding J. Nuclear mechanics during cell migration. Curr Opin Cell Biol 2011; 23: 55–64.
57. Beadle C, Assanah MC, Monzo P, et al. The role of myosin II in glioma invasion of the brain. Mol Biol Cell 2008; 19: 3357–3368.
58. Tom VJ, Doller CM, Malouf AT, et al. Astrocyte-associated fibronectin is critical for axonal regeneration in adult white matter. J Neurosci 2004; 24: 9282–9290.
59. Hirsch S, Bahr M. Immunocytochemical characterization of reactive optic nerve astrocytes and meningeal cells. Glia 1999; 26: 36–46.
60. Gladson CL, Cheresh DA. Glioblastoma expression of vitronectin and the alpha v beta 3 integrin. Adhesion mechanism for transformed glial cells. J Clin Invest 1991; 88: 1924–1932.
61. Naganuma H, Satoh E, Asahara T, et al. Quantification of thrombospondin-1 secretion and expression of alphavbeta3 and alpha3beta1 integrins and syndecan-1 as cell-surface receptors for thrombospondin-1 in malignant glioma cells. J Neurooncol 2004; 70: 309–317.
62. Fidler IJ. The role of the organ microenvironment in brain metastasis. Semin Cancer Biol 2011; 21: 107–112.
63. Leenders WP, Kusters B, Verrijp K, et al. Antiangiogenic therapy of cerebral melanoma metastases results in sustained tumor progression via vessel co-option. Clin Cancer Res 2004; 10: 6222–6230.
64. Carbonell WS, Ansorge O, Sibson N, et al. The vascular basement membrane as 'soil' in brain metastasis. PLoS One 2009; 4: e5857.
65. Kienast Y, von Baumgarten L, Fuhrmann M, et al. Real-time imaging reveals the single steps of brain metastasis formation. Nat Med 2010; 16: 116–122.
66. Maller O, Martinson H, Schedin P. Extracellular matrix composition reveals complex and dynamic stromal–epithelial interactions in the mammary gland. J Mammary Gland Biol Neoplasia 2010; 15: 301–318.
67. Fata JE, Werb Z, Bissell MJ. Regulation of mammary gland branching morphogenesis by the extracellular matrix and its remodeling enzymes. Breast Cancer Res 2004; 6: 1–11.
68. Exposito JY, Valcourt U, Cluzel C, et al. The fibrillar collagen family. Int J Mol Sci 2010; 11: 407–426.
69. Colige A, Ruggiero F, Vandenberghe I, et al. Domains and maturation processes that regulate the activity of ADAMTS-2, a metalloproteinase cleaving the aminopropeptide of fibrillar procollagens types I–III and V. J Biol Chem 2005; 280: 34397–34408.
70. Colige A, Vandenberghe I, Thiry M, et al. Cloning and characterization of ADAMTS-14, a novel ADAMTS displaying high homology with ADAMTS-2 and ADAMTS-3. J Biol Chem 2002; 277: 5756–5766.
71. Colige A, Nuytinck L, Hausser I, et al. Novel types of mutation responsible for the dermatosparactic type of Ehlers–Danlos syndrome (type VIIC) and common polymorphisms in the ADAMTS2 gene. J Invest Dermatol 2004; 123: 656–663.
72. Kessler E, Takahara K, Biniaminov L, et al. Bone morphogenetic protein-1: the type I procollagen C-proteinase. Science 1996; 271: 360–362.
73. Fernandez M, Keyrilainen J, Serimaa R, et al. Small-angle x-ray scattering studies of human breast tissue samples. Phys Med Biol 2002; 47: 577–592.
74. Wolf K, Alexander S, Schacht V, et al. Collagen-based cell migration models in vitro and in vivo. Semin Cell Dev Biol 2009; 20: 931–941.

75. Siegel RC. Biosynthesis of collagen crosslinks: increased activity of purified lysyl oxidase with reconstituted collagen fibrils. Proc Natl Acad Sci U S A 1974; 71: 4826–4830.
76. Robins SP. Biochemistry and functional significance of collagen cross-linking. Biochem Soc Trans 2007; 35: 849–852.
77. Sweeney SM, Orgel JP, Fertala A, et al. Candidate cell and matrix interaction domains on the collagen fibril, the predominant protein of vertebrates. J Biol Chem 2008; 283: 21187–21197.
78. Birk DE. Type V collagen: heterotypic type I/V collagen interactions in the regulation of fibril assembly. Micron 2001; 32: 223–237.
79. Singh P, Carraher C, Schwarzbauer JE. Assembly of fibronectin extracellular matrix. Annu Rev Cell Dev Biol 2010; 26: 397–419.
80. Scott JE. Proteoglycan: collagen interactions in connective tissues. Ultrastructural, biochemical, functional and evolutionary aspects. Int J Biol Macromol 1991; 13: 157–161.
81. Schonherr E, Witsch-Prehm P, Harrach B, et al. Interaction of biglycan with type I collagen. J Biol Chem 1995; 270: 2776–2783.
82. Schwarzbauer JE, DeSimone DW. Fibronectins, their fibrilloge nesis, and in vivo functions. Cold Spring Harbor Perspect Biol 2011; 3: a005041.
83. Sasisekharan R, Shriver Z, Venkataraman G, et al. Roles of heparan-sulphate glycosaminoglycans in cancer. Nature Rev Cancer 2002; 2: 521–528.
84. Toole BP. Hyaluronan: from extracellular glue to pericellular cue. Nature Rev Cancer 2004; 4: 528–539.
85. Wu YJ, La Pierre DP, Wu J, et al. The interaction of versican with its binding partners. Cell Res 2005; 15: 483–494.
86. Pierleoni C, Verdenelli F, Castellucci M, et al. Fibronectins and basal lamina molecules expression in human subcutaneous white adipose tissue. Eur J Histochem 1998; 42: 183–188.
87. Sbarbati A, Accorsi D, Benati D, et al. Subcutaneous adipose tissue classification. Eur J Histochem 2010; 54: e48.
88. Mariman EC, Wang P. Adipocyte extracellular matrix composition, dynamics and role in obesity. Cell Mol Life Sci 2010; 67: 1277–1292.
89. Julien P, Despres JP, Angel A. Scanning electron microscopy of very small fat cells and mature fat cells in human obesity. J Lipid Res 1989; 30: 293–299.
90. Glukhova M, Koteliansky V, Sastre X, et al. Adhesion systems in normal breast and in invasive breast carcinoma. Am J Pathol 1995; 146: 706–716.
91. Cowin P, Rowlands TM, Hatsell SJ. Cadherins and catenins in breast cancer. Curr Opin Cell Biol 2005; 17: 499–508.
92. Yoder BJ, Wilkinson EJ, Massoll NA. Molecular and morphologic distinctions between infiltrating ductal and lobular carcinoma of the breast. Breast J 2007; 13: 172–179.
93. Ewald AJ, Brenot A, Duong M, et al. Collective epithelial migration and cell rearrangements drive mammary branching morphogenesis. Dev Cell 2008; 14: 570–581.
94. Jeschke U, Mylonas I, Kuhn C, et al. Expression of E-cadherin in human ductal breast cancer carcinoma in situ, invasive carcinomas, their lymph node metastases, their distant metastases,carcinomas with recurrence and in recurrence. Anticancer Res 2007; 27: 1969–1974.
95. Friedl P, Gilmour D. Collective cell migration in morphogenesis, regeneration and cancer. Nature Rev Mol Cell Biol 2009; 10: 445–457.
96. Brennan K, Offiah G, McSherry EA, et al. Tight junctions: a barrier to the initiation and progression of breast cancer? J Biomed Biotechnol 2010; 2010: 460607.
97. Kowalski PJ, Rubin MA, Kleer CG. E-cadherin expression in primary carcinomas of the breast and its distant metastases. Breast Cancer Res 2003; 5: R217–R222.
98. Guelstein VI, Tchypysheva TA, Ermilova VD, et al. Myoepithelial and basement membrane antigens in benign and malignant human breast tumors. Int J Cancer 1993; 53: 269–277.
99. Egeblad M, Nakasone ES, Werb Z. Tumors as organs: complex tissues that interface with the entire organism. Dev Cell 2010; 18: 884–901.
100. Shumate SD, El-Shenawee M. Computational model of ductal carcinoma in situ: the effects of contact inhibition on pattern formation. IEEE Trans Biomed Eng 2009; 56: 1341–1347.
101. Koukoulis GK, Howeedy AA, Korhonen M, et al. Distribution of tenascin, cellular fibronectins and integrins in the normal, hyperplastic and neoplastic breast. J Submicrosc Cytol Pathol 1993; 25: 285–295.
102. Kadar A, Tokes AM, Kulka J, et al. Extracellular matrix components in breast carcinomas. Semin Cancer Biol 2002; 12: 243–257.
103. Egeblad M, Rasch MG, Weaver VM. Dynamic interplay between the collagen scaffold and tumor evolution. Curr Opin Cell Biol 2010; 22: 697–706.
104. Lotz T, Simpson PD, Stocker D, et al. In vitro evaluation of surface based non-invasive breast cancer screening with digital image based Elasto tomography (DIET). Conf Proc IEEE Eng Med Biol Soc 2010; 2010: 3077–3080.
105. Levental KR, Yu H, Kass L, et al. Matrix crosslinking forces tumor progression by enhancing integrin signaling. Cell 2009; 139: 891–906.
106. Kim BG, An HJ, Kang S, et al. Laminin-332-rich tumor microenvironment for tumor invasion in the interface zone of breast cancer. Am J Pathol 2011; 178: 373–381.
107. Verhoeven D, Bourgeois N, Buyssens N, et al. Ultrastructural demonstration of type IV collagen deposits in periductal elastosis in breast cancer. Pathol Res Pract 1993; 189: 144–149.
108. Ioachim E, Charchanti A, Briasoulis E, et al. Immunohistochemical expression of extracellular matrix components tenascin, fibronectin, collagen type IV and laminin in breast cancer: their prognostic value and role in tumour invasion and progression. Eur J Cancer 2002; 38: 2362–2370.
109. Aznavoorian S, Stracke ML, Krutzsch H, et al. Signal transduction for chemotaxis and haptotaxis by matrix molecules in tumor cells. J Cell Biol 1990; 110: 1427–1438.
110. Kischel P, Waltregny D, Dumont B, et al. Versican overexpression in human breast cancer lesions: known and new isoforms for stromal tumor targeting. Int J Cancer 2010; 126: 640–650.
111. Potapenko IO, Haakensen VD, Luders T, et al. Glycan gene expression signatures in normal and malignant breast tissue; possible role in diagnosis and progression. Mol Oncol 2010; 4: 98–118.
112. Herrera-Gayol A, Jothy S. Adhesion proteins in the biology of breast cancer: contribution of CD44. Exp Mol Pathol 1999; 66: 149–156.
113. Auvinen P, Tammi R, Parkkinen J, et al. Hyaluronan in peritumoral stroma and malignant cells associates with breast cancer spreading and predicts survival. Am J Pathol 2000; 156: 529–536.
114. Afify A, McNiel MA, Braggin J, et al. Expression of CD44s, CD44v6, and hyaluronan across the spectrum of normal–hyperplasia–carcinoma in breast. Appl Immunohistochem Mol Morphol 2008; 16: 121–127.
115. Clezardin P, Frappart L, Clerget M, et al. Expression of thrombospondin (TSP1) and its receptors (CD36 and CD51) in normal, hyperplastic, and neoplastic human breast. Cancer Res 1993; 53: 1421–1430.
116. Guttery DS, Shaw JA, Lloyd K, et al. Expression of tenascin-C and its isoforms in the breast. Cancer Metastasis Rev 2010; 29: 595–606.
117. Hsiao YH, Lien HC, Hwa HL, et al. SPARC (osteonectin) in breast tumors of different histologic types and its role in the outcome of invasive ductal carcinoma. Breast J 2010; 16: 305–308.
118. Allan AL, George R, Vantyghem SA, et al. Role of the integrin-binding protein osteopontin in lymphatic metastasis of breast cancer. Am J Pathol 2006; 169: 233–246.
119. Zhang Y, Zhang G, Li J, et al. The expression analysis of periostin in human breast cancer. J Surg Res 2010; 160: 102–106.
120. Tuck AB, Arsenault DM, O'Malley FP, et al. Osteopontin induces increased invasiveness and plasminogen activator expression of human mammary epithelial cells. Oncogene 1999; 18: 4237–4246.

121. Senger DR, Perruzzi CA. Cell migration promoted by a potent GRGDS-containing thrombin-cleavage fragment of osteopontin. Biochim Biophys Acta 1996; 1314: 13–24.
122. Wang TN, Qian X, Granick MS, et al. Thrombospondin-1 (TSP-1) promotes the invasive properties of human breast cancer. J Surg Res 1996; 63: 39–43.
123. Kyutoku M, Taniyama Y, Katsuragi N, et al. Role of periostin in cancer progression and metastasis: inhibition of breast cancer progression and metastasis by anti-periostin antibody in a murine model. Int J Mol Med 2011; 28: 181–186.
124. Tuck AB, Chambers AF, Allan AL. Osteopontin overexpression in breast cancer: knowledge gained and possible implications for clinical management. J Cell Biochem 2007; 102: 859–868.
125. Kii I, Nishiyama T, Li M, et al. Incorporation of tenascin-C into the extracellular matrix by periostin underlies an extracellular meshwork architecture. J Biol Chem 2010; 285: 2028–2039.
126. Bristow J, Carey W, Egging D, et al. Tenascin-X, collagen, elastin, and the Ehlers–Danlos syndrome. Am J Med Genet C Semin Med Genet 2005; 139C: 24–30.
127. Conklin MW, Eickhoff JC, Riching KM, et al. Aligned collagen is a prognostic signature for survival in human breast carcinoma. Am J Pathol 2011; 178: 1221–1232.
128. Goetz JG, Minguet S, Navarro-Lerida I, et al. Biomechanical remodeling of the microenvironment by stromal caveolin-1 favors tumor invasion and metastasis. Cell 2011; 146: 148–163.
129. Wolf K, Wu YI, Liu Y, et al. Multi-step pericellular proteolysis controls the transition from individual to collective cancer cell invasion. Nature Cell Biol 2007; 9: 893–904.
130. Alexander S, Koehl GE, Hirschberg M, et al. Dynamic imaging of cancer growth and invasion: a modified skin-fold chamber model. Histochem Cell Biol 2008; 130: 1147–1154.
131. Condeelis J, Segall JE. Intravital imaging of cell movement in tumours. Nature Rev Cancer 2003; 3: 921–930.
132. Ilina O, Bakker GJ, Vasaturo A, et al. Two-photon laser-generated microtracks in 3D collagen lattices: principles of MMP-dependent and -independent collective cancer cell invasion. Phys Biol 2011; 8: 015010.
133. Yamaguchi J, Ohtani H, Nakamura K, et al. Prognostic impact of marginal adipose tissue invasion in ductal carcinoma of the breast. Am J Clin Pathol 2008; 130: 382–388.
134. Fiedler S, Bravin A, Keyrilainen J, et al. Imaging lobular breast carcinoma: comparison of synchrotron radiation DEI-CT technique with clinical CT, mammography and histology. Phys Med Biol 2004; 49: 175–188.
135. Bon G, Folgiero V, Di Carlo S, et al. Involvement of alpha6beta4 integrin in the mechanisms that regulate breast cancer progression. Breast Cancer Res 2007; 9: 203.
136. Morini M, Mottolese M, Ferrari N, et al. The alpha 3 beta 1 integrin is associated with mammary carcinoma cell metastasis, invasion, and gelatinase B (MMP-9) activity. Int J Cancer 2000; 87: 336–342.
137. Park CC, Zhang H, Pallavicini M, et al. Beta1 integrin inhibitory antibody induces apoptosis of breast cancer cells, inhibits growth, and distinguishes malignant from normal phenotype in three dimensional cultures and in vivo. Cancer Res 2006; 66: 1526–1535.
138. Tuck AB, Elliott BE, Hota C, et al. Osteopontin-induced,integrin-dependent migration of human mammary epithelial cells involves activation of the hepatocyte growth factor receptor (Met). J Cell Biochem 2000; 78: 465–475.
139. Felding-Habermann B, O'Toole TE, Smith JW, et al. Integrin activation controls metastasis in human breast cancer. Proc Natl Acad Sci U S A 2001; 98: 1853–1858.
140. Murphy-Ullrich JE. The de-adhesive activity of matricellular proteins: is intermediate cell adhesion an adaptive state? J Clin Invest 2001; 107: 785–790.
141. Sloan EK, Pouliot N, Stanley KL, et al. Tumor-specific expression of alphavbeta3 integrin promotes spontaneous metastasis of breast cancer to bone. Breast Cancer Res 2006; 8: R20.
142. Subbaram S, Dipersio CM. Integrin alpha3beta1 as a breast cancer target. Expert Opin Ther Targets 2011; 15: 1197–1210.
143. Klinowska TC, Alexander CM, Georges-Labouesse E, et al. Epithelial development and differentiation in the mammary gland is not dependent on alpha 3 or alpha 6 integrin subunits. Dev Biol 2001; 233: 449–467.
144. Chen J, Diacovo TG, Grenache DG, et al. The alpha(2) integrin subunit-deficient mouse: a multifaceted phenotype including defects of branching morphogenesis and hemostasis. Am J Pathol 2002; 161: 337–344.
145. Li N, Zhang Y, Naylor MJ, et al. Beta1 integrins regulate mammary gland proliferation and maintain the integrity of mammary alveoli. EMBO J 2005; 24: 1942–1953.
146. Baluk P, Morikawa S, Haskell A, et al. Abnormalities of basement membrane on blood vessels and endothelial sprouts in tumors. Am J Pathol 2003; 163: 1801–1815.
147. Arnaout-Alkarain A, Kahn HJ, Narod SA, et al. Significance of lymph vessel invasion identified by the endothelial lymphatic marker D2-40 in node negative breast cancer. Mod Pathol 2007; 20: 183–191.
148. Van den Eynden GG, Van der Auwera I, Van Laere SJ, et al. Distinguishing blood and lymph vessel invasion in breast cancer: a prospective immunohistochemical study. Br J Cancer 2006; 94: 1643–1649.
149. Dai J, Li B, Shi J, et al. A humanized anti-osteopontin antibody inhibits breast cancer growth and metastasis in vivo. Cancer Immunol Immunother 2010; 59: 355–366.
150. McAllister SS, Gifford AM, Greiner AL, et al. Systemic endocrine instigation of indolent tumor growth requires osteopontin. Cell 2008; 133: 994–1005.
151. Lammermann T, Bader BL, Monkley SJ, et al. Rapid leukocyte migration by integrin-independent flowing and squeezing. Nature 2008; 453: 51–55.
152. Mechtersheimer G, Munk M, Barth T, et al. Expression of beta 1 integrins in non-neoplastic mammary epithelium, fibroadenoma and carcinoma of the breast. Virchows Arch A Pathol Anat Histopathol 1993; 422: 203–210.
153. Zutter MM, Mazoujian G, Santoro SA. Decreased expression of integrin adhesive protein receptors in adenocarcinoma of the breast. Am J Pathol 1990; 137: 863–870.
154. Pignatelli M, Cardillo MR, Hanby A, et al. Integrins and their accessory adhesion molecules in mammary carcinomas: loss of polarization in poorly differentiated tumors. Hum Pathol 1992; 23: 1159–1166.
155. Jones JL, Critchley DR, Walker RA. Alteration of stromal protein and integrin expression in breast—a marker of premalignant change? J Pathol 1992; 167: 399–406.
156. Gould VE, Koukoulis GK, Virtanen I. Extracellular matrix proteins and their receptors in the normal, hyperplastic and neoplastic breast. Cell Differ Dev 1990; 32: 409–416.
157. D'Ardenne AJ, Richman PI, Horton MA, et al. Co-ordinate expression of the alpha-6 integrin laminin receptor sub-unit and laminin in breast cancer. J Pathol 1991; 165: 213–220.
158. Previtali S, Quattrini A, Nemni R, et al. Alpha6 beta4 and alpha6 beta1 integrins in astrocytomas and other CNS tumors. J Neuropathol Exp Neurol 1996; 55: 456–465.
159. Allen MD, Vaziri R, Green M, et al. Clinical and functional significance of alpha9beta1 integrin expression in breast cancer: a novel cell-surface marker of the basal phenotype that promotes tumour cell invasion. J Pathol 2011; 223: 646–658.
160. Zutter MM, Krigman HR, Santoro SA. Altered integrin expression in adenocarcinoma of the breast. Analysis by in situ hybridization. Am J Pathol 1993; 142: 1439–1448.
161. Bello L, Francolini M, Marthyn P, et al. Alpha(v)beta3 and alpha(v)beta5 integrin expression in glioma periphery. Neurosurgery 2001; 49: 380–389; discussion 390.
162. Lendorf ME, Manon-Jensen T, Kronqvist P, et al. Syndecan-1 and syndecan-4 are independent indicators in breast carcinoma. J Histochem Cytochem 2011; 59: 615–629.
163. Henry MD, Cohen MB, Campbell KP. Reduced expression ofdystroglycan

in breast and prostate cancer. Hum Pathol 2001; 32: 791–795.
164. Cross SS, Lippitt J, Mitchell A, et al. Expression of beta-dystroglycan is reduced or absent in many human carcinomas. Histopathology 2008; 53: 561–566.
165. Auvinen P, Tammi R, Tammi M, et al. Expression of CD 44 s, CD 44 v 3 and CD 44 v 6 in benign and malignant breast lesions: correlation and colocalization with hyaluronan. Histopathology 2005; 47: 420–428.
166. Gotte M, Yip GW. Heparanase, hyaluronan, and CD44 in cancers: a breast carcinoma perspective. Cancer Res 2006; 66: 10233–10237.
167. Burim RV, Teixeira SA, Colli BO, et al. ICAM-1 (Lys469Glu) and PECAM-1 (Leu125Val) polymorphisms in diffuse astrocytomas. Clin Exp Med 2009; 9: 157–163.
168. Schroder C, Witzel I, Muller V, et al. Prognostic value of intercellular adhesion molecule (ICAM)-1 expression in breast cancer. J Cancer Res Clin Oncol 2011; 137: 1193–1201.
169. Duenisch P, Reichart R, Mueller U, et al. Neural cell adhesion molecule isoform 140 declines with rise of WHO grade in human gliomas and serves as indicator for the invasion zone of multiform glioblastomas and brain metastases. J Cancer Res Clin Oncol 2011; 137: 399–414.
170. Todaro L, Christiansen S, Varela M, et al. Alteration of serum and tumoral neural cell adhesion molecule (NCAM) isoforms in patients with brain tumors. J Neurooncol 2007; 83: 135–144.
171. Yamamoto J, Ohshima K, Nabeshima K, et al. Comparative study of primary mammary small cell carcinoma, carcinoma with endocrine features and invasive ductal carcinoma. Oncol Rep 2004; 11: 825–831.
172. Tsuzuki T, Izumoto S, Ohnishi T, et al. Neural cell adhesion molecule L1 in gliomas: correlation with TGF-beta and p53. J Clin Pathol 1998; 51: 13–17.
173. Izumoto S, Ohnishi T, Arita N, et al. Gene expression of neural cell adhesion molecule L1 in malignant gliomas and biological significance of L1 in glioma invasion. Cancer Res 1996; 56: 1440–1444.
174. Yang M, Adla S, Temburni MK, et al. Stimulation of glioma cell motility by expression, proteolysis, and release of the L1 neural cell recognition molecule. Cancer Cell Int 2009; 9: 27.
175. Schroder C, Schumacher U, Fogel M, et al. Expression and prognostic value of L1-CAM in breast cancer. Oncol Rep 2009; 22: 1109–1117.
176. Asano K, Kubo O, Tajika Y, et al. Expression and role of cadherins in astrocytic tumors. Brain Tumor Pathol 1997; 14: 27–33.
177. Utsuki S, Sato Y, Oka H, et al. Relationship between the expression of E-, N-cadherins and beta-catenin and tumor grade in astrocytomas. J Neurooncol 2002; 57: 187–192.
178. Bassarova AV, Torlakovic E, Sedloev T, et al. Simultaneous bilateral breast carcinoma: histopathological characteristics and CD44/catenin–cadherin profile. Histol Histopathol 2005; 20: 791–799.
179. Prasad CP, Rath G, Mathur S, et al. Expression analysis of E-cadherin, Slug and GSK3beta in invasive ductal carcinoma of breast. BMC Cancer 2009; 9: 325.

CHAPTER 3

RECAPITULATING IN VIVO-LIKE PLASTICITY OF GLIOMA CELL INVASION ALONG BLOOD VESSELS AND IN ASTROCYTE-RICH STROMA

Pavlo Gritsenko[1], William Leenders[2], Peter Friedl[1,3,4]

[1] Microscopical Imaging of the Cell, Department of Cell Biology, Radboud Institute for Molecular Life Sciences, Radboud University Medical Centre, Nijmegen, The Nederlands
[2] Department of Pathology, Radboud University Medical Center, Nijmegen, The Netherlands
[3] David H Koch Center for Applied Research of Genitourinary Cancers, Department of Genitourinary Medical Oncology, The University of Texas, MD Anderson Cancer Center, Houston, Texas, USA
[4] Genomics Centre (CGC.nl), 3584 Utrecht, The Netherlands

Histochemistry and Cell Biology (2017); DOI 10.1007/s00418-017-1604-2

ABSTRACT

Diffuse invasion of glioma cells into the brain parenchyma leads to nonresectable brain tumors and poor prognosis of glioma disease. *In vivo*, glioma cells can adopt a range of invasion strategies and routes, by moving as single cells, collective strands and multicellular networks along perivascular, perineuronal and interstitial guidance cues. Current in vitro assays to probe glioma cell invasion, however, are limited in recapitulating the modes and adaptability of glioma invasion observed in brain parenchyma, including collective behaviours. To mimic *in vivo*-like glioma cell invasion *in vitro*, we here applied three tissue-inspired 3D environments combining multicellular glioma spheroids and reconstituted microanatomic features of vascular and interstitial brain structures. Radial migration from multicellular glioma spheroids of human cell lines and patient-derived xenograft cells was monitored using (i) reconstituted basement membrane/hyaluronan interfaces representing the space along brain vessels; (ii) 3D scaffolds generated by multi-layered mouse astrocytes to reflect brain interstitium; and (iii) freshly isolated mouse brain slice culture *ex vivo*. The invasion patterns in vitro were validated using histological analysis of brain sections from glioblastoma patients and glioma xenografts infiltrating the mouse brain. Each 3D assay recapitulated distinct aspects of major glioma invasion patterns identified in mouse xenograft and patient brain samples, including individually migrating cells, collective strands extending along blood vessels, and multicellular networks of interconnected glioma cells infiltrating the neuropil. In conjunction, these organotypic assays enable a range of invasion modes used by glioma cells and will be applicable for mechanistic analysis and targeting of glioma cell dissemination.

INTRODUCTION

Gliomas represent the most common primary brain tumor type in adults, with glioblastoma as one of the most detrimental cancers in humans[1]. The high lethality of glioma patients is mainly caused by diffuse invasion of glioma cells into the brain parenchyma, the extent of which typically precludes curative surgical resection and radiotherapy[2]. This diffuse invasive character is a relatively unique characteristic of gliomas and rarely seen in other brain cancers[3]. The structures of the brain tissue along which glioma cells migrate are complex and their microanatomic and molecular organization varies. Guiding structures include myelinated axons and astrocyte processes (white matter tracks) as well as basement membranes of blood vessels and the meninges (perivascular tracks)[2,4]. Both brain regions contain hyaluronan as main component of the brain extracellular matrix (ECM)[5]. Disseminating glioma cells orient preferentially along aligned myelinated fibers and astrocyte processes throughout the white matter[2,4]. In parallel, glioma cell invasion occurs along the interface between blood vessels and brain parenchyma[2,4,6]. Glioma cells invade the brain tissue either individually, after detaching from neighboring glioma cells, or as cohesive groups preferentially moving along blood vessels[6–12]. In addition, glioma cells may form multicellular networks with long filaments connecting glioma cells *in vivo*, and these networks were recently implicated in glioma cell invasion and resistance signaling[13].

In recent years, different assays were developed to model glioma microenvironments of the brain tissue and test the extent and mechanisms of glioma cell invasion[14,15]. Widely used 2D assays are based on coating of the culture dish with ECM molecules, including laminin, fibronectin or collagen[16,17]. However, these models lack crucial parameters of 3D brain environments which modulate migration mechanisms, including (i) low substrate stiffness, (ii) anatomically complex 3D organization, (iii) 3D space confinements which enable adhesion-dependent and adhesion-independent migration, and (iv) molecularly rich ECM composition maintained by brain cells and containing chemotactic factors[14]. Reconstituted 3D migration assays are based on natural or synthetic hydrogels with various molecular components, including fibrillar collagen, reconstituted basement membrane (rBM) rich in laminin and type IV collagen, and composite hydrogels containing polyacrylamide, fibronectin and/or cross-linked hyaluronan[18–21]. In unperturbed brain fibrillar collagens are expressed mainly along blood vessels but not in the parenchyma[4,22], and upregulated in a subset of clinical gliomas in the tumor mass and perivascular regions[23–25]. Type I collagen scaffolds are effectively invaded by glioma cells[18,26,27], however the relevance of collagen as substrate for diffuse glioma cell infiltration beyond the tumor core remains unclear[14]. rBM and cross-linked hyaluronan both represent key components of the brain stroma and, like synthetic hydrogels, provide soft environments similar to brain tissue; however they lack other adhesion ligands and cell-derived brain structures, such as astrocyte networks and myelinated axons[4].

Migration assays comprising brain-derived cells in monolayer culture, including primary astrocytes, provide 2D interaction scaffolds for glioma cells[28–30]. Astrocyte monolayers support glioma cell invasiveness via gap-junction communications and by secretion of promigratory molecules[28–30]. As 3D modification, primary rat astrocytes were combined with electrospun nanofiber scaffolds, and this approach revealed a contribution of astrocytes to single cell migration of glioma cells by secreting migration-enhancing factors[15]. However, both astrocyte monolayers and electrospun scaffolds lack the complexity and, likely, softness of 3D brain stroma[14].

Consequently, live brain slice assays are considered as "gold standard" recapitulating the complexity of brain tissue, however they support mainly perivascular but not parenchymatous routes of glioma cell invasion[31–33]. To this end, we hypothesize that the complexity of glioma invasion requires the combined application of a set of complementary *in vitro* models to enable an adaptive range of glioma invasion types, including collective perivascular invasion and network-like interstitial invasion patterns[13,34].

We here developed a set of 3D assays mimicking brain-like structures to analyse glioma cell invasion patterns from 3D multicellular spheroids. When compared to *in vivo* invasion of the same cell types in the mouse brain and to histopathology of human lesions, each assay delivers dedicated *in vivo*-like invasion programs, including single cell migration, collective sheets and strands, and/or multicellular glioma networks.

MATERIALS AND METHODS

Antibodies and reagents

The following antibodies were used: anti-mouse β-catenin (mouse clone 14/beta-catenin, 1:100, BD Biosciences); anti-human β-catenin (rabbit polyclonal, 1:1000, Abcam); anti-mouse N-cadherin (mouse, clone GC-4, 1:200, Sigma); anti-mouse laminin (rabbit polyclonal, 1:100, Sigma); anti-human collagen-IV (mouse, clone Col-94, 1:300, Sigma); anti-human vimentin (rabbit, SP20 clone, human specific,1:300, Thermo Scientific), anti-bovine glial fibrillary acidic protein (GFAP) (chicken polyclonal, 1:1000, Abcam); anti-human nestin (rabbit polyclonal, human specific,1:100, Millipore). Primary antibodies were visualized with secondary AlexaFluor-conjugated goat-anti-mouse, goat-anti-rabbit or goat-anti-chicken polyclonal antibodies (Invitrogen; 5 µg/ml). For background controls, isotype-matched unspecific mouse IgG (BD Biosciences) was used for monoclonal antibody stainings, and for polyclonal antibody stainings samples were incubated only with secondary AlexaFluor-conjugated antibodies. Cell nuclei were stained with 4',6-diamidino-2-phenylindole (DAPI; 2.5 µg/ml). F-actin was labelled with AlexaFluor-conjugated phalloidin (Invitrogen). Growth factor-reduced reconstituted basement membrane (rBM) (Matrigel, BD Biosciences; 9.8 mg/ml) was used for rBM interface culture.

Cell lines and culture

Human glioblastoma E-98 and E-468 cells were maintained as patient-derived xenografts by serial subcutaneous (E-98) and intracerebral (E-468) inoculation without in vitro culture[35]. E-468 cells were freshly isolated from mouse brain 7-8 days prior to each spheroid preparation for migration assays to minimize adaptation to in vitro culture. E-468 cells were maintained in neurobasal medium (Invitrogen) supplemented with human EGF (20 ng/ml), human bFGF (20 ng/ml), B27 Supplement (1:50), L-glutamine (2 mM) (all from Invitrogen), heparin (2 mg/ml, Sigma), penicillin (100 U/ml) and streptomycin (100 µg/ml; both PAA). Cells were maintained for up to 2 passages (E-468) in 2D culture on flasks coated with growth factor-reduced reconstituted basement membrane (rBM) (BD Biosciences; 30 µg/ml in PBS). Accutase digestion (10 min, 400-600 units/ml; Sigma) was used for cell detachment and dissociation of multicellular spheroids. A subline of E-98 cells was propagated in vitro in flasks for up to passage 35. Human glioblastoma U-251MG cells (kind gift from Dr. J. Schalkwijk, Nijmegen) were maintained permanently in in vitro culture. Primary mouse astrocytes immortalized with SV40 large T-antigen and additionally transformed with retrovirus pBabe puro H-Ras V12 (kindly provided by Amparo Acker-Palmer, Institute of Cell Biology and Neuroscience and BMLS, Goethe University Frankfurt, Germany), were maintained as described[36,37]. H2B/eGFP-expressing U-251 and E-98 cells were generated by lentiviral transduction with pLenti6.2/V5-DEST™ Gateway (Invitrogen) containing histone2B/eGFP. For in vitro invasion assays murine astrocytes and human E-98 and U-251 cells were maintained in Dulbecco's Modified Eagle's Medium (DMEM; Invitrogen) supplemented with 10% fetal bovine serum (Sigma-Aldrich), penicillin (100 U/ml) and streptomycin (100 µg/ml; both PAA), L-glutamine (2 mM, Invitrogen) and sodium pyruvate (1 mM, Invitrogen).

Generation of glioma cell spheroids

Glioma cell spheroids were generated using the hanging drop method[38]. Cells were cultured in DMEM until subconfluency, detached with 1 mM EDTA/0.075% trypsin or with Accutase (400-600 units/ml; Sigma), washed with PBS, and maintained for 24h in complete DMEM/methylcellulose (2.4%; Sigma) as hanging droplets (25 µL) containing 1000 (U-251, E-468) or 2000 (E-98) cells.

Reconstituted basement membrane interface migration assays

3D rBM/hyaluronan interface cultures were generated by polymerizing growth factor-reduced rBM on a culture dish (30 min, 37°C), followed by addition of glioma spheroids over polymerized rBM in complete DMEM with further incubation (2h, 37°C, 10% CO_2), replacement of media by complete DMEM supplemented with sodium hyaluronate (Sigma, Cat: 53747, from Streptococcus equi, Mr ~ 1.5 – 1.8 ´10^6 Da, 10 mg/ml) or methyl-cellulose (Sigma, Cat: M6385, viscosity 25 cP, 15 mg/ml) and incubation for 24–48 h. For rBM-plastic interface cultures, glioma spheroids were placed on 96-well plates (Greiner Bio One, PS, F-bottom, mClear, Black, CELLSTAR) coated with growth factor reduced rBM (30 µg/ml, diluted in PBS, preadsorbed overnight at 4°C). After spheroid addition, cultures were incubated in complete DMEM or neurobasal media (2h, 37°C, 10% CO_2), overlaid with growth factor reduced rBM (5 mg/ml, diluted in PBS) and incubated to allow rBM

polymerization (30 min, 37°C). After 24 or 48h of migration culture in complete DMEM or neurobasal media, samples were fixed (4% PFA, 30 min, RT) and analysed by bright-field or confocal microscopy.

3D astrocyte scaffold invasion assay

3D astrocyte-derived scaffolds were generated by immortalized murine astrocytes maintained at high cell density in 96-well plates (Greiner Bio One, PS, F-bottom, mClear, Black, CELLSTAR; 20,000 cells/well, coated with growth factor-reduced rBM) for 2-3 days resulting in consolidated 3D scaffolds of up to 3 - 4 cell layers in height. Glioma cell spheroids expressing H2B/eGFP were cultured on top of astrocyte scaffolds (4-5 spheroids/well) for 2 days, fixed (4% PFA, 30 min, RT), and stained to visualize glioma cells (human specific anti-vimentin antibody), astrocytes and ECM proteins.

Organotypic mouse brain slice invasion assay

To probe glioma cell invasion into 3D brain slices, the assay from[39] was modified for multicellular spheroid culture. Brains from female mice (5-6 weeks old; Charles River or Jackson Laboratories) were dissected, using the strain C57BL/6-Tg(TcraTcrb)1100Mjb/Crl (OT1) which was crossed with B6.Cg-Tg(CAG-DsRed*MST)1Nagy/J (dsRed) in our laboratory. Brains were freshly sectioned as 400 µm-thick tissue slices using a vibratome (Leica, VT1000s). Slices were maintained on transwell insert membranes (Costar, 12-well plate; 8 µm pore diameter) in complete DMEM (37°C, 5% CO_2) for 1h. Glioma cell spheroids expressing H2B/eGFP were added on top of brain slices (8-10 spheroids per slice), cultured in complete DMEM for 48h, fixed (4% PFA, 1h, 20°C), washed and stained with human-specific anti-vimentin antibody to discriminate glioma cells from DsRed-expressing blood vessels.

Confocal microscopy and quantification of glioma cell migration

Confocal microscopy (Olympus FV1000) was performed using long working distance 20× NA 0.50 and 40× NA 0.80 objectives at a vertical step size of 2-3 µm. 3D reconstruction of Z-stacks was performed using Imaris V.6.1.5 (Bitplane).

For quantitative image analysis, operator-assisted image segmentation of bright-field or confocal 3D stacks was performed (Fiji software, V.1.49g [40]). The average cell migration distance representing radial migration of glioma cells from spheroids was calculated according to the following formula:

$$\text{Average distance of cell migration} = \sqrt{\text{Total cell area} / \pi} - \sqrt{\text{spheroid area} / \pi}$$

Glioblastoma xenografts in mouse brain

Female athymic Balb/C nu/nu mice (6–8 weeks old), were obtained from Charles River Laboratories and maintained under specific pathogen-free conditions at the central animal facility of Radboudumc, Nijmegen. The animal experiments were approved by the Ethical Committee on Animal Experiments of the Radboud University, Nijmegen, The Netherlands (RU-DEC-2013-251) and performed in accordance with the Dutch Animal Experimentation Acts and the European FELASA protocol (www.felasa.eu/guidelines.php). U-251-Fluc-mCherry and E-98-Fluc-mCherry parental cells[41,42] were cultured as spheroids in neurobasal media for 1 month, enzymatically dissociated by Accutase digestion, and intracranially implanted (5 ´ 10^5 cells in 20 µL PBS) by guided injection into the right parieto-occipital hemisphere of isofluorane-anesthetized mice 2 mm from the midline.

3D reconstruction of glioma lesions

Paraffinized clinical samples from four anonymized glioma patients (primary glioblastoma) were obtained from the archives of the Department of Pathology, Radboudumc, Nijmegen. Informed patient consent and ethical committee approval for the use of (archival) brain tissue was obtained and the material was used in a manner compliant with the Declaration of Helsinki. Slices of 100 µm thickness were obtained by microtome slicing (HM 340E, Thermo Scientific Microm), deparaffinized (100% xylene), gradually rehydratated (sequential 100, 96, 70, 50% v/v ethanol/water), heated for antigen retrieval (98°C, 15 min in Tris-EDTA, pH 9.0), incubated with blocking solution (0.1% Tween-20 and 1% bovine serum albumin in PBS) and stained with antibodies. To reach saturated antibody conditions and efficient washing in the 3D sample, prolonged incubation periods with primary and secondary antibodies and each washing step (0.1% tween-20/PBS; 0.05% NaN_3) were 8-24h at room temperature to ascertain antigen saturation and complete removal of unbound antibody. The presence of nestin in the absence of astrocytic and neuronal markers GFAP and myelin basic protein (MBP), respectively, was used to identify glioma cells[43]. 200 µm thick sections from glioblastoma xenografts (U-251, E-98 and E-468 cells) in mouse brains were obtained after fixation (4% PFA, 20h) by vibratome slicing (Leica, VT1000s) followed by counterstaining to detect murine astrocytes by anti-GFAP pAbs, basement membranes by anti-laminin pAb and glioma cells by human-specific anti-vimentin or anti-nestin pAbs.

RESULTS AND DISCUSSION

Glioma cell migration along reconstituted basement membrane interfaces

To recapitulate perivascular glioma cell invasion along interfaces formed by brain parenchyma and basement membranes, we used polymerized rBM, which comprises structural glycoproteins constituting basement membrane[44,45], overlaid with hyaluronan, the most abundant component of interstitial brain ECM[5] (Fig. 1a). When overlaid on 3D

rBM without hyaluronan in the supernatant, U-251 glioma cells invaded into, but not along the rBM, and E-98 cells failed to establish radial migration but grew as compact spheroids (Fig. 1b). When hyaluronan was overlaid, both U-251 and E-98 cells developed sheet-like migration (Fig. 1b) with the speed increasing in dependence of the hyaluronan concentration reaching up to 10 mg/ml, a supra-physiological concentration at which hyaluronan formed a viscous, semi-solid solution (Fig. 1c, d). In gliomas, extracellular hyaluronan concentrations may range from 0.2 up to 5 mg/ml[46,47]. In control experiments using methylcellulose as non-physiological, inert polysaccharide in combination with rBM, migration of U-251 and E-98 cells was equally well supported (Fig. 1b, c). This indicates a generic pro-migratory function of a protein interface adjacent to viscous polysaccharide. In previous work, glioma cell migration was primarily assessed in single-cell migration assays, using cell suspensions after enzymatic dispersion[16,17]. However, when tested as tumor-like multicellular spheroids, which allow cells to establish cell-cell junctions, both U-251 and E-98 cells migrated collectively, as a cohesive sheet of cells, along the rBM-hyaluronan interface (Fig. 1d, e). Similarly, when spheroids were positioned at the interface between rBM overlaying the plastic substrate of the culture plate (Fig. 2a), U-251 glioma cells migrated as epithelial-like sheets and collective strands, whereas E-98 cells formed thinner strands and complex-shaped multicellular networks with cells retaining both linear junctions and connecting filaments between cell bodies (Fig. 2b, c). Glioma invasion modes observed in hyaluronan-rBM vs rBM-plastic interfaces may result from the different molecular and mechanical characteristics of the interface along which they migrated, including coverage of rBM proteins by hyaluronan which may provide confinement and further modulate ligand availability for cell adhesion systems and the stiffness of migration substrate. These parameters may cooperatively influence the retention of cell-cell junctions, migration mode and speed[48–51]. Accordingly, both glioma cell lines moving collectively under rBM established linear or focal adherens junctions at cell-cell contacts which were positive for N-cadherin and β-catenin, whereas glioma cells migrating on a 2D surface lacked junctional β-catenin and showed its redistribution to the cytoplasm (Fig. 2d, e). The average distance of glioma cell migration under rBM was decreased by 60-80%, compared to migration along rBM-hyaluronan interfaces (compare Fig. 2c with Fig. 1c), indicating speed regulation in dependence of variations of confinement and/or substrate stiffness.

Invasion into 3D astrocyte scaffolds

To reproduce diffuse glioma cell invasion in astrocyte-rich brain stroma we generated 3D scaffolds formed by immortalized murine astrocytes in hyperconfluent culture (Fig. 3a). Astrocytes proliferated and formed dense multicellular networks with up to 3 cell layers in thickness (~35 µm) during 3 days of culture (Fig. 3b). Astrocytes of the bottom layer typically aligned in parallel, whereas the top layer developed more varied and randomly orientated network-like organization (Fig. 3b). Hyperconfluent astrocyte cultures produced

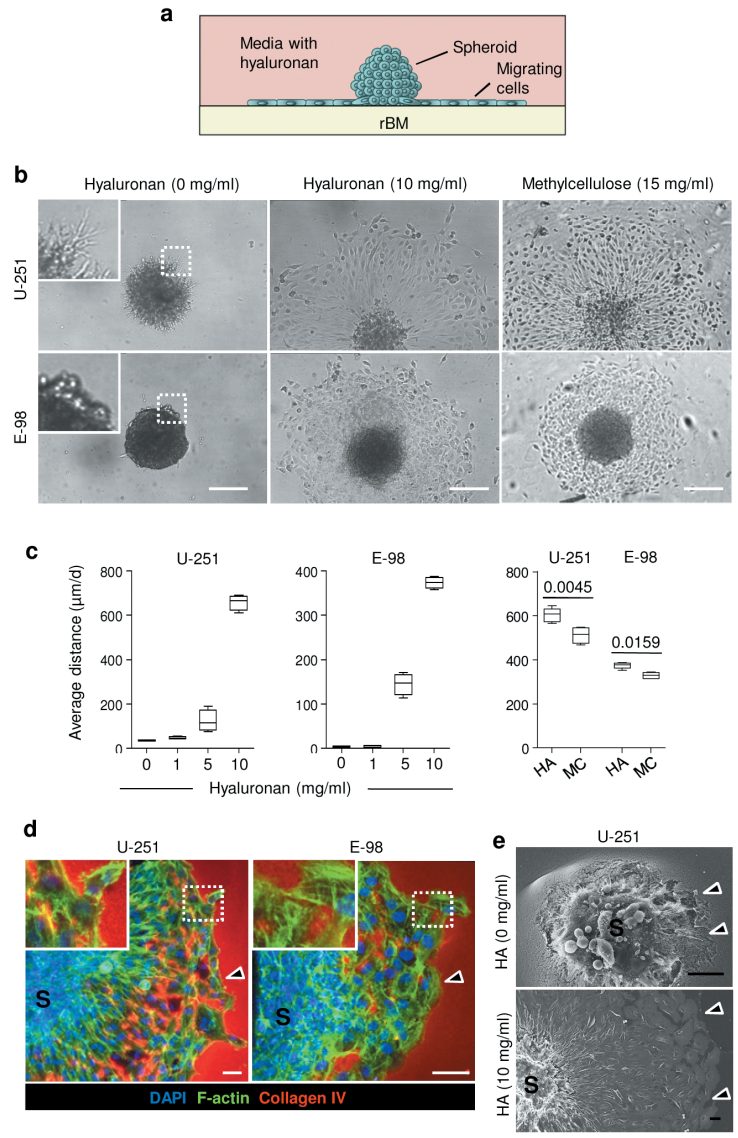

Figure 1. Reconstituted basement membrane/hyaluronan interface migration assay. **a** Assay design. **b** Radial migration of U-251 and E-98 cells from spheroids along the rBM - hyaluronan (HA) or methylcellulose (MC) interface after 1 day of culture, detected by bright-field microscopy. **c** Average distance migrated by U-251 and E-98 cells along the rBM/HA or rBM/MC interface at different concentration of HA or MC; values display medians (black line), 25/75 percentiles (boxes) and maximum/minimum (whiskers) from 3 independent experiments. P values, Mann Whitney test. **d** 3D projection from confocal z-stack of U-251 and E-98 cell migration from multicellular spheroids (S) along rBM/HA interface (10 mg/ml HA concentration). Arrowheads indicate the invasion front. **e** Scanning electron microscopy of U-251 cells after 1 day of radial migration from spheroids (S) on rBM in media without or with HA (10 mg/ml). Arrowheads, invasion front with signs of degradation of rBM (HA, 0 mg/ml) or without rBM degradation (HA, 10 mg/ml)**.** Scale bars, 200 µm (**b**), 50 µm (**d, e**).

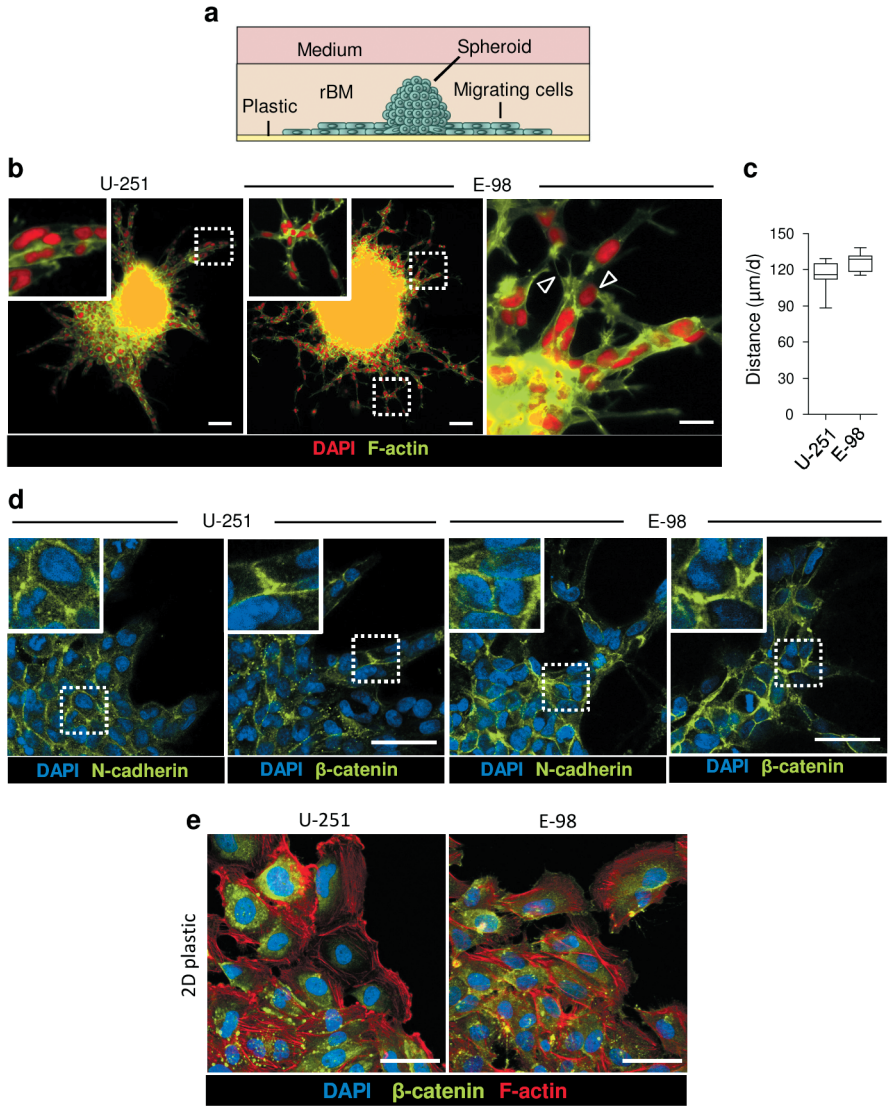

Figure 2. rBM-plastic interface migration assay. **a** Assay design. **b** Overviews of U-251 and E-98 cells after 2 days of radial migration from spheroids under rBM in neurobasal media. Arrowheads, focal cell-cell interactions. **c** Average migration distance of U-251 and E-98 cells under rBM. Values display median (black line), 25/75 percentiles (boxes) and maximum/minimum (whiskers) from 3 independent experiments. **d** Molecular topology of adherens junction proteins in U-251 and E-98 cells migrating under rBM. Images were obtained by epifluorescence (b) and confocal microscopy (d). **e** Maximum z-projection of U-251 and E-98 cells after 2 days of emigration from multicellular spheroids maintained on polystyrene surface coated with rBM. Scale bars, 100 µm **(b)**, 20 µm (zoomed insert **b**), 50 µm **(d,e)**.

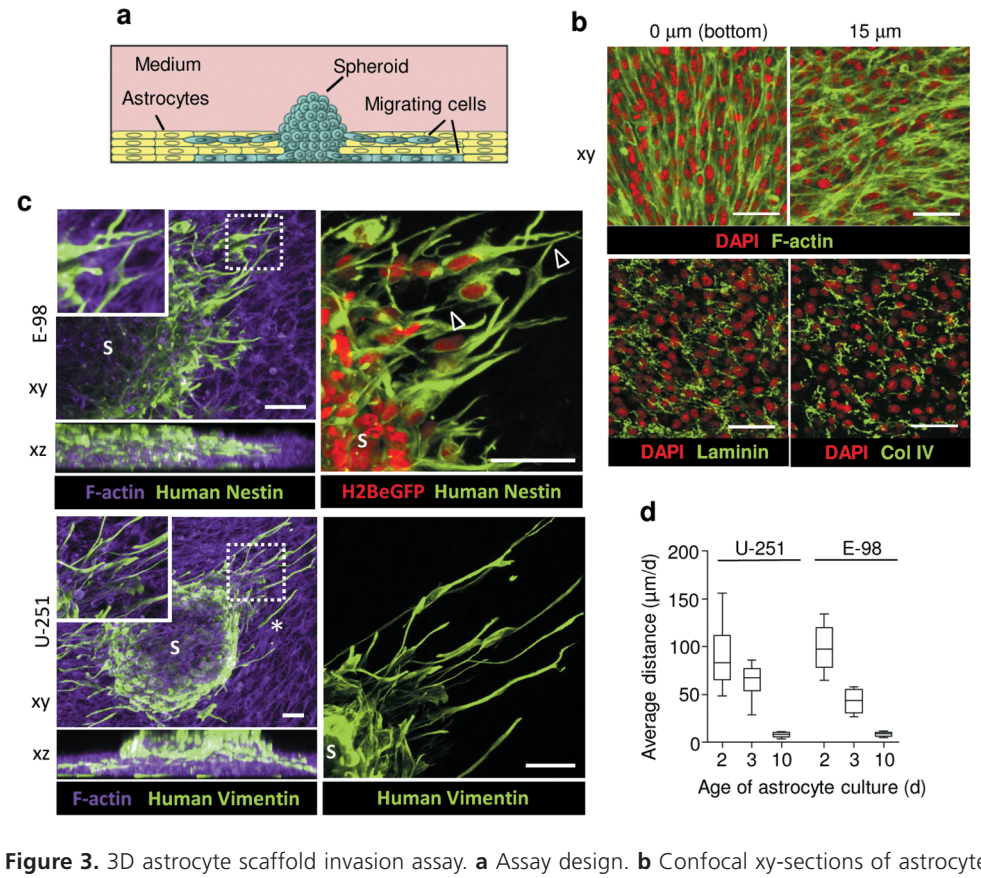

Figure 3. 3D astrocyte scaffold invasion assay. **a** Assay design. **b** Confocal xy-sections of astrocyte culture (3 days) stained for F-actin, laminin and collagen type IV (Col IV). **c** 3D reconstruction (confocal z-stack, 90 µm, horizontal and orthogonal projections) of E-98 and U-251 cell invasion from spheroids (S) into 3-day old mouse astrocyte scaffolds. Glioma cells were identified by vimentin staining with human-specific antibody and constitutive expression of H2BeGFP in the nucleus, and murine astrocytes using phalloidin (F-actin). *Arrowheads* point to contacts between glioma cells via dendrite-like filaments. *Asterisk*, detached single cell. **d** Average migration distance of U-251 and E-98 cells invading astrocyte scaffolds matured for 2, 3 or 10 days before addition of glioma spheroids. Values display median (black line), 25/75 percentiles (boxes) and maximum/minimum (whiskers) from 3 independent experiments. Scale bars, 50 µm.

extracellular matrix molecules along their cell boundaries, including laminin and collagen IV (Fig. 3b), resulting in a dense cell- and ECM-rich 3D scaffold.

Glioma cells readily invaded astrocyte scaffolds, by aligning along and intercalating between astrocytes and penetrating all scaffold layers (Fig. 3c). The speed of glioma cell invasion correlated inversely with the duration of astrocyte scaffold conditioning, with average distances covered decreasing from ~100 µm/d in 2-day old scaffolds to less than 10 µm/day in 10-day old scaffolds (Fig. 3d). Notably, and in contrast to rBM based culture, U-251 and E-98 cells invaded astrocyte scaffolds as both, single cells (Fig. 3c, asterisk) and

multicellular networks of individual cells connecting with neighbor cells via long dendrite-like filaments (Fig. 3c, arrowheads).

Invasion into mouse brain slices

The brain blood vessels have a complex anatomical and molecular organization[52,53], and in vitro assays fail to reconstitute these microanatomic features. To recapitulate the perivascular niche for U-251 and E-98 cell invasion and validate the results obtained in rBM culture, we used organotypic brain slice culture (Fig. 4a). U-251 and E-98 cells both invaded the brain slice tissue effectively and preferentially associated with blood vessels (Fig. 4b, c). Using end-point analysis of the position of individual cells relative to the spheroid boundary, the invasion speed was ~10 to 50 µm/day (median ~25 µm/day) for both cell lines (Fig. 4d), similar to the invasion speed in 3-day matured astrocyte scaffolds (Fig. 3d). The invasion pattern of U-251 and E-98 glioma cells in brain slice culture was adaptive and was dominated by collective cell strands while extending along blood vessels (Fig. 4b, arrowheads) and occasional detached single cells (Fig. 4b, asterisks). Thus, glioma cell invasion from spheroid culture on brain slices displays plastic adaptation in dependence of the tissue subregion.

Validation of in vitro assays by glioma invasion in vivo

To benchmark each in vitro invasion model, we compared the respective invasion patterns obtained in rBM, 3D astrocyte scaffolds and brain slice cultures with brain invasion in vivo, using 3D reconstructions of patient-derived xenografts in mouse brain and glioblastoma patient samples (Fig. 5a, b). Orthotopically injected in mouse brain, perivascular invasion of U-251 and E-98 glioma cells progressed as collective, finger-like strands along capillaries and larger blood vessels (Fig. 5a), and this pattern was reminiscent to their cohesive strand migration along rBM interfaces (Fig. 5a). Among other invasion patterns, similar cohesive, strand-like glioma cell invasion along blood vessels were previously observed by intravital two-photon microscopy in the mouse brain[11,12]. The number of connections per cell in perivascular invasion strands was similar for in vitro rBM and in vivo mouse models, with 70% of the cells in direct contact with 3 to 7 neighbor cells (Fig. 5c). rBM is often used for coating transwell filters to model cell invasion through, rather than along, basement membrane[54]. However, the data from the perivascular invasion in vivo confirm that glioma cells preferentially migrate along basement membranes and follow the perivascular space, but typically do not intravasate[6,12].

Likewise, the in vitro/in vivo correlation was high for multicellular glioma network organization. Glioma cells connected with long filaments were found both in peritumoral regions of E-468 patient derived xenografts (PDX) in the mouse brain and glioblastoma lesions from patient samples (Fig. 5b, arrowheads), which was consistent with the filament-based network-like pattern of E-468 cells (Fig. 5b) during infiltration of 3D astrocyte scaffolds. The number of filament-based connections between E-468 cells in 3D astrocyte

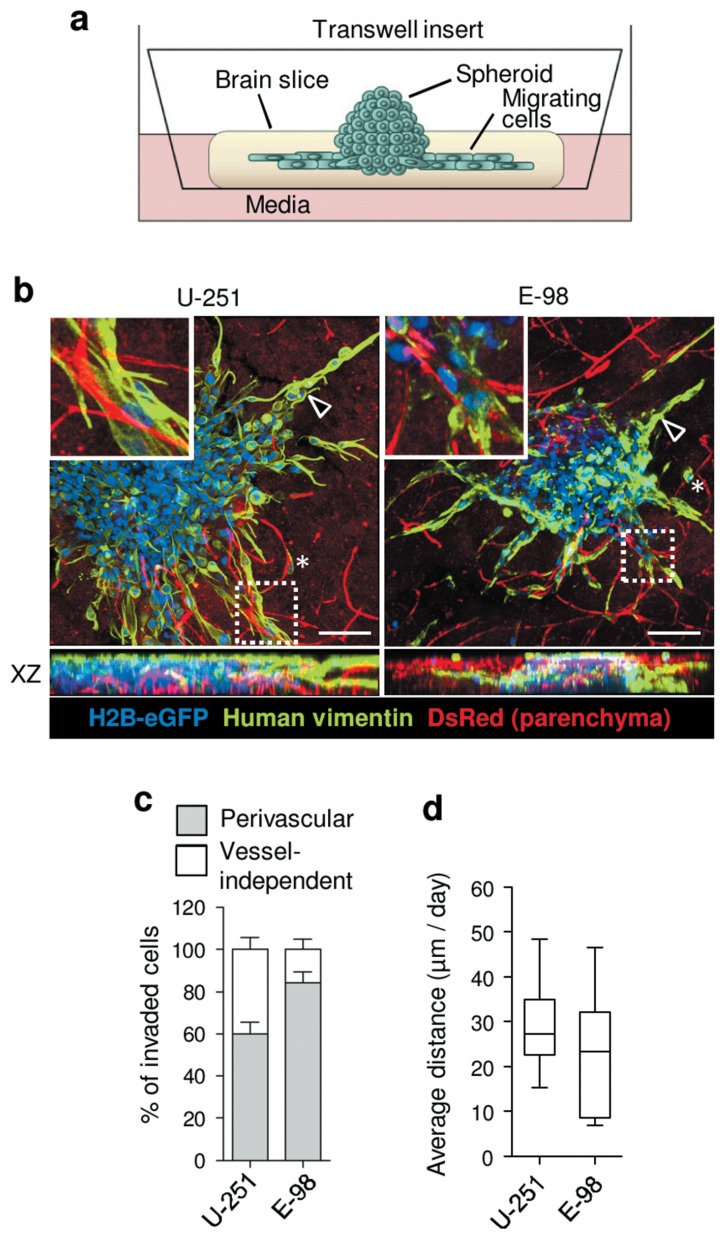

Figure 4. Organotypic mouse brain slice invasion assay. **a** Assay design. **b** 3D reconstruction (confocal z-stack, 90 µm, horizontal and orthogonal projections) of U-251 and E-98 cell migration from spheroids in mouse brain slices after 2 days of culture. Arrowheads indicate multicellular strands. Asterisks, detached single cells. Red signal originates from the DsRed mouse background, as contrast of vessels (bright signals) and stromal cells (dim signal). **c** Fractions of glioma cells associated with blood vessels, identified by vimentin staining with human-specific antibody. **d** Average distance of U-251 and E-98 cell migration in mouse brain slices. Values display median (black line), 25/75 percentiles (boxes) and maximum/minimum (whiskers) from 3 independent experiments. Scale bars, 100 µm.

Figure 5. Validation of in vitro assays by glioma invasion in murine and human brain in vivo. **a** 3D reconstruction of U-251 cell invasion along rBM-plastic interface in vitro compared to invasion pattern in the mouse brain 1 month after orthotopic implantation of U-251 cells. Glioma cells were identified using human-specific anti-vimentin, basement membranes with anti-laminin, and astrocytes and glia limitans perivascularis with anti-GFAP antibody. *Arrowhead* indicates glioma cells invading along basement membrane of a linear brain vessel under glia limitans. V - vessel lumen. In vivo images are projections from 100 µm-thick z-stacks. **b** E-468 patient-derived glioblastoma cells invading (2 days) 3D astrocyte scaffolds in vitro, or mouse brain 2 months after orthotopic implantation, compared with the peritumoral region of a primary glioblastoma (PGB) patient sample. Images represent 100 µm-thick z-stacks. *Arrowheads* denote contacts between glioma cells via dendrite-like filaments. Glioma cells were positive for vimentin (E-468) or nestin (E-468 and human sample), detected with human specific antibodies. Astrocytes were detected by anti-GFAP antibody. **c** Number of cell-cell junctions between U-251 and E-98 glioma cells in different assays, including collective strands under rBM compared to perivascular invasion in mouse brain. Values represent the number of cell contact per glioma cell (colour code of stacked boxes) and their relative frequency in the population. The number of connected neighbour cells is indicated as median (red square), 25/75 percentiles (whiskers), representing 3 independent in vitro experiments and 2 mice per cell line in mouse brain. **d** Number of filaments connecting glioblastoma cells during astrocyte scaffold invasion compared with mouse brain tissue and primary glioblastoma lesion. Values display median (black line), 25/75 percentiles (boxes) and maximum/minimum (whiskers). Data represent 3 independent in vitro experiments; 2 E-468 xenografts in mouse brain, and 4 glioblastoma patients. Scale bars, 50 µm.

scaffolds (median 4 connections/cell) matched the number of filamentous connections between E-468 cells in the mouse brain (median 4 connections/cell) as well as in human glioblastoma samples (median 5 connections/cell) (Fig. 5d). The plasticity of glioma cell invasion modes, including cohesive strand- and sheet-like structures along rBM interfaces and in perivascular space, and diffuse multicellular networks in astrocyte scaffolds likely reflect the geometry of the environment, including microtracks of least resistance and confinement effects[55].

Thus, the rBM interface and 3D astrocyte scaffold assays reliably represent two major routes of glioma dissemination in brain tissue in vivo: strand-like collective perivascular invasion along basement membranes and multicellular networks in astrocyte-rich stroma. Because rBM interface and astrocyte scaffold invasion assays are performed in 96-well plate format, both assays may be amenable for pharmacological compound screens and other experimental treatments.

ACKNOWLEDGEMENTS

We acknowledge Esther Wagena and Bianca Lemmers-Van de Weem for the excellent support for animal experiments, Anneke Navis for expert technical support for E-468 cell isolation from mouse brain, and Mietske Wijers-Rouw for expert technical assistance in scanning electron microscopy. We are greatful to Amparo Acker-Palmer for provading immortalized mouse astrocytes and Pieter Wesseling for supply of glioblastoma samples. This work was supported by NWO-VICI (918.11.626), Pieken in the Delta Oost Nederland and the Cancer Genomics Center, The Netherlands (to P.F.).

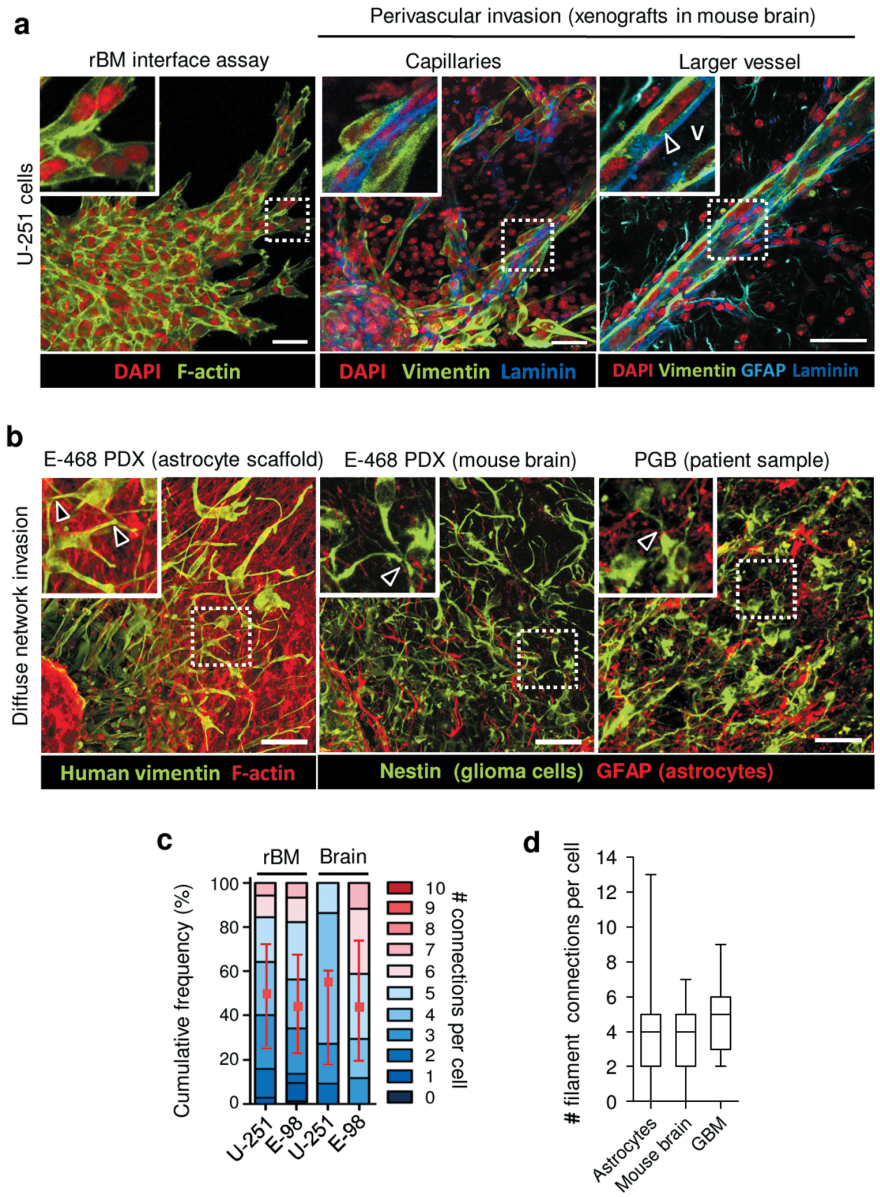

CONFLICT OF INTEREST

The authors declare that they have no conflict of interest.

REFERENCES

1. Wen, P. Y. & Reardon, D. A. Neuro-oncology in 2015: Progress in glioma diagnosis, classification and treatment. *Nat. Rev. Neurol.* **12,** 69–70 (2016).
2. Cuddapah, V. A., Robel, S., Watkins, S. & Sontheimer, H. A neurocentric perspective on glioma invasion. *Nat. Rev. Neurosci.* **15,** 455–465 (2014).
3. Lenting, K., Verhaak, R., Ter Laan, M., Wesseling, P. & Leenders, W. Glioma: experimental models and reality. *Acta Neuropathol.* **133,** 263–282 (2017).
4. Gritsenko, P. G., Ilina, O. & Friedl, P. Interstitial guidance of cancer invasion. *J. Pathol.* **226,** 185–199 (2012).
5. Zimmermann, D. R. & Dours-Zimmermann, M. T. Extracellular matrix of the central nervous system: from neglect to challenge. *Histochem Cell Biol* **130,** 635–653 (2008).
6. Farin, A. *et al.* Transplanted glioma cells migrate and proliferate on host brain vasculature: a dynamic analysis. *Glia* **53,** 799–808 (2006).
7. Hirata, E. *et al.* In vivo fluorescence resonance energy transfer imaging reveals differential activation of Rho-family GTPases in glioblastoma cell invasion. *J. Cell Sci.* **125,** 858–868 (2012).
8. Assanah, M. C. *et al.* PDGF stimulates the massive expansion of glial progenitors in the neonatal forebrain. *Glia* **57,** 1835–1847 (2009).
9. Baker, G. J. *et al.* Mechanisms of glioma formation: iterative perivascular glioma growth and invasion leads to tumor progression, VEGF-independent vascularization, and resistance to antiangiogenic therapy. *Neoplasia* **16,** 543–561 (2014).
10. Krusche, B. *et al.* EphrinB2 drives perivascular invasion and proliferation of glioblastoma stem-like cells. *Elife* **5,** (2016).
11. Winkler, F. *et al.* Imaging glioma cell invasion in vivo reveals mechanisms of dissemination and peritumoral angiogenesis. *Glia* **57,** 1306–1315 (2009).
12. Watkins, S. *et al.* Disruption of astrocyte-vascular coupling and the blood-brain barrier by invading glioma cells. *Nat. Commun.* **5,** 4196 (2014).
13. Osswald, M. *et al.* Brain tumour cells interconnect to a functional and resistant network. *Nature* **528,** 93–98 (2015).
14. Rape, A., Ananthanarayanan, B. & Kumar, S. Engineering strategies to mimic the glioblastoma microenvironment. *Adv. Drug Deliv. Rev.* **79–80,** 172–183 (2014).
15. Rao, S. S., Lannutti, J. J., Viapiano, M. S., Sarkar, A. & Winter, J. O. Toward 3D biomimetic models to understand the behavior of glioblastoma multiforme cells. *Tissue Eng. Part B. Rev.* **20,** 314–327 (2014).
16. Nakada, M. *et al.* Integrin α3 is overexpressed in glioma stem-like cells and promotes invasion. *Br. J. Cancer* **108,** 2516–24 (2013).
17. Chen, H. & Nalbantoglu, J. Ring cell migration assay identifies distinct effects of extracellular matrix proteins on cancer cell migration. *BMC Res. Notes* **7,** 183 (2014).
18. Yang, Y., Motte, S. & Kaufman, L. J. Pore size variable type I collagen gels and their interaction with glioma cells. *Biomaterials* **31,** 5678–5688 (2010).
19. Gordon, V. D. *et al.* Measuring the mechanical stress induced by an expanding multicellular tumor system: a case study. *Exp. Cell Res.* **289,** 58–66 (2003).
20. Ulrich, T. A., de Juan Pardo, E. M. & Kumar, S. The mechanical rigidity of the extracellular matrix regulates the structure, motility, and proliferation of glioma cells. *Cancer Res.* **69,** 4167–4174 (2009).
21. Ananthanarayanan, B., Kim, Y. & Kumar, S. Elucidating the mechanobiology of malignant brain tumors using a brain matrix-mimetic hyaluronic acid hydrogel platform. *Biomaterials* **32,** 7913–7923 (2011).
22. Bellail, A. C., Hunter, S. B., Brat, D. J., Tan, C. & Van Meir, E. G. Microregional extracellular matrix heterogeneity in brain modulates glioma cell invasion. *Int. J. Biochem. Cell Biol.* **36,** 1046–1069 (2004).
23. Payne, L. S. & Huang, P. H. The pathobiology of collagens in glioma. *Mol. Cancer Res.* **11,** 1129–1140 (2013).
24. Huijbers, I. J. *et al.* A role for fibrillar collagen deposition and the collagen internalization receptor endo180 in glioma invasion. *PLoS One* **5,** e9808 (2010).
25. Motegi, H., Kamoshima, Y., Terasaka, S., Kobayashi, H. & Houkin, K. Type 1 collagen as a potential niche component for CD133-positive glioblastoma cells. *Neuropathology* **34,** 378–385 (2014).
26. Frolov, A. *et al.* Imatinib and Nilotinib increase glioblastoma cell invasion via Abl-independent stimulation of p130Cas and FAK signalling. *Sci. Rep.* **6,** 27378 (2016).
27. Kaufman, L. J. *et al.* Glioma expansion in collagen I matrices: analyzing collagen concentration-dependent growth and motility patterns. *Biophys. J.* **89,** 635–650 (2005).
28. Hong, X., Sin, W. C., Harris, A. L. & Naus, C. C. Gap junctions modulate glioma invasion by direct transfer of microRNA. *Oncotarget* **6,** 15566–15577 (2015).
29. Oliveira, R. *et al.* Contribution of gap junctional communication between tumor cells and astroglia to the invasion of the brain parenchyma by human glioblastomas. *BMC Cell Biol.* **6,** 1–17 (2005).
30. Rath, B. H., Fair, J. M., Jamal, M., Camphausen, K. & Tofilon, P. J. Astrocytes enhance the invasion potential of glioblastoma stem-like cells. *PLoS One* **8,** e54752 (2013).
31. Alfi, S. T. P., Eguerinel, C. A. L. & Asset, M. I. M. Invasion of human glioma biopsy specimens in cultures of rodent brain slices: a quantitative analysis. *J Neurosurg* **97,** 169–176 (2002).
32. Miao, H. *et al.* EphA2 promotes infiltrative invasion of glioma stem cells in vivo through cross-talk with Akt and regulates stem cell properties. *Oncogene* **34,** 558–567 (2015).
33. Fayzullin, A. *et al.* Time-lapse phenotyping of invasive glioma cells ex vivo reveals subtype-specific movement patterns guided by tumor core signaling. *Exp. Cell Res.* **349,** 199–213 (2016).
34. Osswald, M., Solecki, G., Wick, W. & Winkler, F. A malignant cellular network in gliomas: potential clinical implications. *Neuro. Oncol.* **18,** 479–485 (2016).
35. Claes, A. *et al.* Phenotypic and Genotypic Characterization of Orthotopic Human Glioma Models and Its Relevance for the Study of Anti-glioma Therapy. *Brain Pathol.* **18,** 423–433 (2008).
36. Sawamiphak, S. *et al.* Ephrin-B2 regulates VEGFR2 function in developmental and tumour angiogenesis. *Nature* **465,** 487–491 (2010).
37. Depner, C. *et al.* EphrinB2 repression through ZEB2 mediates tumour invasion and anti-angiogenic resistance. *Nat. Commun.* **7,** 12329 (2016).
38. Korff, T. & Augustin, H. G. Integration of endothelial cells in multicellular spheroids prevents apoptosis and induces differentiation. *J. Cell Biol.* **143,** 1341–1352 (1998).
39. Montana, V. & Sontheimer, H. Bradykinin promotes the chemotactic invasion of primary brain tumors. *J. Neurosci.* **31,** 4858–4867 (2011).
40. Schindelin, J. *et al.* Fiji: an open-source platform for biological-image analysis. *Nat. Methods* **9,** 676–682 (2012).
41. Mir, S. E. *et al.* In silico analysis of kinase expression identifies WEE1 as a gatekeeper against mitotic catastrophe in glioblastoma. *Cancer Cell* **18,** 244–257 (2010).
42. Wurdinger, T. *et al.* A secreted luciferase for ex vivo monitoring of in vivo processes. *Nat. Methods* **5,** 171–173 (2008).
43. Kitai, R. *et al.* Nestin expression in astrocytic tumors delineates tumor infiltration. *Brain Tumor Pathol.* **27,** 17–21 (2010).
44. Hughes, C. S., Postovit, L. M. & Lajoie, G. A. Matrigel : A complex protein mixture required for optimal growth of cell culture. *Proteomics* **10,** 1886–1890 (2010).
45. Albini, A. *et al.* A rapid in vitro assay for quantitating the invasive potential of tumor cells. *Cancer Res.* **47,** 3239–3245 (1987).
46. Delpech, B. *et al.* Hyaluronan and hyaluronectin in the extracellular matrix of human brain tumour stroma. *Eur. J. Cancer* **29A,** 1012–1017 (1993).
47. Sykova, E. & Nicholson, C. Diffusion in brain extracellular space. *Physiol Rev* **88,** 1277–1340 (2008).
48. Canver, A. C., Ngo, O., Urbano, R. L. & Clyne, A. M. Endothelial directed collective migration depends on substrate stiffness via localized myosin contractility and cell-matrix interactions. *J. Biomech.* **49,** 1369–1380 (2016).

49. Bangasser, B. L. *et al.* Shifting the optimal stiffness for cell migration. *Nat. Commun.* **8,** 15313 (2017).
50. Haeger, A., Krause, M., Wolf, K. & Friedl, P. Cell jamming: collective invasion of mesenchymal tumor cells imposed by tissue confinement. *Biochim. Biophys. Acta* **1840,** 2386–2395 (2014).
51. Asano, S. *et al.* Matrix stiffness regulates migration of human lung fibroblasts. *Physiol. Rep.* **5,** e13281 (2017).
52. Yousif, L. F., Di Russo, J. & Sorokin, L. Laminin isoforms in endothelial and perivascular basement membranes. *Cell Adh. Migr.* **7,** 101–110 (2013).
53. Di Russo, J. *et al.* Vascular laminins in physiology and pathology. *Matrix Biol.* **57–58,** 140–148 (2017).
54. Benton, G., Arnaoutova, I., George, J., Kleinman, H. K. & Koblinski, J. Matrigel: from discovery and ECM mimicry to assays and models for cancer research. *Adv. Drug Deliv. Rev.* **79–80,** 3–18 (2014).
55. Monzo, P. *et al.* Mechanical confinement triggers glioma linear migration dependent on formin FHOD3. *Mol. Biol. Cell* **27,** 1246–1261 (2016).

CHAPTER 4

P120-CATENIN DEPENDENT COLLECTIVE BRAIN INFILTRATION BY GLIOMA-CELL NETWORKS

Pavlo G. Gritsenko[1], Nader Altasy[2], Cindy E.J. Dieteren[1], Anna C. Navis[3], Jan-Hendrik Venhuizen[1], Cornelia Veelken[1], Dirk Schubert[4], Amparo Acker-Palmer[5,6], Bart A. Westerman[7], Thomas Wurdinger[7], William Leenders[3], Pieter Wesseling[3,8,9], Hendrik G. Stunnenberg[2], Peter Friedl[1,10,11]

[1] Department of Cell Biology, Radboud University Medical Center, Nijmegen, The Netherlands
[2]Department of Molecular Biology, Radboud University Nijmegen, The Netherlands
[3] Department of Pathology, Radboud University Medical Center, Nijmegen, The Netherlands
[4] Cognitive Neuroscience Department, Donders Institute, Radboud University Medical Center, Nijmegen, The Netherlands
[5]Institute of Cell Biology and Neuroscience and BMLS, Goethe University Frankfurt, Germany
[6] Max Planck Institute for Brain Research, Max von Laue Strasse 4, 60438 Frankfurt, Germany
[7]Department of Neurosurgery, VU University Medical Center, Amsterdam, The Netherlands
[8] Department of Pathology, VU University Medical Center, Amsterdam, The Netherlands
[9]Department of Pathology, Princess Máxima Center for Pediatric Oncology and University Medical Center Utrecht, Utrecht, The Netherlands
[10]The University of Texas MD Anderson Cancer Center, Houston, Texas, USA
[11]Cancer Genomics Center (CGC.nl), Utrecht, The Netherlands

ABSTRACT

Diffuse brain infiltration represents a detrimental progression step of glioma disease, the cellular and mechanochemical basis of which is poorly understood. Using quantitative 3D tissue segmentation of human lesions and patient-derived xenografts in mouse brain, we here identify moving multicellular glioma cell networks as a collective organization principle for diffuse brain infiltration. Contacts between moving glioma cells were adaptive epithelial-like or filamentous junctions stabilized by N-cadherin, b-catenin and p120-catenin, which underwent kinetic turn-over to secure intercellular synchronization and directional persistence. Downregulation of p120-catenin destabilized collective networks and severely compromised diffuse brain infiltration with marginalized microlesions as outcome. Differential transcriptomics by next-generation sequencing identified p120-cateninas upstream regulator of axonal guidance and neurogenesis pathways and as strong predictor of poor clinical outcome in human glioma. The data suggest that neoplastic brain infiltration recapitulates mechanisms of brain morphogenesis with kinetically adaptive adherens junctions and intercellular communication driving glioma cell migration as multicellular network. Targeting adherens junctions thus may offer an unanticipated strategy to halt glioma progression.

INTRODUCTION

Malignant gliomas represent a molecularly defined group of consistently invasive and fatal primary brain tumors with astrocytic and oligodendroglial subtypes and glioblastoma (GBM) as the most malignant astrocytic variant. Gliomas are maintained by a limited set of driver mutations affecting isocitrate dehydrogenase (IDH), RTK/RAS/PI3K, p53 and RB pathways as well as δ2-catenin, all implicated in reprogramming cell differentiation and stemness by deranging cell cycle, metabolic programs, cell-cell interaction and migration[1–4]. Irrespective of their divergent cell origin and level of dedifferentiation, all diffuse glioma types share the dual capability of devastating brain infiltration and therapy resistance, with progressing disease even during high-dose chemo- and radiation therapy[5,6]. Through signaling cross-talk, glioma invasion, growth and resistance signaling cooperate[7], and additional protection arises from the intact blood-brain barrier which shields diffusely infiltrated brain stroma from systemic therapy. Thus, understanding the organization of glioma invasion and identifying glioma cell-intrinsic or microenvironmental regulators of invasion and survival programs are critical for developing effective targeted intervention strategies[7].

Glioma cells infiltrate brain tissue by at least two topographic and likely interconvertible programs, including perivascular and diffuse perineural invasion. Perivascular invasion, by chemotactic and/or tissue-guided motion, occurs along vascular basement membranes bordering perivascular spaces and eventually disrupts the neurovascular niche[8–10]. Diffuse infiltration of the neuropil depends upon glioma cell guidance along extracellular matrix, nerve and astrocytic tracts which consumes and ultimately destroys brain tissue[9]. Progressing gliomas retain an epithelial-to-mesenchymal transition (EMT)-like state of single cell growth, migration and survival programs, as suggested by molecular profiling and in vitro functional analyses[10,11]. Therefore, glioma invasion and survival programs are typically understood as cell-autonomous processes, with unclear cross-talk between glioma cells themselves and with non-neoplastic glial or neuronal cells[8,12,13].

In potential conflict with single-cell dissemination concepts, three-dimensional (3D) reconstruction of glioma lesions recently identified multicellular networks with dendrite-like microtubules connecting glioma cells in developing and established glioma lesions in human brain and mouse models[14]. By ensuring multicellular communication the glioma cell network depends upon connexin 43 for gap junctional intercellular communication and survival during experimental radiation therapy, indicating multicellular connectivity as important contributor to glioma progression and therapy resistance[14].

To reconcile the organization principle of glioma networks with mechanisms of glioma cell migration and brain infiltration, we here address whether cell-cell junctions are a property moving glioma cells and required for tissue infiltration. We identify a novel type of collective invasion deployed by cells with particular plasticity and interconversion between epithelial-like and filamentous intercellular junctions and further reveal p120-catenin dependent adherens junctions (AJs) as central hub stabilizing cell-cell interactions and network infiltration into brain parenchyma.

RESULTS

Network organization of glioma lesions in vivo

To revisit the cellular and molecular basis of brain infiltration by glioma cells, we first mapped the three-dimensional (3D) microanatomy of clinical glioma samples of different histological subtypes. In conventional single-slice pathology staining, infiltrating gliomas consist of spatially dispersed cell bodies with small filamentous protrusions and little sign of intercellular connectivity. However, when assessed by 3D image reconstruction using immunohistochemical staining for IDH1^{R132H} and nestin to discriminate glioma from non-neoplastic glial and other brain cells[15] both tumor center and diffusely infiltrating margins revealed extensive multicellular glioma cell networks (Supplementary Fig. 1a-f and Supplementary Video 1).

These data confirm network-like organization of glioma lesions[14]. The network pattern was present in different glioma subtypes, including low-grade astrocytomas, secondary

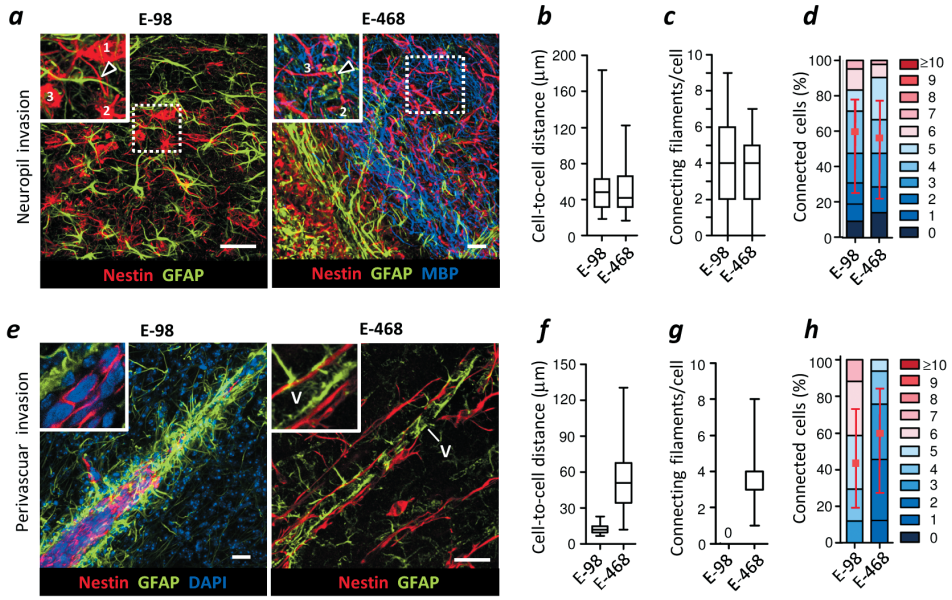

Figure 1. Perivascular invasion and multicellular glioma cell networks *in vivo*. Morphological pattern and quantitative cell-cell junction analysis of perivascular invasion (**a-d**) and interstitial networks (**e-h)** in human glioblastoma xenografts. E-98 and E-468 cell lines were implanted into mouse brain and after 28d peritumor regions were assessed by confocal microscopy (in 200 mm-thick brain slices). Identification of glioma cells by human nestin staining, brain stroma was detected by GFAP (astrocytes) and MBP staining (myelinated axons). Values display the median (black line), 25/75 percentiles (boxes) and maximum/minimum values (whiskers) or relative fractions of connected glioma cells interacting with 0 up to 10 connected cells (boxes), median (red square), 25/75 percentiles (whiskers). Data were obtained from two random mice (from 19 independent tumors) with 42 to 84 cells analyzed per mouse. Bars, 50 µm.

glioblastoma (originating from low-grade astrocytoma) and primary GBM, indicating general relevance. Two morphological types of cell-cell junctions were identified, (i) filamentous networks between glioma cells reaching deeply into the brain parenchyma (Supplementary Fig. 1a,f) and (ii) compact linear junctions present in cell-dense regions of the tumor core and collective invasion strands extending along the perivascular niche (Supplementary Fig. 1g, h).

Both, compact perivascular and network-like diffuse invasion types were present in two different human glioma models diffusely infiltrating both grey and white matter of the mouse brain, including patient-derived pro-neuronal E-98 and mesenchymal/classical patient-derived xenograft (PDX) E-468 cells[16,17] (Fig. 1a and Supplementary Fig. 2a). Consistent with the topology of clinical lesions, the organization of networks consisted of dispersed cell bodies connected by branched filaments to an average number of 4 to 8 (Fig. 1b-d, Supplementary Fig. 1b-d; Supplementary Videos 2, 3). Through filaments, glioma cell bodies separated by distances between 10 and up to 200 mm (Fig. 1b, Supplementary Fig. 1b) retained anatomical contacts to an average of 4 to 6 (total range 1 to >10) neighboring glioma cells in 3D space, with a trend for higher connectivity to neighbors in low-grade astrocytoma compared with GBM (Fig. 1c, d, Supplementary Fig. 1c, d and Supplementary Table 1). Filamentous, dendrite-like branched protrusions between glioma cells contained microtubules and the intermediate filament proteins vimentin and nestin (Supplementary Fig. 1i; Supplementary Video 4), in morphological reminiscence of filamentous junctions between astrocytes or neuronal networks during morphogenesis[18,19]. Alternatively, perivascular invasion zones comprised either directly adjacent cells bordered by epithelial-like AJs with linear junctional b-catenin or, when aligned along glia limitans, sparsely distributed cells connected with filamentous junctions (Fig. 1e-h, Supplementary Fig.1 g, h)[20,21]. Thus, during both diffuse and vessel-associated invasion, glioma cells retain cell-cell junctions.

Collective invasion of glioma cell networks

This abundance of either filamentous or epithelial-like junctions between glioma cells during brain infiltration is a morphological indication of collective invasion[22]. Collective invasion is defined as the movement of cells retaining adhesive cell-cell junctions and mechanochemical cooperativity while moving across surfaces or through 3D tissue[22,23],[24]. Using complementary 3D in vitro models mimicking brain invasion, we next addressed whether cell-cell junctions hinder or support tissue infiltration by glioma cells. Glioma cells invaded as compact capillary-like strands at the interphase between two layers of reconstituted basement membrane (rBM) (Fig. 2a), similar to collective patterns formed by glioma cells in rBM culture[25]. Moving glioma cells retained connections with 3 to 5 neighboring cells (Supplementary Fig. 3c) while generating speeds of 300-350 mm/day, consistent with sheet-like collective invasion in monolayer culture[23,26].

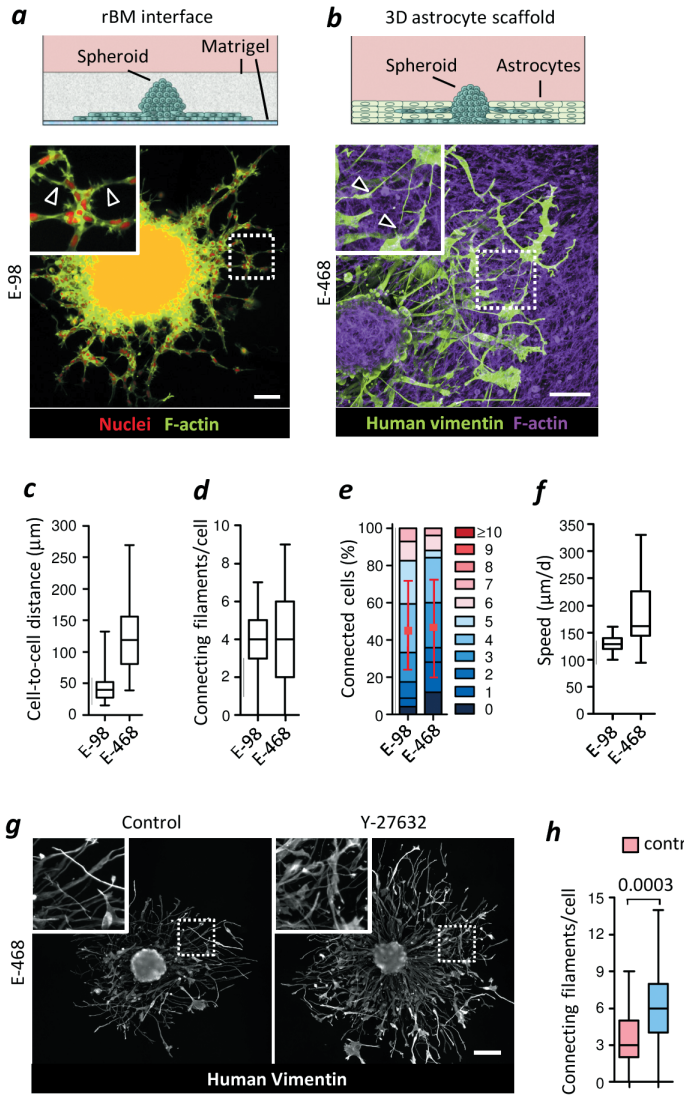

Figure 2. Collective glioma cell invasion in 3D assays representing different anatomical structures of brain tissue. Glioma cell invasion from 3D spheroids in mechanically distinct environments in vitro including (**a**) the interface between two layers of reconstituted basement membranes (rBM) and (**b**) 3D astrocyte scaffolds. Arrowheads, cell-cell junctions. Quantification of next-neighbor proximity (**c**), cell-cell connecting filaments (**d**), number of connected cells (**e**), and invasion speed (**f**) in astrocyte scaffolds. Quantitative analysis of glioma cell invasion in rBM assays is shown in Supplementary Fig. 3c. **g, h.** Enhanced glioma cell network formation and invasion in response to ROCK inhibition. Overviews and quantification of E-468 glioma cell invasion in 3D astrocyte scaffolds with or without ROCK inhibitor Y-27632 (10 µM). Values display the median (black line), 25/75 percentiles (boxes) and maximum/minimum values (whiskers) or relative fractions of connected glioma cells interacting with 0 up to 10 connected cells (boxes), median (red square), 25/75 percentiles (whiskers). Data represent 12 to 15 spheroids per condition from three independent experiments. P values, Mann Whitney test (**h**). Bars, 50 µm (**a-c**) and 200 µm (**g**).

To model diffuse infiltration into brain parenchyma in an organotypic model which provides structural complexity but retains high transparency for 3D microscopy, we monitored glioma cell invasion along 40-50 mm-thick 3D scaffolds consisting of transformed mouse astrocytes and astrocyte-derived interstitial matrix (Supplementary Fig. 3a). Similar to neuropil infiltration, glioma cells formed invading networks by aligning along astrocyte processes with tip-like cell junctions to an average of 3 to 4 adjacent glioma cells, while complete detachment of individual cells occurred rarely (Fig. 2b, e; Supplementary Fig. 3b, c).

Thus, E-98 and E-468 cells developed very similar cell-to-cell distance, number of connecting filaments and the number of connected glioma cells across interstitial in vitro and in vivo models (Fig. 1f-h; Fig. 2c-e), indicating multicellular connectivity between moving cells as default strategy across tissue subtype and experimental model.

The filamentous interactions between glioma cells are reminiscent of dendritic protrusions and interactions between neuronal cells and astrocytes[27,28]. The connectivity between neuronal cells is compromised by high actomyosin contractility under the control of RhoA/ROCK signaling[29,30]; we therefore tested whether limiting Rho/ROCK further supports glioma cell interactions and network dynamics. ROCK inhibition significantly enhanced filamentous intercellular connectivity and invasion efficiency of E-468 cells into astrocyte scaffolds (Fig. 2g, h). This indicates that the invasion activity of glioma cell networks is enhanced when actomyosin contractility is limited, similar to developing neuronal networks[27], but unlike epithelial tumors where limiting RhoA/ROCK signaling reduces invasive and metastatic competence[31,32].

Epithelial collective invasion results from relatively long-lived AJs between cells[22], however the organization and stability of AJs in moving glioma networks is unclear. Collectively moving glioma cells comprised high junction plasticity with interconversion between epithelial-like and filamentous junctions, dependent on cell density. Linear junctions were a continuous feature of cohesive emigration from the spheroid where cell density was high (Fig. 2a), while filamentous junctions formed and resolved over distance between moving cells towards the invasion front where cell density was low, revealed by 3D time-lapse microscopy (Fig. 3a,b; Supplementary Video 5). We therefore analyzed how cell movement and junction stability are balanced. Anterior, lateral and rear filaments formed, persisted for several (up to 10) hours and resolved while interacting cells translocated (Fig. 3c). Because multiple junctions were engaged in parallel at any time point, with a steady-state number of 2 to 6 connections/cell (Fig. 3d), cell movement allowed the network to expand (Supplementary Video 5). While maintaining junctional plasticity, cells leading the network maintained an oscillatory stop-go pattern with an average speed of 10 to 12 µm/h (Fig. 3c), similar to the speed of moving glioma cells in the mouse brain (5-15 µm/h)[33].

This variability of junction organization was consistent between in vitro models, glioma cells in the mouse brain and in patient glioblastoma samples (Fig. 3e, f), with epithelial-like linear or filament-based focal AJs between neighbor cells containing F-actin, b-catenin

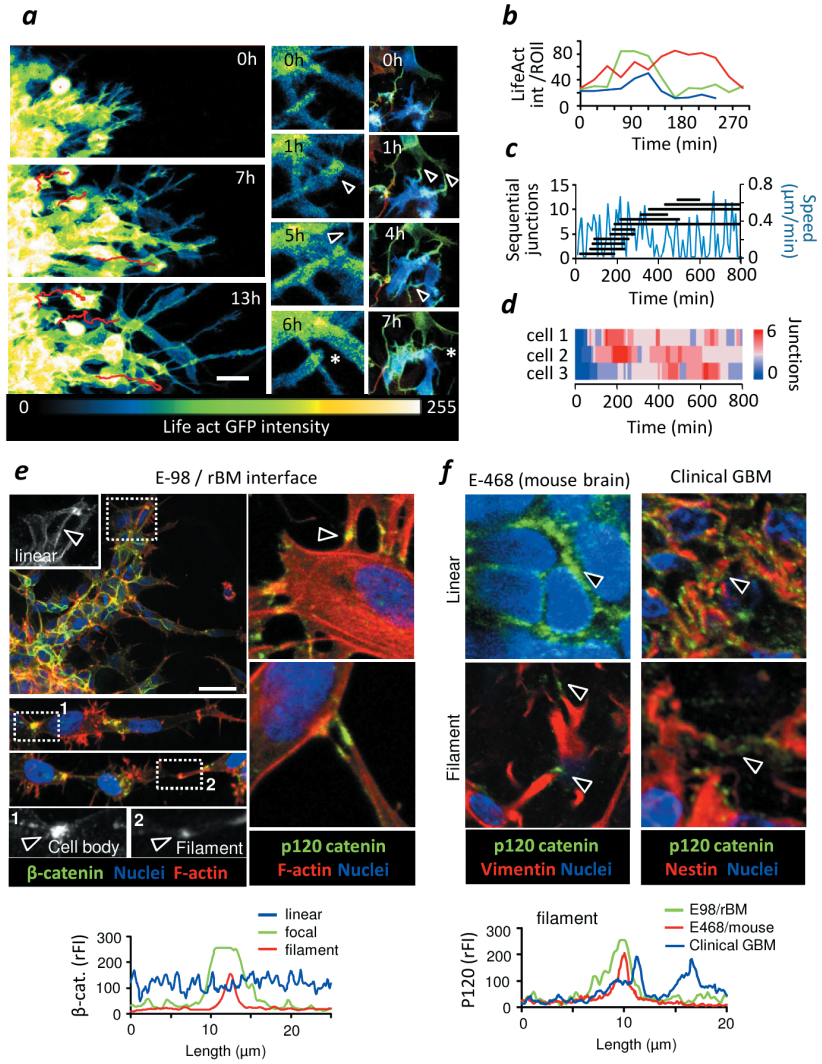

Figure 3. Topology, kinetics and molecular organization of cell-cell junctions during glioma network invasion. **a,** Actin dynamics. Sequence analysis of E-468 cell network migration from spheroid culture on 3D astrocyte scaffolds. Formation (arrowheads) and resolution of cell-cell junctions (asterisk) was monitored in LifeAct/GFP expressing E-468 cells. **b**, LifeAct/GFP intensity at filamentous cell-cell junctions over time (3 different junctions; Roi defined by filamentous cell-cell-junctions). **c,** Steady-state speed (blue line) and accompanying formation and turn-over of cell-cell junctions in representative single cell. **d,** Steady-state number of intercellular connections in three moving cells (depicted by paths in Video 6), represented as time-dependent heat-map. Sph, spheroid. **e,** Heterogeneity of junction organization, including linear, focal and filamentous cell-cell interactions between glioma cells. Subcellular distribution of β-catenin and p120 catenin in E-98 cells (rBM assay), E-468 cells (xenograft in mouse brain) and glioblastoma cells in patient sample (GBM) (top panels). Arrowheads, β- and p120 catenin accumulation along the cell-cell interface. β-catenin and p120 catenin accumulation quantified as relative fluorescence intensity (rFI) along (linear) or perpendicular (focal, filamentous) to the cell-cell junction (bottom panels). Bars, 50 µm.

and p120 catenin (Fig. 3e, f; Supplementary Fig. 4c). Thus, dependent on cell density and environmental context, glioma cells maintain cohesive or network-based junctions and anatomically adaptive collective invasion, not unlike astrocyte precursors that migrate collectively during retina development[34] and reactive astrocytes after wounding[18,19].

Cell-cell signaling between invading glioma cells

In morphogenesis and mature brain parenchyma, astrocyte networks share coordinated multicellular calcium oscillations, which are implicated in glial cell growth and neuronal signaling[35]. Moving individual glioma cells exhibit non-coordinated calcium transients[10] but depend upon calcium channel activity for invasion[36], whereas stable glioma networks constitutively and during radiation therapy exhibit calcium transients across multiple cells[14]. To test whether collectively moving glioma cells retain intercellular signaling, intracellular calcium ($[Ca^{2++}]i$) levels were recorded by the calcium indicator Fura-2AM in the spheroid migration assay. Connected E-98 and E-468 cells produced $[Ca^{2++}]i$ oscillations originating in individual or multiple cells that have emigrated from the spheroid (Fig. 4a,b) followed by signal spreading across fields of up to 20 cells (Fig. 4c; Supplementary Videos 6, 7). As in neuronal or astrocyte networks[37], calcium transients and field size were compromised by the connexin channel inhibitor carbenoxolone (CBX) (Supplementary Fig. 3d,e; Supplementary Video 8), confirming that invading glioma cells maintain gap junctional cell-cell signaling, similar to stable glioma cells networks[14]. Thus, collectively migrating glioma cells retain adhesive cell-cell junctions and intercellular signaling.

Mechanical glioma-cell coupling by AJs

To test whether glioma-cell connections are critical for tissue invasion and disease outcome, or rather represent functionally irrelevant morphological variants, we mapped and disrupted mechanisms of cell-cell cooperation. In epithelial, mesenchymal and neuronal cells during morphogenesis and homeostasis, AJs depend upon partially overlapping E- and N-cadherin-mediated mechanical and functional coupling[20,21]. E-98 and E-468 cells expressed multiple classical cadherins (Supplementary Fig. 2c) and additional adhesion molecules implicated in homophilic cell-cell adhesion, including ALCAM and NCAM (Supplementary Fig. 4a). Deregulation of N-cadherin, b-catenin and p120-catenin by transient RNA interference (RNAi) consistently disrupted cell-cell junctions and facilitated cell individualization, with negligible impact by additional downregulation of ALCAM and NCAM (Supplementary Fig. 5a). This identifies classical cadherins in maintaining AJ between glioma cells.

p120-catenin as gatekeeper of glioma cell cooperation

As non-redundant intracellular regulator of AJs formed by a range of classical cadherins, p120-catenin (p120) is essential in enabling mechanical and signaling cell-cell interaction[38,39]. In neuronal cells p120 stabilizes dendritic intercellular junctions[40] and

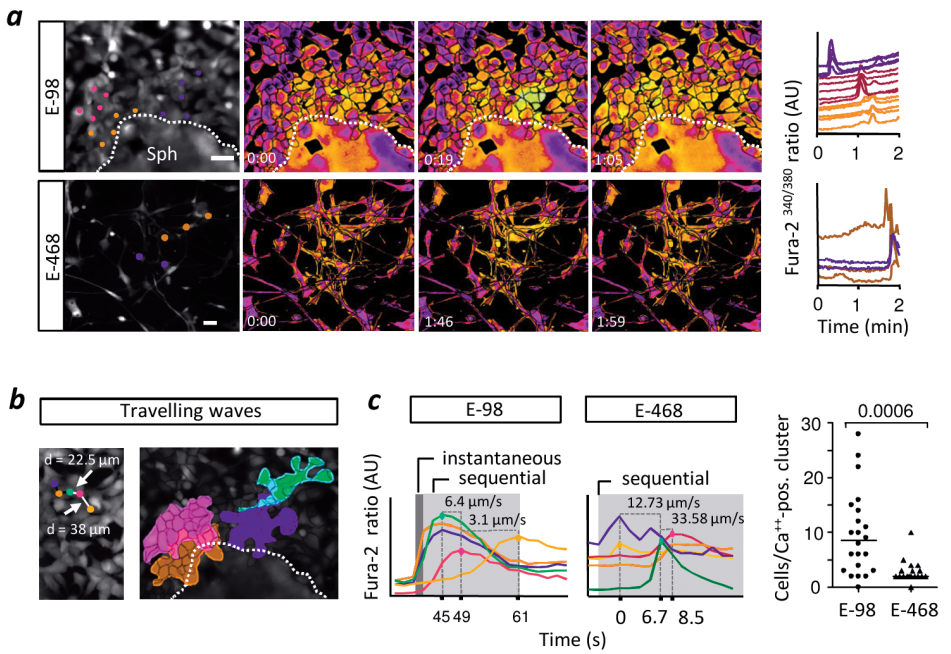

Figure 4. Functional coupling of glioma cellsin networks. **a,** Functional cell-cell coupling in E-98 and E-468 cells measured as intracellular calcium transients. Cell identification for ratiometric time-series (left panels) and derived calcium transients in neighboring cells (right panel). **b,** Near-instantaneous and sequential calcium transients in E-98 and E-468 cell clusters and networks. Example micrograph highlighting neighboring cells participating in calcium wave (left panel) and fields of connected cells recorded over 2 min (right image). **c,** Calcium waves and propagation speed (left panels, speed in brackets) and number of connected cells (right panel) in E-98 and E-468 cells. The propagation speed in E-98 is consistent with the velocity of calcium waves between astrocytes (approx. 6 mm/s)[35]. Sph, spheroid. Values display the median (black line) and individual values from individual cells (dots). Data represent 22 (E-98) and 17 (E-468) cell clusters from three independent experiments. P value, Mann Whitney test. Bars, 50 µm.

network stability[39]. In astrocytes p120 supports collective migration in vitro[23]. P120 is upregulated in glioma lesions[1] (Supplementary Fig. 4b) and detectable in both bulky and diffusely infiltrating regions of clinical glioma samples (Supplementary Fig. 4b,c). In addition, cadherin-associated protein/δ2-catenin, an endogenous p120 antagonist primarily expressed in cells with neuronal differentiation, is target of inactivating driver mutations in glioblastomas[2]. These correlative data point towards a role for AJs and particularly p120 in glioma progression, yet with unclear mechanism. We thus stably downregulated p120 by shRNA to test its role in glioma network organization and function. In both cell lines, p120 downregulation using 4 independent RNA sequences (70-80% efficacy verified by qPCR and Western blot analysis) impaired cell-cell interactions followed by cell individualization, compromised cell cycle progression with diminished mitosis rate and geminin expression, and either de-novo (E-98) or persisting severe growth deficit

(E-468 PDX cells) (Supplementary Fig. 5b-e). Downregulation of p120 further caused a severe junction defect with loss of cell-cell interactions followed by cell individualization (Fig. 5a) and the inability to participate in multicellular calcium wave propagation (Fig. 5b,c; Supplementary Video 9).

To address how perturbed cell-cell junctions affect the coordination of moving glioma networks, we recorded their migration on 3D astrocyte scaffolds. After downregulation of p120 catenin, the loss of filament-like cell-cell junctions resulted in poorly polarized and uncoordinated migration with compromised ability to migrate outward (Fig. 5d-g and Supplementary Video 10). Importantly, whereas migration speed was moderately decreased after p120 silencing (Supplementary Fig. 5f), migration persistence and outward propagation away from the spheroid were impaired (Fig. 5e; "running on the spot"). This reveals a critical role of p120 in securing collective polarity and migration persistence in glioma cells, similar to normal astrocytes[23].

We next tested whether the promotion of de novo formation of filamentous junctions or rather mechanical junction stabilization by p120 was critical for maintaining glioma cell coordination. P120 catenin limits the RhoA/ROCK pathway and down-stream actomyosin contractility including the light chain of myosin II (MLC)[41,42]. Downregulation of p120 caused an elevation of pMLC, and ROCK inhibitor Y27632 reverted pMLC levels in p120 knock-down cells to near-control level (Supplementary Fig. 5g,h) and further increased the number of filamentous connections (Fig. 5h,i); however ROCK inhibition failed to restore network propagation and invasion into astrocyte scaffolds (Fig. 5i). Thus, filamentous junctions require stabilization by AJs to support cell-cell coupling, cell polarity and network migration. Taken together, moving networks reflect a novel, neuronal type of collective migration in complex environments which depends upon morphologically plastic intercellular connections via AJs of variable duration. These particular cell and junction topologies and kinetics between glioma cells are distinct from stable junctions connecting moving epithelia or co-attraction engaged in collectively moving mesenchymal cells[43,44].

P120-catenin dependent networks mediate diffuse brain infiltration

We next aimed to delineate whether glioma cell networks maintained by AJs are indeed required for diffuse brain infiltration. Luciferase-expressing E-98 cells as well as non-luminescent E-468 cells were implanted into the mouse brain and the effect of p120 downregulation on tumor growth and brain infiltration was monitored by bioluminescence in live mice after up to 4 weeks (Fig. 6a) and/or whole-brain reconstruction and volumetric analysis *post mortem* after 4 weeks (Fig. 6b and Supplementary Video 11). Whereas multifocal control tumors developed reliably over weeks, all p120-deficient models lacked large or multifocal lesions and further failed to diffusely infiltrate the brain parenchyma (Fig. 6c; Supplementary Fig. 6a1). Overall, the reduction of diseased brain parenchyma after p120 targeting was profound, amounting to minus 90-98% (Fig. 6c). To detect

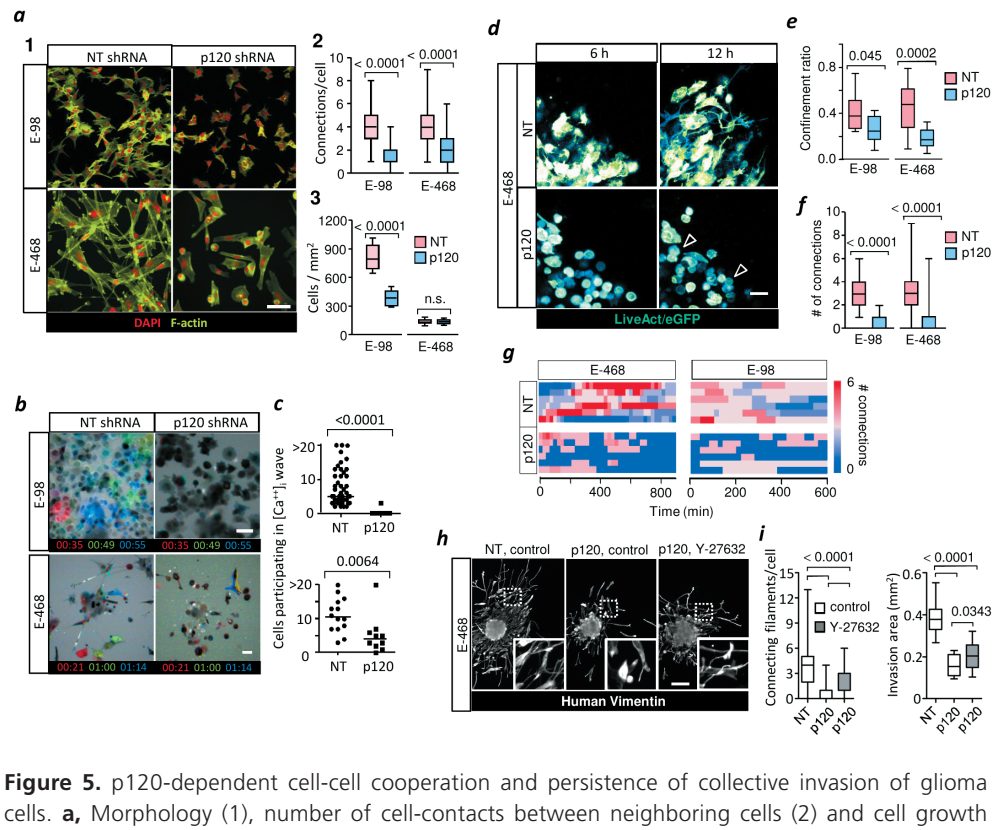

Figure 5. p120-dependent cell-cell cooperation and persistence of collective invasion of glioma cells. **a,** Morphology (1), number of cell-contacts between neighboring cells (2) and cell growth (3) in response to stable expression of non-targeting (NT) and p120 shRNA in E-98 and E-468 cells. Data represent 196 to 208 cells from duplicate wells from three independent shRNA lentiviral transductions. Efficiency, stability of downregulation and validation using independent shRNA probes are shown in Supplementary Fig. 5c. **b-f,** Impact of p120 downregulation on glioma cell network functions. **b,c,** Morphology and quantitative impact of p120 downregulation on calcium wave propagation between neighbor cells in E-98 and E-468 cells. Data represent 10 - 19 spheroids per condition from two independent shRNA lentiviral transductions. **d,** Time-lapse sequence of E-468 cells from spheroid on 3D astrocyte scaffold expressing NT or p120 shRNA. Arrowheads, non-polar cells deficient of protrusions and intercellular connections. **e,** Decreased migration persistence, measured as confinement ratio (distance start-end point / total length of path) over a period of 10-13 h. **f,g,** Image-sequence based quantification of the median number (**f**) and time-dependent cell-cell interactions (g) in moving cells during 13h of migration. Data represent 6 to 8 representative movies with each 3 spheroids from 3 independent experiments. **h**,**i**, Marginal rescue of filamentous connectivity and invasion efficiency of E-468 cells after p120 catenin downregulation by ROCK inhibitor Y-27632 (10 µM) in 3D astrocyte scaffolds. Overview images (**h**) and quantitative analysis (**i**). Data represent 25 to 30 spheroids from three independent shRNA lentiviral transductions. Values display the median (black line), 25/75 percentiles (boxes) and maximum/minimum values (whiskers). P values, Mann Whitney test. Bars, 100 µm (a), 50 µm (b, d), 200 µm (h).

whether networks were disrupted by p120 downregulation in vivo, we performed 3D high-resolution morphometry of large-field sections capturing both tumor center and invasion front of E-468 PDX tumors (Fig. 6d). In control lesions, both tumor center and invasion front were composed of glioma cell networks with filamentous cell-cell junctions and an average of 3 cell-cell contacts (Fig. 6e) with gradual decrease of connection density towards the outward edge (Fig. 6f). Likewise, the network organization was lost and replaced by individualized less polarized or rounded cells in E-98 lesions after p120 downregulation with abolished interstitial invasion (Supplementary Fig. 6a). Residual microlesions contained few clustered cells lacking p120-positive intercellular junctions (Supplementary Fig. 6c) or individualized cells with shortened filaments positioned along interstitial tracks (Fig. 6d, Supplementary Fig. 6a2; Video 12), together with compromised cell cycle progression detected by diminished geminin-positive cell subsets (Supplementary Fig. 6b). In line with defective brain infiltration, colonization of the spinal cord was lacking in E-98 cells upon follow-up for up to 4 weeks (Fig. 6a). Thus, diffuse glioma cell invasion in brain tissue depend on cell-cell junctions and p120 availability, resulting in poorly invasive, marginalized microlesions.

Glioma cell networks recapitulate a neuronal morphogenesis program

To map the putative signaling mechanisms by which AJs may support glioma progression, we performed next-generation RNA sequencing and gene ontology (GO) analysis. Differential response patterns in glioma cells expressing non-targeting or p120 shRNA were largely cell-type specific with unique sets of down- or up-regulated genes, however with a significant cluster common to both E-98 and E-468 cells (Supplementary Fig. 2b and Supplementary Fig. 7a). GO-term analysis of downregulated gene sets identified perturbation of neuron development, differentiation and axonogenesis in both cell lines (Fig. 7a, Supplementary Fig. 7b). Deregulated ephrins, netrins, neurofascin and contactin-2, among other targets (Fig. 7a) are critically involved in cell-cell interactions, neuronal development and synaptic transmission[45] as well as GAP43 which was identified in the radiation resistance response of glioma networks[14] (Fig. 7a, Supplementary Table 3). Thus, p120 is a critical upstream regulator of protein networks required for neuronal-like features in glioma cells.

High p120-catenin expression correlates with poor clinical outcome

To validate the role of p120 in glioma progression for human disease, we generated a p120 downstream gene signature using two independent datasets from human gliomas[17,46]. Genes that were up- and down-regulated after knock-down of p120 in E-98 cells were directionally weighed-matched with gene expression data of the clinical samples. The p120 signature significantly matched with signatures of genes involved in cell migration and extracellular matrix remodeling (Supplementary Fig. 7c; Supplementary Table 4), using the list of scanned 3875 Broad curated gene signatures. When stratified

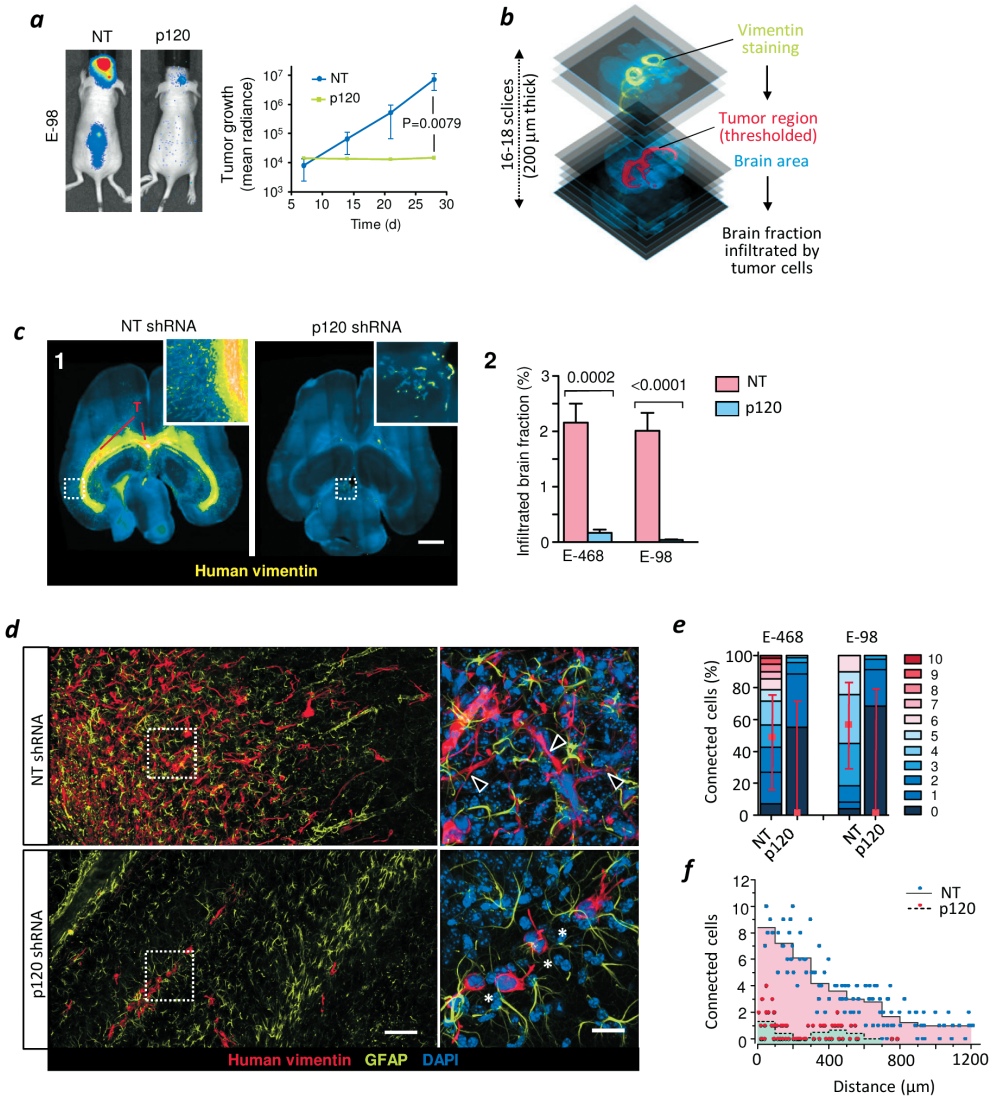

Figure 6. p120 is indispensable for glioma growth, network formation and diffuse brain infiltration. **a,** Bioluminescence distribution and intensity after implantation into the mouse brain. Data represent the means and SEM from 5 mice/group. **b**, Ex vivo technique to quantify the mouse brain volume infiltrated with glioma cells. **c1,** Impaired tumor growth and diffuse brain infiltration of E-468 cells after p120 downregulation. Overviews and detail (insets) from 200 µm thick brain slices. Bar, 2 mm. **c2,** Extent of brain volume consumption by three glioma lines, expressed as cumulative percent of brain section area containing vimentin-positive cells 4 weeks post-implantation. Data represent the mean values ± SEM 19 mice (E-98) and 16 mice (E-468) from two independent implantation series. P values, Mann Whitney test. **d,** Diffuse brain infiltration of E-468 cells as multicellular networks and perturbation after p120 downregulation 30d post-implantation (3D confocal microscopy from 200 mm thick brain slices). Arrowheads, filaments in multicellular networks of vimentin-positive E-468 cells. Bars, 100 µm (overview) and 25 µm (detail). **e,** Perturbation of cell-cell interactions in two glioma models in 4 weeks post-implantation. Data represent 49 to 108 cells from two mice per condition. Relative fractions of connected glioma cells interacting with 0 up to 10 connected cells (boxes), median (red square), 25/75 percentiles (whiskers). **f,** Frequency of cell-cell junctions from the region of maximum cell density ("0") to the front of the diffuse infiltration zone covering >1200 mm in cells expressing NT or p120 shRNA. Bar, 25 µm.

for p120 expression, overall survival of glioma patients was significantly prolonged in the subgroup with low p120 level (Fig.7b). Thus, in PDX models and clinical glioma samples, p120 regulated genes are associated with neuronal network and migration functions and strongly associated with glioma progression.

DISCUSSION

These findings implicate multicellular networks as a novel pathomechanistic principle of glioma disease and identify p120-catenin as integrator of neuronal-like functions in glioma cells required for diffuse brain infiltration. As a consequence, multicellular networks rather than individualized cells secure mechanocoupling, signaling and large-scale brain infiltration, similar to astrocytic or neuronal networks[27,47,48]. Although glioma networks may contain functional subunits and intratumoral heterogeneity[3] and occasional cell individualization, the extensive intercellular connections imply that diffuse gliomas should be considered as a single functional operon, rather than a collection of individual cells, which as a whole sustain particularly aggressive growth, invasion and survival ability, as proposed[14].

As basis for network function, AJs provide cell-cell adhesion and signaling for both neuronal-like network function in collective migration programs and growth, in potential reminiscence of certain epithelial tumors which rely upon p120 signaling for anchorage-independent growth, anoikis resistance and metastasis[49–52]. Our data establish p120 as a central gatekeeper of AJs[38,39] in glioma tumors and suggest oncogene-like functions of p120 in glioma and disrupting p120-dependent signaling disables glioma aggressiveness. The emerging roles for cell-cell cooperation in tumor progression, including in glioma, indicate that targeting of AJs may suffice to revert detrimental neoplastic growth and tissue infiltration programs congruently.

Plasticity of collective invasion programs

In glioma, collective migration strategies are remarkably adaptive, in a tissue-context dependent manner. Perivascular cohesive strands move through aligned confined space form epithelial-like AJs whereas multicellular networks with dynamic and relatively short-lived neuronal-like filaments support intercellular connections during interstitial invasion of brain stroma (Fig. 7c). While cohesive cell migration with linear cell-cell junctions is a well-established collective invasion mode utilized by epithelial embryonic and cancer cells[22,53], glioma multicellular network migration combines neuronal network plasticity present with transient cell-cell interactions in dynamic crest cell and neuronal networks in

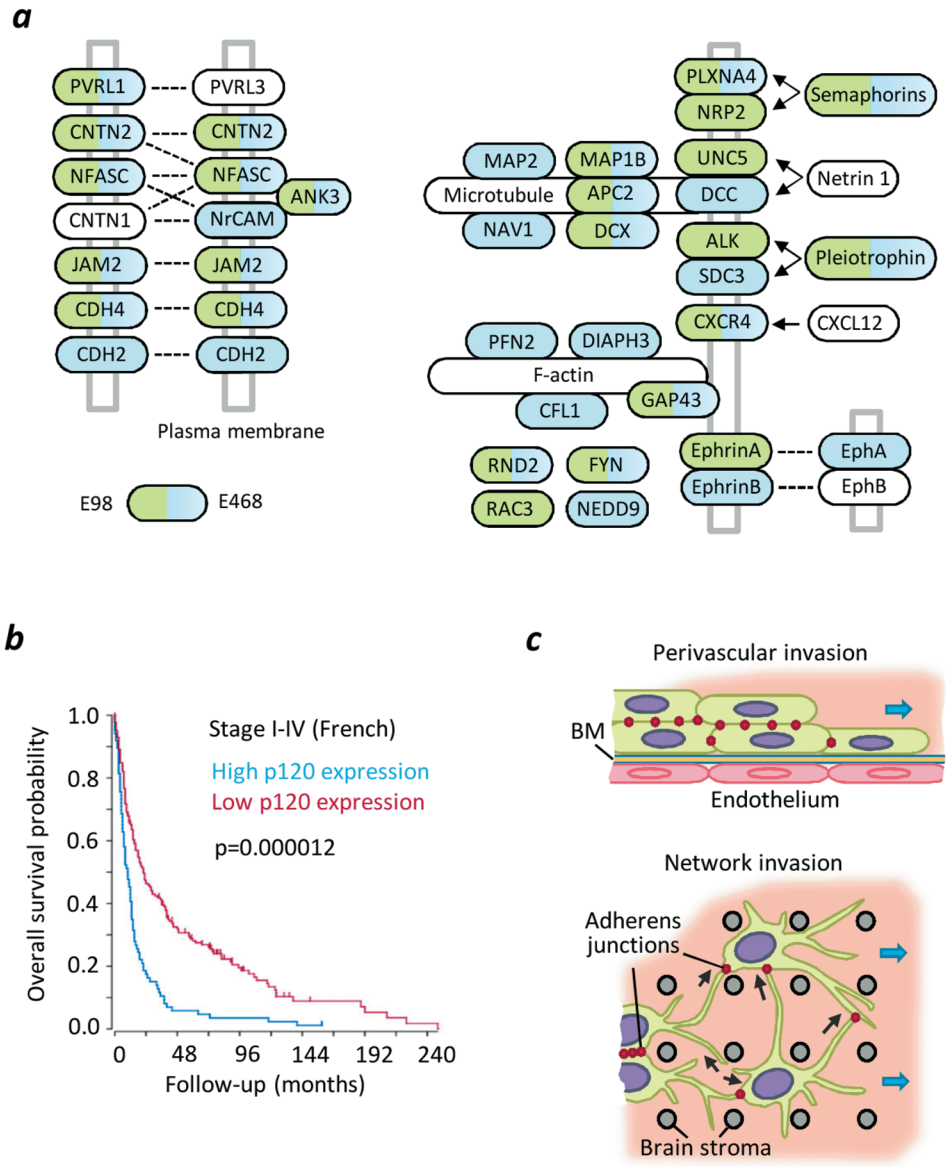

Figure 7. Neuronal related pathways regulated by p120 catenin in glioma cells and clinical relevance in glioma patients. **a,** Deregulated cell adhesion and axon guidance after downregulation of p120 catenin in glioma cells, based on Gene Ontology term analysis and the KEGG network maps "Cell-cell adhesion" and "Axonogenesis" biological functions. Pathway-related genes significantly down-regulated in E98 or E468 cell lines upon p120-shRNA targeting are annotated in respective green or blue fillings. The underlying RNA expression analysis and clustering are shown in Supplementary Fig. 7a,b. **b**, Overall survival of glioma patients (grade I – IV) with high or low p120 mRNA expression (French dataset, 284 samples). P-value was obtained after Bonferroni correction. **c,** Types of collective glioma cell invasion in response to different microanatomy of brain subregions. Epithelial-like cohesive pattern during perivascular invasion (1) may convert into diffusely-infiltrating neuronal-like networks during neuropil infiltration. Black arrows, kinetics of cell-cell interactions. Blue arrows, direction of migration.

embryogenesis[54–56], and with ongoing mechanical and chemical coupling between cells, thus fulfilling key criteria of collective invasion[22].

Molecular profiling after p120 downregulation indicates defects in the expression of neurofascin, contactin 2, ankyrin G, MAP1B, doublecortin, GAP43 and other molecules (Fig. 7a and Supplementary Table 3), which regulate neuronal polarization and cytoskeleton dynamic in neuronal network formation[27,57,58]. Beyond intercellular signaling, relevance for AJs was shown for collective durotaxis of epithelial monolayers, when compared to individually-moving cells, as they provide mechanical coupling across multiple cell bodies required for collective persistence towards stiffer substrate[24]. Likely, AJs thus deliver combined mechanical and molecular signals to sustain front-rear polarity and create a morphogenesis-like program in glioma cell networks. P120 catenin is an established modulator of Rho GTPases which control the polarity of collective invasion and axonal growth[29,30,41,59,60]. Accordingly, by diminishing RhoA and engaging Rac1 activities p120 catenin promotes extension of processes in neuronal cells[40,61]. However, the marginal effects of ROCK inhibition in reverting the loss of network function and invasion after p120 downregulation indicates that increasing filament formation is insufficient to secure collective behaviors when AJs are dysfunctional. Besides mechanical cell-cell cohesion and junctional signaling, additional functions of p120 reside in translocation to the nucleus and transcription regulation of genes implicated in neuronal differentiation via the transcriptional repressors REST and GLIS2[62] as well as Kaiso; these effectors, which antagonize β-catenin/TCF/LEF transcriptional activity and modulate Wnt signaling pathways in axonal guidance and cell proliferation[41,62–64], may be engaged and support glioma networks.

In conclusion, mechanical and signaling functions of p120 catenin are indispensable for structural and signaling integrity of axonal guidance and neurogenesis programs in glioma cell networks, implicating classical AJs as central hub maintaining collective brain infiltration and ultimately brain consumption. Future targeting of AJs or their downstream effectors will offer yet unappreciated strategies to overcome diffuse brain infiltration and fatal outcome.

ACKNOWLEDGEMENTS

We acknowledge Esther Wagena, Manon Vullings, Kiek Verrijp, Jeroen Mooren and Bianca Lemmers-Van de Weem for expert technical support in animal experiments, image analyses and immunohistochemistry. We further acknowledge Mirjam Zegers for critical reading of the manuscript. This work was supported by NWO-VICI (918.11.626), Pieken in the Delta Oost Nederland and the Cancer Genomics Center, The Netherlands (to P.F.), NWO-VENI (863.13.019) to C.D. and SFB834 to A.A.-P.

AUTHOR CONTRIBUTIONS

P.G., C.D., W.L., P.W., A.A.-P. T.W., N.A., H.G.S. and P.F. designed the experiments and interpreted the data. P.G., C.D., A.N., J.H.V., C.V. and D.S. performed experiments and

quantitatively analyzed the data. P.G. and P.F. wrote the paper. All authors read and corrected the manuscript.

AUTHOR INFORMATION

The authors declare no competing financial interests. Correspondence and requests for materials should be addressed to peter.friedl@radboudumc.nl.

SUPPLEMENTARY INFORMATION

Materials and Methods

Antibodies and reagents

The following antibodies were used for immunolabeling: anti-human IDH1 R132H (mouse, clone H09, 1:20, Dianova); anti-bovine GFAP (chicken polyclonal, 1:1000, Abcam); anti-human myelin basic protein (rabbit polyclonal, 1:200, Sigma); anti-human nestin (mouse, clone 10C2, human specific, 1:200, Millipore); anti-human nestin (rabbit polyclonal, human specific,1:100, Millipore); anti-human vimentin (chicken polyclonal, 1:400, Abcam); anti-human vimentin (rabbit, SP20 clone, human specific,1:300, Thermo Scientific); anti-human tubulin (rabbit polyclonal, 1:200, Abcam); anti-mouse laminin β1 (rat, clone LT3, 1:100, Thermo Scientific); anti-mouse laminin (rabbit polyclonal, 1: 100, Sigma); anti-mouse p120 catenin (mouse, clone 98/pp120, 1:200, BD Biosciences); anti-human p120 catenin (rabbit, clone YE372, human specific, 1:200, Millipore); anti mouse β-catenin (mouse clone 14/beta-catenin, 1:100, BD Biosciences); anti-human β-catenin (rabbit polyclonal, 1:1000, Abcam); anti-mouse N-cadherin (mouse, clone GC-4, 1:200, Sigma); anti-human β1 integrin (mouse, clone 4B4, human specific, 1:100, BD Biosciences); anti-human ALCAM (mouse, clone 3A6, 1:50, BD Biosciences); anti-human NCAM (mouse, clone NCAM16.2, 1:100, BD Biosciences); anti-human collagen-IV (mouse, clone Col-94, 1:300, Sigma); anti-human collagen-I (rabbit polyclonal, 1:100, Rockland); anti-human geminin (rabbit polyclonal, 1 : 500, Thermo Scientific).

3D reconstruction of glioma lesions

Paraffinized clinical samples from glioma patients were obtained from the archives of the Department of Pathology, Radboudumc, Nijmegen. Samples included lower grade astrocytomas, anaplastic oligodendroglioma (with the characteristic complete deletion of chromosome arms 1p and 19q), secondary GBM (originating from low-grade astrocytoma) and primary GBM (Supplementary Table 1). Informed patient consent and ethical committee approval for the use of (archival) brain tissue was obtained and the material was used in a manner compliant with the Declaration of Helsinki. Slices of 100 µm thickness were obtained by microtome slicing (HM 340E, Thermo Scientific Microm), deparaffinized (100% xylene), gradually rehydratated (sequential 100, 96, 70, 50% v/v ethanol/water), heated for antigen retrieval (98°C, 15 min in Tris-EDTA, pH 9.0), incubated with blocking solution (0.05% Tween-20 and 1% bovine serum albumin in PBS) and stained with antibodies. Likewise, 200 µm thick sections from glioblastoma xenografts in mouse brain were obtained after fixation (4 % PFA, 20h) using vibratome slicing (Leica, VT100s). To reach saturated antibody conditions and efficient washing in the 3D sample, incubation periods with primary and secondary antibodies and each washing step (0.05% tween-20/PBS; 0.05% NaN_3) were 8-24h at room temperature. Glioma cell populations in LGA and in secondary glioblastoma were identified by positivity for the IDH1 R132H mutation colocalized with nestin in the majority of cells. In primary glioblastoma, due to the absence of IDH1 R132H, the presence of nestin in the absence of astrocytic and neuronal markers GFAP and MBP, respectively, was used to identify glioma cells[65].

Cell lines and culture

Human glioblastoma E-98 and E-468 cells were maintained as patient-derived xenografts by serial intradermal (E-98) and intracerebral (E-468) inoculation without in vitro culture[16]. E-468 cells were freshly isolated from mouse brain 8-10 days prior each transduction to minimize adaptation to in vitro culture, underwent showed very low baseline proliferation. A subline of E-98 cells was propagated in vitro in flasks for up to passage 35. For in vivo monitoring, E-98-Fluc-mCherry was generated by lentiviral transduction using firefly luciferase (Fluc) and mCherry construct (CSCW-Fluc-mCherry), as described[66,67].

Glioma cells were maintained in neurobasal medium (Invitrogen) supplemented with human EGF (20 ng/ml), human bFGF (20 ng/ml), B27 Supplement (1:50), L-glutamine (2 mM) (all from Invitrogen), heparin (2 mg/ml, Sigma), penicillin (100 U/ml) and streptomycin (100 µg/ml; both PAA). Cells were cultured either as 2D culture on flasks coated with growth factor-reduced reconstituted basement membrane (rBM) (BD Biosciences; 30 µg/ml in PBS, overnight at 4°C) or as neurobasal spheroids. Accutase digestion (10 min, 400-600 units/ml; Sigma) was used for cell detachment and dissociation of the spheroids. Cells were cultured at a minimum for 1 month with regular change of media before their use for migration assays, lentiviral transduction or brain implantation. Murine astrocytes and, for selected experiments, glioma cells were maintained in Dulbecco's Modified Eagle's Medium (DMEM; Invitrogen) supplemented with 10% fetal bovine serum (Sigma-Aldrich), penicillin (100 U/ml) and streptomycin (100 µg/ml; both PAA), L-glutamine (2 mM, Invitrogen) and sodium pyruvate (1mM, Invitrogen).

Generation of glioma cell spheroids

Spheroids from E-98 and E-468 cells used in short-term migration assays were generated using the hanging drop method[68]. Cells were cultured in neurobasal media to subconfluency, detached with accutase (400-600 units/ml; Sigma) washed with PBS, suspended in medium/methylcellulose (2.4 - 4.8 %; Sigma) and maintained as hanging droplets (25 µL) containing 2000 (E-98) or 1000 (E-468) cells for 24 or 48 h.

Reconstituted basement membrane interface invasion assay

Glioma cell spheroids were placed on 96-well-plates coated with growth factor-reduced rBM and, after initial attachment (2h), overlaid with 3D rBM (5 mg/ml). After matrix polymerization, cultures were overlaid with neural basal media, incubated for radial emigration (1d), fixed and stained for 3D confocal reconstruction and quantitative image analysis.

Murine astrocyte invasion assay

Primary mouse astrocytes were immortalized with SV40 large T-antigen and additionally transformed with retrovirus pBabe puro H-Ras V12, as described[69]. To generate 3D scaffolds, immortalized astrocytes were detached from subconfluent culture (1 mM EDTA /0.075% trypsin), transferred to 96-well plates (20,000 cells/well) coated with growth factor-reduced rBM). For invasion culture, 3-4 glioma cell spheroids/well were placed on top of consolidated astrocyte scaffolds (2d), incubated for 1-2 additional days, fixed (4%PFA), stained and quantified for invasion efficacy and pattern by 3D confocal microscopy. 3D organotypic tissue organization and matrix proteins deposited in glioma-cell free 3D astrocyte-derived scaffolds after 4d of culture were analyzed by 3D confocal microscopy.

Confocal microscopy and quantitative image analysis

Confocal imaging was performed on an Olympus FV1000 microscope, using long working distance 20× NA 0.50 and 40× NA 0.80 objectives at step size of 2-3 µm. Large-field microscopy of tissue sections from murine glioma lesions as well as multi-well in vitro culture of E-98 cells on rBM was performed by automated high-content microscopy and image stitching (Leica DMI6000B). Imaris V.6.1.5 software (Bitplane) was used for 3D reconstruction of Z-stacks. For quantitative image analysis, operator-assisted image segmentation of 3D stacks and analysis were performed using Fiji analysis software (V.1.49g) for the following parameters: number of nestin-, vimentin- or IDH1 R132H-positive filaments extending per cell with connections to neighboring glioma cells; number of connected cells, as the number of neighboring glioma cells engaged with each glioma cell by nestin- or vimentin-positive connecting filaments; number of neighbors by epithelial-like junctions; distance between connecting glioma cell bodies as the direct line between 4',6-diamidino-2-phenylindole-(DAPI) or H2B/eGFP-positive nuclei; organization of cell-cell junctions as the fluorescence intensity of cell-cell junction and filament markers along the intercellular junction line; migration speed, as the distance of either leading invasion edge or all cells from the spheroid margin.

Time-lapse confocal microscopy of LifeAct/GFP expressing E-98 and E-468 cells was performed on a Leica-SP8 SMD confocal scanner equipped with high-sensitivity HyD detectors using 0.05 mW for excitation (488nm). Multicellular glioma cell spheroids were overlaid on non-fluorescent astrocyte scaffolds (day 2) and 3D stacks comprising the entire volume of the invasion zone were recorded every 20 - 25 min. The position of the cell body (centroid) for each cell was recorded manually for every frame using the maximum intensity projection to calculate speed for each step and confinement ratio (distance from start to end-point divided by total length of the path for an observation period of 10 to 13 hours). The number of cell-cell connections/cell during migration was obtained from individual slices to exclude false-positive projections.

Live-cell calcium imaging

Glioma cell spheroids after growth in neurobasal media for 1 month were placed on high-grade 96-well imaging plates (BD Biosciences) coated with growth factor- reduced rBM. After 3 -5 days of emigration from spheroids, cells were loaded with Fura-2AM (2.5 µM, 40 min; Invitrogen), washed once with neurobasal medium (20 min) followed by washing twice with Krebs solution (5.5 mM KCl, 147 mM NaCl, 1.2 mM $MgCl_2$, 1.5 mM $CaCl_2$, 10 mM glucose, and 10 mM HEPES/NaOH, pH 7.4) prior to imaging. Gap junctional communication was inhibited by carbenoxolone (CBX) (50 µM; Sigma) in Krebs solution at least 30 min before imaging. Imaging was performed by automated epifluorescence microscopy (BD Pathway 855, BD Biosciences; 37°C, 5% CO_2) using excitation at 340/26 nm and 387/11 nm and emission detection at 435LP nm with a 1.75s sampling interval. Ratiometric 340/380 analysis was performed using Attovision software 1.6/855 (BD Bioscience) and post-processed for spatiotemporal mapping using Fiji. For visualization of calcium waves, the cell fraction was masked in the 380 nm channel (thresholding followed by median filtering, radius 2.0 pixels) to define the cell regions for 340/380 ratiometric analysis. Cell boundaries were manually defined.

Transient and stable downregulation of protein expression

Transient downregulation of adherens junction proteins and adhesion receptors was obtained for monolayer cultures on growth factor-reduced rBMusing specific or matched non-targeting smart-pool RNAi (Dharmacon) or 4 individual RNA probes (Sigma). For stable downregulation of p120 with lentiviral particles pLKO.1 (MISSION shRNA, Sigma), the following sequences were used:

Specificity / product code	Sequence
Non-target shRNA	CCGG**CAACAAGATGAAGAGCACCAA**CTCGAG**TTGGTGCTCTTC ATCTTGTTG**TTTTTG
Non human or mouse shRNA	
CTNND1 shRNA TRCN0000122988	CCGG**CTCCCAATGTTGCCAACAATA**CTCGAG**TATTGTTGGCAAC ATTGGGAG**TTTTTG
CTNND1 shRNA TRCN0000344830	CCGG**ACTACCCTCCTGATGGTTATA**CTCGAG**TATAACCATCAGG AGGGTAG**TTTTTTG
CTNND1 shRNA TRCN0000344770	CCGG**GCTTCGAAAGGCTCGTGATAT**CTCGAG**ATATCACGAGCC TTTCGAAGC**TTTTTG
CTNND1 shRNA TRCN0000333514	CCGG**CGCCACTATGAAGATGGTTAT**CTCGAG**ATAACCATCTTCAT AGTGGCG**TTTTTG

After lentiviral transduction E-98 cells were propagated in neurobasal media using flasks coated with growth factor reduced rBM. Stability of p120 downregulation was verified monthly by Western blot analysis. For transduction of patient-derived E-468 xenograft cells, intracranial tumors from 6 mice were isolated, suspended, cultured (10 days) in neurobasal media on growth factor reduced rBM-coated flasks and transfected with lentiviruses. For in vitro and in vivo assays, cells were used after 8 day-culture after transduction in neurobasal media without subculturing. Efficiency of downregulation was verified by quantitative PCR, Western blot for total and/or flow cytometry for cell surface proteins.

Reverse transcription and real-time quantitative PCR (RT-qPCR)

p120 mRNA levels after shRNA knock-down were analyzed by RT-qPCR. cDNA was prepared from 500 ng RNA with the SuperScript Reverse Transcriptase II kit (Invitrogen) using random hexamer primers. RNases were inhibited using RNaseOUT (Invitrogen). Pre-designed KiCqStart primers that were pre-validated according to the Minimal Information for Publication of Quantitative Real-Time PCR Experiments (MIQE) guidelines (Sigma) and the following three p120 primer pairs were used:

Primer pair		Sequence
P120-1	Forward	AGCAATATGGGATCAAACAC
	Reverse	TAAATCTTCTGCATCAAGGG
P120-2	Forward	GGAGCTATGAAGACATGATTG
	Reverse	CAAGCTTGCTAAACTTCCTC
P120-3	Forward	TGTGGAGCTCTCAAGAATATC
	Reverse	CCGGTAATAACTTCAGTAAGG

RT-qPCR was performed using CFX96 Real-Time PCR Detection System on a C1000 Thermocycler (Bio-Rad) and analyzed using the Bio-Rad CFX Manager software (version 2.0). For RT-qPCR, forward and reverse primers were used at a final concentration of 400 nM in 1x iQ SYBR Green Supermix (BioRad). The thermocycling program was: 10 min at 95˚C to denature the cDNA, followed by 40 cycles of 15 s at 95˚C and 50 s at 60˚C, and another 95˚C denaturing step for 15 s prior to a melting curve sequence from 65˚C to 95˚C at 0.5˚C increments. The threshold cycles (Ct) were normalized on a pool of 5 reference genes (GAPDH, β-actin, PSMB3, CANX, HMBS). The identity of the amplicon was confirmed by melting curve data. Appropriate no-template and no-reverse transcriptase negative controls included in each RT-qPCR run confirmed negativity in all cases.

Next-generation RNA sequencing. The RNA expression profile of wild-type and cells after stable transfection with p120 or NT shRNA were analyzed by RNA sequencing. Cells were maintained in culture with neural basal medium for at least 4 weeks (E-98) or for 8 days (E-468) after lentiviral transduction. Total RNA was extracted using the column based RNeasy micro kit (Qiagen) and the integrity and quality of obtained RNA was evaluated using the Experion RNA HighSens Analysis Kit (Biorad; #7007105) on a 2100 Bioanalyzer platform (Agilent). For cDNA synthesis starting from 1-10 ng total RNA, SMARTer Ultra low Input RNA kit (Clontech) was used and processed according to the manufacture protocol. The transcribed cDNA was sheared into fragments of 200-600 bp using Diagenode Pico sonicater. Subsequently the library preparation for Next Generation Sequencing has been carried out according to the Illumina standard protocol using the KAPA Hyper prep kit (KAPA Biosystems).

Raw data was aligned to the human genome using GSNAP aligner[70] and aligned reads annotation and counting was performed using HTSeq-count[71]. Differential expression analysis was performed using the DESeq package in R[72]. The log2 of fold changes +-1.5, p value < 0.05 and FDR < 0.05 are used as criteria to determine the significant deregulated genes in p120-knock down samples compared to their matched NT-shRNA samples. Gene ontology analysis was performed using DAVID (https://david.ncifcrf.gov) and the KEGG database (http://www.genome.jp/kegg/) was used for pathway analysis. Clustering analysis of datasets was performed using GENE-E (http://www.broadinstitute.org/cancer/software/GENE-E/). Gene set enrichment analysis was performed using GSEA[73,74]. Non-supervised clustering was performed using normalized read counts table as input and the one minus pearson correlation was used as metrics distance.

Bio-informatic analysis of human samples

Human samples were analyzed using the online platform R2 (r2.amc.nl). For gene ontology (GO) analysis, shp120 knockdown experiments in E98 GBM cells resulted in a list of up and downregulated genes from which a directional gene signature was generated, taking the amount of genes into account (i.e. a directional and weighed signature). Using this signature, samples present in the GBM (Verhaak, TCGA 540 tumors, ID2000-01-01)[17] and low- to high-grade glioma (French dataset, 284 samples including normal controls, GEO ID: gse16011)[46] datasets were scanned for their match to the signature as based on the expression values of these genes and displayed as z-value with positive match displayed in red and inverse match in blue color. Kaplan-Meier analysis was done using p120 expression levels as a determinant of disease outcome, using the significance scanner option to identify the most optimal expression cut-off level to provide the highest, Bonferroni corrected statistical significance. Reactive and dynamic GO term analysis was performed by correlating the E-98 derived p120 signature with 3875 curated gene sets as provided by the Broad Institute (www.broadinstitute.org/gsea), using the TCGA 540 GBM dataset. Results were top-ranked according to the correlation coefficient.

Glioma growth and invasion in mouse brain

Female athymic Balb/C nu/nu mice (6–8 weeks old), were obtained from Charles River Laboratories, maintained under specific pathogen-free conditionsat the central animal

facility, Radboudumc, Nijmegen. E-98-Fluc-mCherry parental cells were cultured as spheroids in neurobasal media for 1 month, enzymatically dissociated by accutase digestion, and intracranially implanted (5 ´ 10^5 cells in 20 µL PBS) by guided injection into the right parieto-occipital hemisphere of isofluorane-anesthetized mice 2 mm from the midline (animal ethics approval number RU-DEC-2013-251).

E-98-Fluc-mCherry and unlabeled E-468 cells with control and p120 shRNA (sequence TRCN0000122988) were cultured for more than 4 weeks (E-98) or 8 days (E-468) in neurobasal media on growth factor reduced rBM-coated flasks and intracranially implanted in 20 µL PBS per mouse - 0.4 or 0.8 ´ 10^5 of E-98 and 0.4 or 1.0 ´ 10^5 of E-468 cells. The extent to tumor growth and diffuse brain infiltration was quantified by whole-brain vibratome sectioning (200 µm thickness) followed by counterstaining to detect murine astrocytes by anti-GFAP pAb and glioma cells by human-specific anti-vimentin pAb. The extent of glioma infiltration was obtained by automated high-content microscopy (Leica DMI6000B) from whole-brain vibratome slices (200 µm thickness) followed by manual segmentation using the vimentin channel (Fiji). Quantitative image analysis from 3D confocal stacks (40x, NA 0.8) was performed to extract the frequency of geminin-positive cells, the number of cell-cell contacts per cell and the subcellular location of p120 in glioma cells using anti-human p120 mAb.

In vivo bioluminescence imaging

Fluc-E98/NTshRNA and Fluc-E98/p120 shRNA in mouse brain and spinal cord was monitored with IVIS Lumina imaging system (Caliber). Luciferine (200 µL; 15 mg/ml in PBS) was injected intraperitoneally in isofluorane-anesthetized mice and bioluminescence was detected in 10 min. Photon emission was normalized to photons per second per centimeter squared per steradian (p/s/cm2/sr).

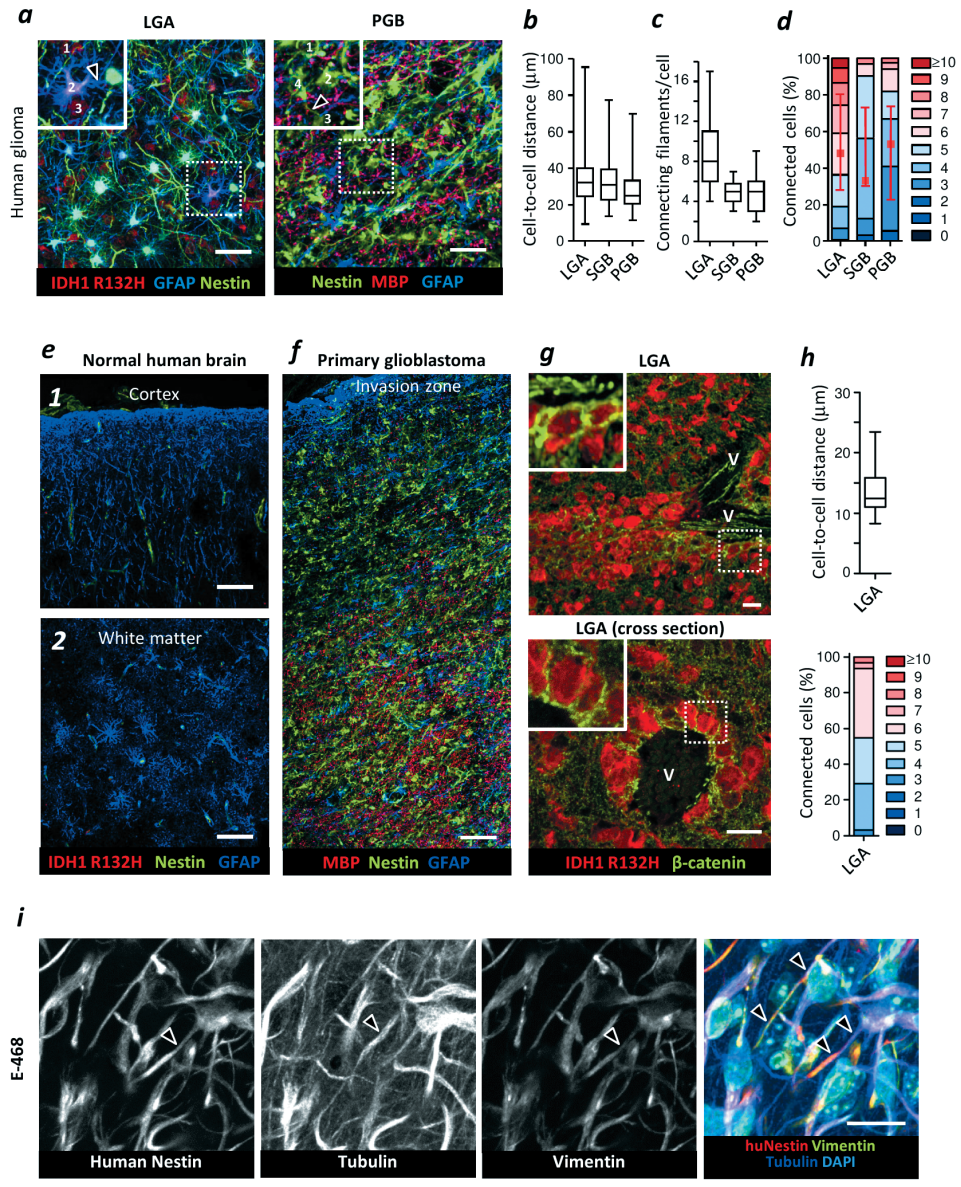

Supplementary Figure 1. Identification of glioma cell networks and cohesive perivascular invasion zones in patient samples. **a-d,** Morphological pattern and quantitative cell-cell junction analysis of glioma cell networks detected in 100 µm-thick tissue slices. Samples included lower-grade astrocytoma, secondary glioblastoma (SGB) originating from low-grade astrocytoma (LGA, grade II and III), and primary glioblastoma (PGB). Images represent the peritumor region of the lesions. Identification of glioma cells in LGA and SGB via colocalization of $IDH1^{R132H}$ and nestin. In PGB, which lacks $IDH1^{R132H}$, nestin-positive but Myelin Basic Protein-(MBP)- and focally GFAP-negative networks represent the glioma cell fraction. **e,** Tumor-free human brain cortex (1) and adjacent white matter region (2) lacking $IDH1^{R132H}$ and interstitial nestin signal, but contain GFAP-positive astrocytes in the parenchyma. **f,** Representative large-field overview used for selecting region ▸

for high-resolution imaging. Nestin-positive but myelin basic protein-(MBP-)negative glioma cell network in primary glioblastoma (PGB) sample intercalating with astrocyte (GFAP) and myelinated axonal (MBP) networks in tumor margin. **g,** Perivascular cohesive glioma cell layers aligning along large vessel, identified by longitudinal lumen (V) in LGA sample. Inset, β-catenin-positive cell-cell junctions. **h,** Cell-cell proximity and number of directly neighboring cells during perivascular invasion (3D image analysis of LGA samples). **i,** Molecular topography of filamentous protrusions connecting glioma cells in patient-derived orthotopic E-468 xenograft. Identification of glioma cells using human-specific anti-nestin mAb. Arrowhead, nestin- and vimentin-positive filament, also containing microtubules. Values display median (black line), 25/75 percentiles (boxes) and maximum/minimum values (whiskers) or relative fractions of connected glioma cells interacting with 0 up to 10 connected cells (boxes), median (red square), 25/75 percentiles (whiskers). 8 patients (LGA), 1 patient (SGB), 4 patients (PGB), 1 - 3 samples (25 - 30 cells) per patient, 3 - 5 imaging fields per sample. Detailed information in Supplementary Table 1. Bars, 50 µm (**a**), 100 µm (**e**, **f**), 20 µm (**i**, **g**).

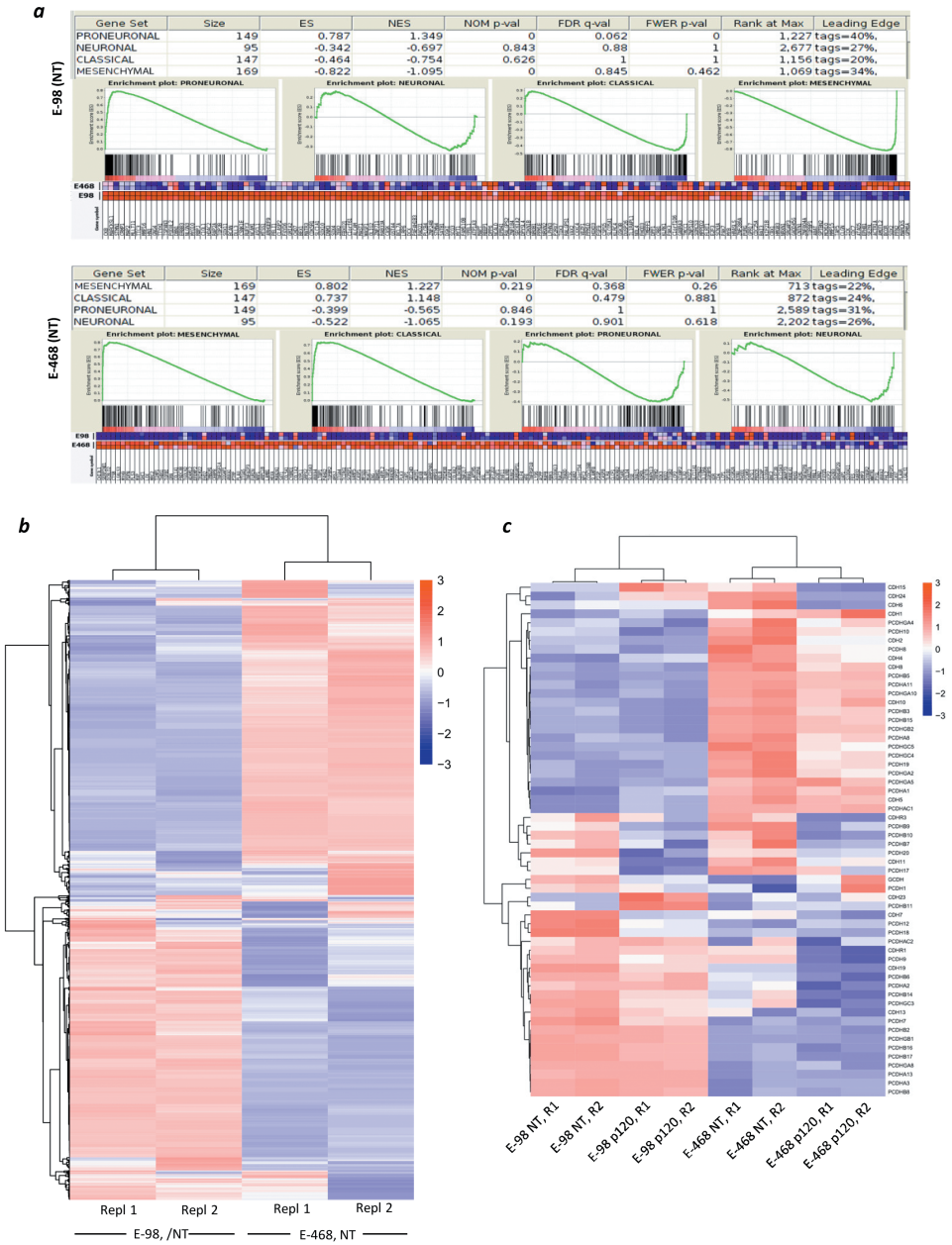

Supplementary Figure 2. Subtype analysis and differential gene expression of E-98 and E-468 glioma cells. **a,** Gene set enrichment analysis on two non-targeting shRNA samples of E-98 and E-468 datasets using 4 glioblastoma subtype gene sets[14]. **b**, Hierarchical clustering and heatmap of mRNA expression of genes found to be deregulated after p120 knock-down (compare Supplementary Figure 7). Data represent the gene expression in cells after transfection with non-targeting shRNA. **c,** Hierarchical clustering and heatmap of cadherin and protocadherin genes detected in at least one of the replicates. The Euclidean distance was used as metrics and the normalized expression level of genes used as input values.

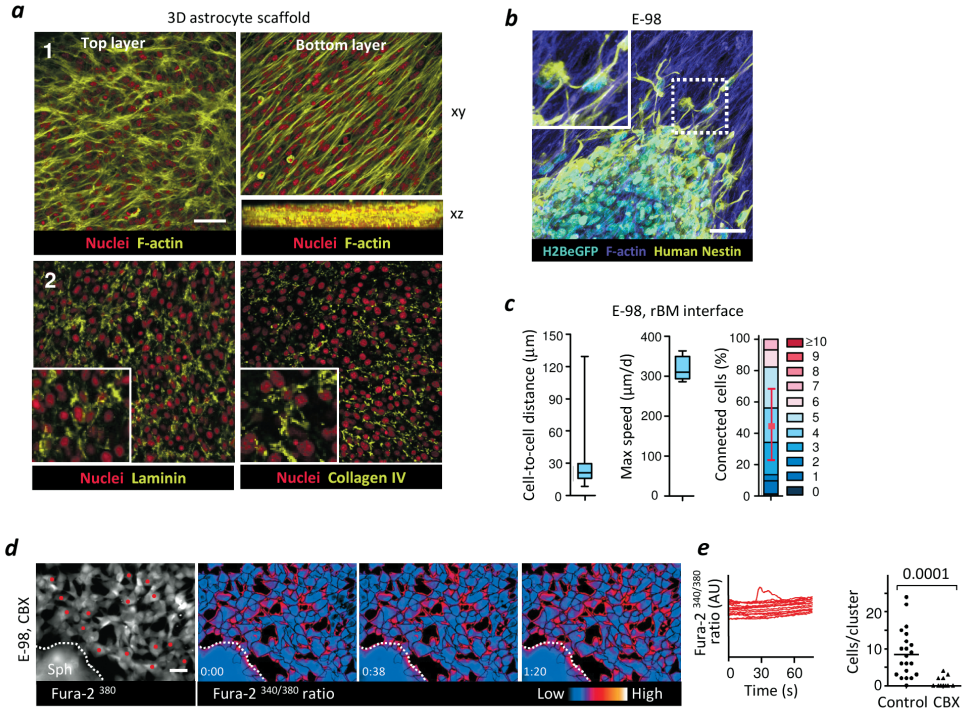

Supplementary Figure 3. Variability of cell-cell interactions and signaling in human glioma cells during invasion in organotypic culture. **a,** 3D organization of scaffold formed by transformed astrocytes, shown by horizontal and orthogonal projections. (1) Random (top section) versus aligned (bottom section) orientation of astrocyte cell bodies. (2) Organization of laminin and collagen-IV between astrocytes, with intercellular pattern (inset). **b,** Cell pattern of E-98 glioma invasion from spheroids (Sph) into 3D astrocyte scaffolds. **c,** Quantification of next-neighbor proximity, migration speed and cell-cell interactions in glioma cell invasion in reconstituted basement membrane (rBM) assays. Values display median (black line), 25/75 percentiles (boxes) and maximum/minimum values (whiskers) or relative fractions of connected glioma cells interacting with 0 up to 10 connected cells (boxes), median (red square), 25/75 percentiles (whiskers). 5 - 10 spheroids, 94 - 272 cells per parameter; data show two representative out of three independent experiments. **d,** Inhibition of multicellular calcium transients in E-98 cells in the presence of carbenoxolone (CBX). Dots, cells assessed for calcium transients displayed in the graphs. **e,** Lack of calcium transients in the presence of CBX (left panel) and quantification for multiple cells (right panel). Values display median (black line) and values (dots); P values, Mann Whitney test. Bars, 50 µm.

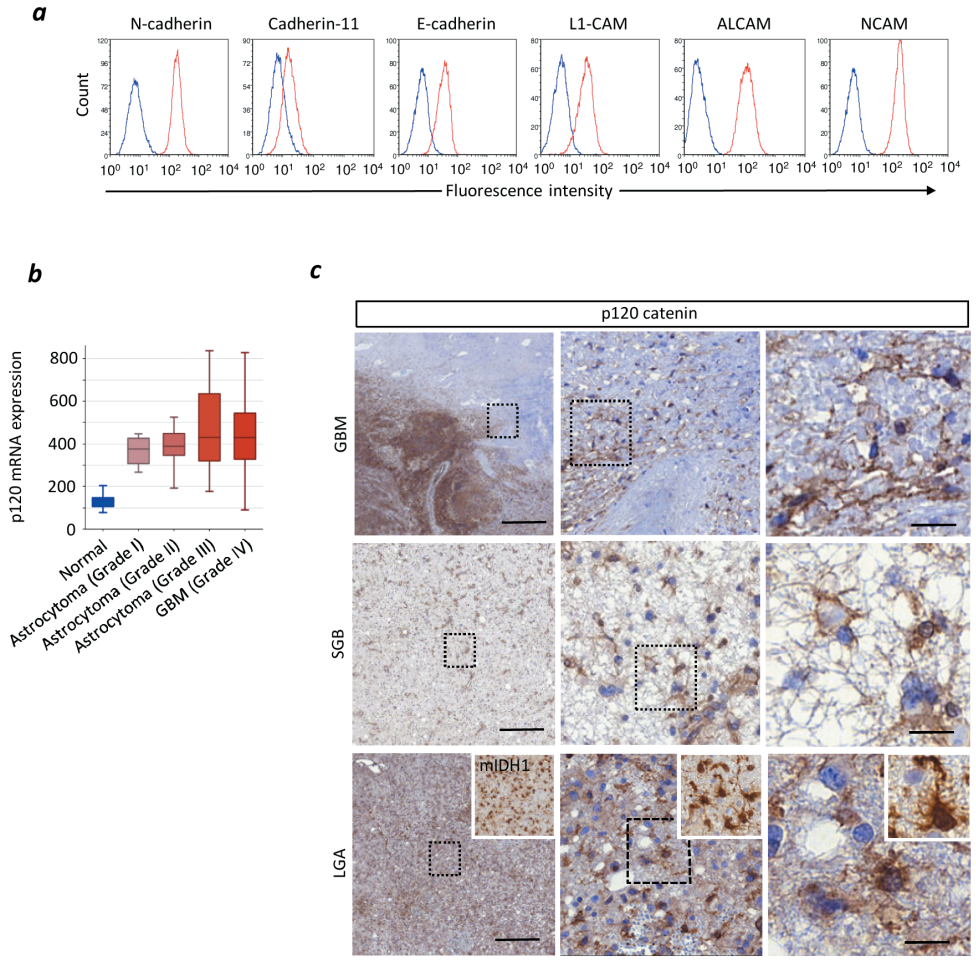

Supplementary Figure 4. Expression and subcellular distribution of p120 and other cell-cell adhesion molecules in human glioma cells. **a,** Surface expression of receptors implicated in cell-cell interactions in E-98 cells (FACS data). **b,** Increased expression of p120 catenin in human gliomas of different grade. Data are derived from the 284 sample cohort from French et al. (MAS5.0-u133p2) comprising grade I-IV gliomas. Expression reflects log level. **c,** p120 (brown label in large panels) and $IDH1^{R132H}$ (insets) immunohistochemistry in primary/ secondary human glioblastoma and low grade glioma samples. P120 positivity in both tumor core and diffuse brain infiltration region. $IDH1^{R132H}$ positivity in grade III glioma sample was used to confirm glioma origin. Bars, 500 µm (overviews) and 20 µm (details).

Supplementary Figure 5. Molecular targeting of cell-cell interaction and collective invasion in vitro. **a,** Transient downregulation of candidate proteins involved in cell-cell junction stability of E-98 cells. (1) Relative protein levels detected by Western blot (total proteins) or flow cytometry (surface receptors) after transient downregulation using SMARTpool siRNA. (2) Numbers in the table express the ratio between p120 and non-targeting (NT) siRNA. (3) Morphology and (4) quantification of single-cell fraction during radial migration of E-98 glioma cells from spheroids on rBM-coated surface after single- or triple interference with cell-cell junction proteins. Color code denotes fold-change compared with non-targeting baseline. Data represent three independent siRNA transfections, with 10 to 20 cell spheroids analyzed per condition. **b-f,** Quality control and functional consequences of stable downregulation of p120 in glioma cells. **b,** Extent of downregulation of p120 protein (1) and mRNA (2) and persistence of vimentin expression in E-468 cells (3). Immunostaining of vimentin was used for the detection of glioma cells in the mouse brain. **c,** Effect of four independent shRNA sequences on p120 catenin protein levels detected by immunofluorescence (1), the number of cell-contacts between neighboring cells (2) and cell density as measure for growth (3). Data represent three independent shRNA lentiviral transductions with 209 to 2353 cells analyzed from 2 wells per shRNA sequence. Based on efficacy of p120 downregulation and representativity, sequence 988 was used for further in vitro and in vivo experiments. **d,** Cells in S/G2/M phase detected by geminin staining >30 (E-98) or 8 days (E-468) after transduction. In contrast to E-98 cells which grew well in liquid culture before p120 downregulation, E-468 cells were derived directly from mouse brains and failed to grow in vitro. Therefore, all functional experiments with E-468 cells were performed 8 days after transduction, including molecular profiling and implantation into mouse brains. **e** Reduced growth of E-98 cells in neurobasal spheroids. **f,** Unperturbed migration speed on 3D astrocyte scaffolds after p120 downregulation, obtained by single cell tracking. **g, h,** Myosin light-chain phosporylation (ROCK target) after p120-catenin downregulation in E-468 cells in the absence or presence of ROCK inhibitor Y-27632 (10 µM) detected by cell-based immunofluorescence. Values display the median (black line), 25/75 percentiles (boxes) and maximum/minimum values (whiskers); P values, Mann Whitney test **(b - h)**. Bars, 50 µm (a3, d), 200 µm (e), 100 µm (g).

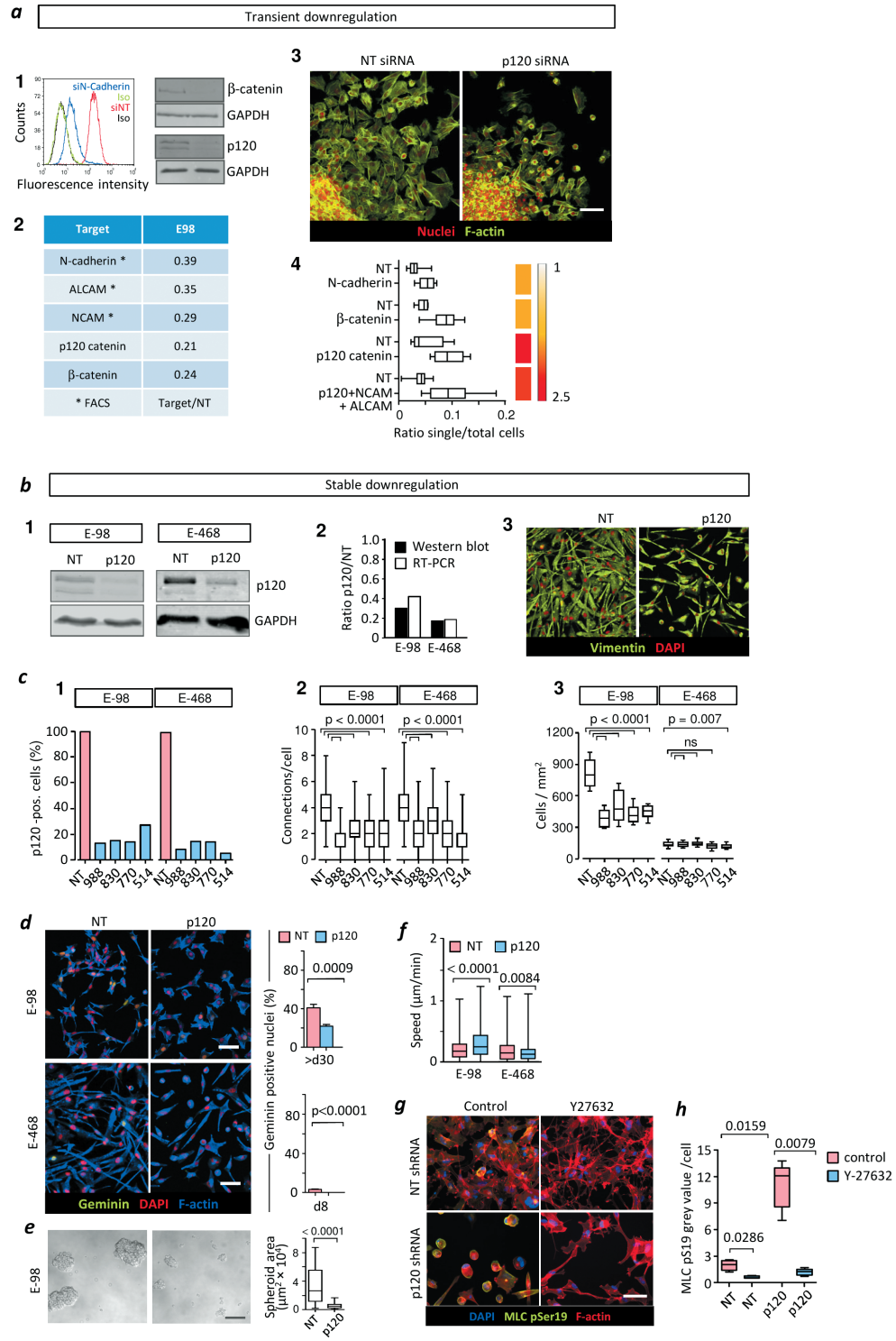

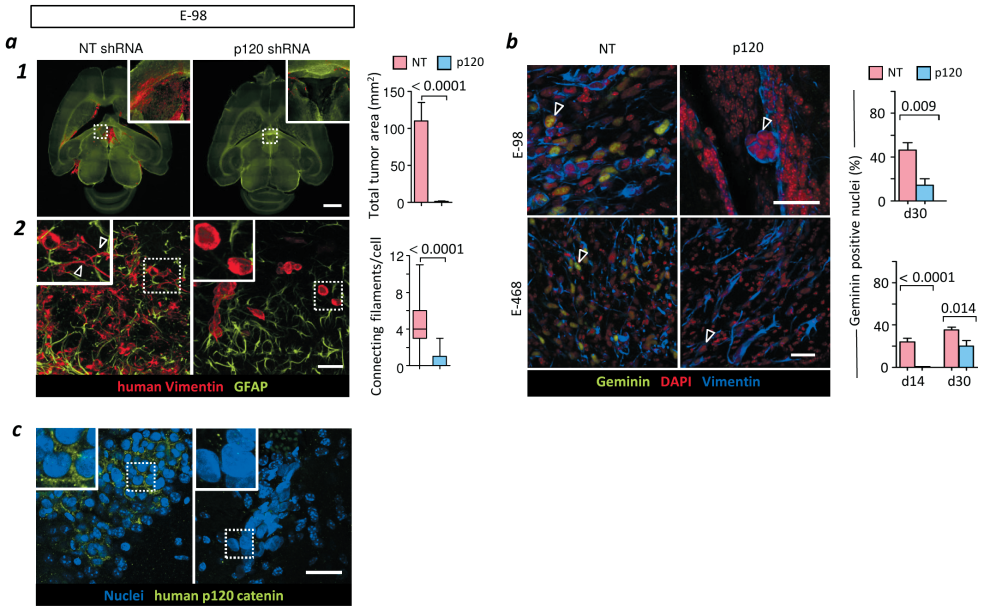

Supplementary Figure 6. Inhibition of multicellular networks and diffuse infiltration into mouse brain after p120 downregulation. **a,** Impaired tumor growth, loss of network formation and diffuse brain infiltration of E-98 cells after p120 downregulation. Overviews (1) and zoom images (2) from 200 µm thick brain slices. Arrowheads, filaments in multicellular networks of vimentin-positive E-98 cells diffusely infiltrating the brain. Data represent 19 independent mice from 2 independent experimental series; mean values ± SEM (a1) or median (black line), 25/75 percentiles (boxes) and maximum/minimum values (whiskers) (a2); P values, Mann Whitney test. **b,** Persistent deficiency of p120 signal in vivo in E-98 p120 shRNA knock-down cells in 4 weeks after intracranial tumor implantation. **c,** Sustained glioma growth deficit in vivo after p120 downregulation. Frequency of geminin-positive glioma cells after the indicated time of post-implantation in mouse brain. Data represent two mice per condition. Values display the median (black line), 25/75 percentiles (boxes) and maximum/minimum values (whiskers); P values, Mann Whitney test. Bars, 2 mm (a1), 50 µm (a2, b, c).

Supplementary Figure 7. Gene expression regulation in glioma cells in response to downregulation of p120. **a,** Proportional Venn diagrams of total number of down- or up-regulated genes in E-98 and E-468 cells after p120 downregulation (*p* values are obtained using hypergeometric test). **b**, Ranked list heatmap of all relevant GO term biological functions resulting from gene ontology analysis of deregulated genes in each p120 knock-down cell lines. Log2 of Benjamini values was used as input. The annotation was carried out using the DAVID server and GO database and the Benjamini -3 was determined as cut off for selecting the relevance of the GO terms. To determine the significance of deregulation, log2-fold change of /-1.5 and p value < 0.05 and FDR < 0.05 were used as cut offs. **c,** Gene enrichment analysis of the p120 signature in human glioma**.** Expression levels of p120 correlate to migration/ECM. Ranked expression panels of p120 RNA expression as determined by MAS5.0 normalized u133a or u133p2 RNA expression arrays (Verhaak, TCGA 540 tumors, ID2000-01-01) and low- to high-grade glioma (French 284 samples including normal controls, GEO ID: gse16011), correlated to z-values of a migration signature[75] (http://www.broadinstitute.org/gsea/msigdb/cards/WU_CELL_MIGRATION.html) and an ECM signature (Segal Stanford cancer modules, http://ai.stanford.edu/~erans/cancer/modules/module_47.html).

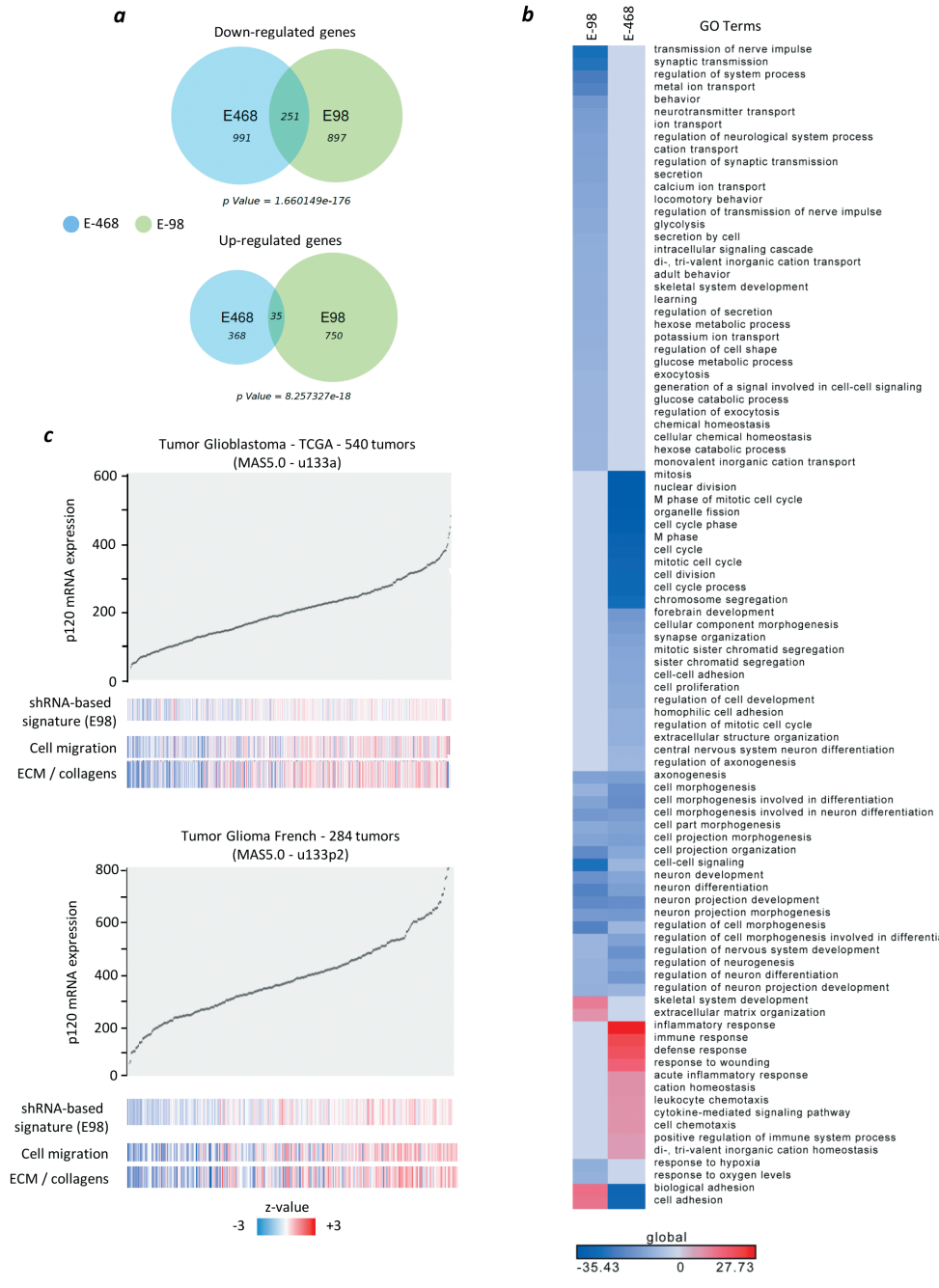

Supplementary Table 1. Patient samples used for 3D reconstruction of glioma networks.

Class	Sample Nr.	Type*	WHO grade	Age	Sex	Tumor location	Connectivity cell network**
Lower grade diffuse glioma	1	A	II	38	female	temporal right	7.5 (6-9)
	2	A	II	48	male	frontal right	7.0 (5-9)
	3	A	II	46	female	thalamus left	4.0 (4-6)
	4	A	II	37	male	frontal right	5.0 (4-6)***
	5	A	II/III	31	male	frontotemporal left	6.0 (5-7)
	6	A	II/III	50	male	frontal right	6.5 (5-8)
	7	O	III	38	male	frontal right	5.0 (4-7)
	8	A	III	38	male	frontal right	5.0 (4-6)***
Secondary glioblastoma	1	A	IV	22	male	frontal left	4.0 (4-5)
Primary glioblastoma	1	A	IV	67	female	frontal left	3.0 (3-4)
	2	A	IV	72	female	parietal right	4.0 (3-6)
	3	A	IV	65	male	temporal left	5.0 (4-6)
	4	A	IV	66	female	frontal right	3.0 (3-4)

* Histological type: A = astrocytic, O = oligodendroglial. ** Values denote medians and 25/75 percentiles.
*** Perivascular invasion.

REFERENCES

1. Network, C. G. A. R. Comprehensive genomic characterization defines human glioblastoma genes and core pathways. *Nature* **455,** 1061–1068 (2008).
2. Frattini, V. *et al.* The integrated landscape of driver genomic alterations in glioblastoma. *Nat. Genet.* **45,** 1141–1149 (2013).
3. Patel, A. P. *et al.* Single-cell RNA-seq highlights intratumoral heterogeneity in primary glioblastoma. *Science* **344,** 1396–1401 (2014).
4. Brat, D. J. *et al.* Comprehensive, Integrative Genomic Analysis of Diffuse Lower-Grade Gliomas. *N. Engl. J. Med.* **372,** 2481–2498 (2015).
5. Gilbert, M. R. *et al.* Dose-dense temozolomide for newly diagnosed glioblastoma: a randomized phase III clinical trial. *J. Clin. Oncol.* **31,** 4085–4091 (2013).
6. Stupp, R. *et al.* Effects of radiotherapy with concomitant and adjuvant temozolomide versus radiotherapy alone on survival in glioblastoma in a randomised phase III study: 5-year analysis of the EORTC-NCIC trial. *Lancet. Oncol.* **10,** 459–466 (2009).
7. Hoelzinger, D. B., Demuth, T. & Berens, M. E. Autocrine factors that sustain glioma invasion and paracrine biology in the brain microenvironment. *J. Natl. Cancer Inst.* **99,** 1583–1593 (2007).
8. Cuddapah, V. A., Robel, S., Watkins, S. & Sontheimer, H. A neurocentric perspective on glioma invasion. *Nat. Rev. Neurosci.* **15,** 455–465 (2014).
9. Gritsenko, P. G., Ilina, O. & Friedl, P. Interstitial guidance of cancer invasion. *J. Pathol.* **226,** 185–199 (2012).
10. Montana, V. & Sontheimer, H. Bradykinin promotes the chemotactic invasion of primary brain tumors. *J. Neurosci.* **31,** 4858–4867 (2011).
11. Cheng, W.-Y., Kandel, J. J., Yamashiro, D. J., Canoll, P. & Anastassiou, D. A multi-cancer mesenchymal transition gene expression signature is associated with prolonged time to recurrence in glioblastoma. *PLoS One* **7,** e34705 (2012).
12. Farin, A. *et al.* Transplanted glioma cells migrate and proliferate on host brain vasculature: a dynamic analysis. *Glia* **53,** 799–808 (2006).
13. Nakada, M. *et al.* Molecular targets of glioma invasion. *Cell. Mol. Life Sci.* **64,** 458–478 (2007).
14. Osswald, M. *et al.* Brain tumour cells interconnect to a functional and resistant network. *Nature* **528,** 93–98 (2015).
15. Skalli, O. *et al.* Astrocytoma grade IV (glioblastoma multiforme) displays 3 subtypes with unique expression profiles of intermediate filament proteins. *Hum. Pathol.* **44,** 2081–2088 (2013).
16. Claes, A. *et al.* Phenotypic and genotypic characterization of orthotopic human glioma models and its relevance for the study of anti-glioma therapy. *Brain Pathol.* **18,** 423–433 (2008).
17. Verhaak, R. G. W. *et al.* Integrated genomic analysis identifies clinically relevant subtypes of glioblastoma characterized by abnormalities in PDGFRA, IDH1, EGFR, and NF1. *Cancer Cell* **17,** 98–110 (2010).
18. Chu, Y., Hughes, S. & Chan-Ling, T. Differentiation and migration of astrocyte precursor cells and astrocytes in human fetal retina: relevance to optic nerve coloboma. *FASEB J. Off. Publ. Fed. Am. Soc. Exp. Biol.* **15,** 2013–2015 (2001).
19. Faber-Elman, A., Solomon, A., Abraham, J. A., Marikovsky, M. & Schwartz, M. Involvement of wound-associated factors in rat brain astrocyte migratory response to axonal injury: in vitro simulation. *J. Clin. Invest.* **97,** 162–171 (1996).
20. Ozaki, C. *et al.* p120-Catenin is essential for N-cadherin-mediated formation of proper junctional structure, thereby establishing cell polarity in epithelial cells. *Cell Struct. Funct.* **35,** 81–94 (2010).
21. Harris, T. J. C. & Tepass, U. Adherens junctions: from molecules to morphogenesis. *Nat. Rev. Mol. Cell Biol.* **11,** 502–514 (2010).
22. Friedl, P., Locker, J., Sahai, E. & Segall, J. E. Classifying collective cancer cell invasion. *Nat. Cell Biol.* **14,** 777–783 (2012).

23. Peglion, F., Llense, F. & Etienne-Manneville, S. Adherens junction treadmilling during collective migration. *Nat. Cell Biol.* **16,** 639–651 (2014).
24. Sunyer, R. *et al.* Collective cell durotaxis emerges from long-range intercellular force transmission. *Science* **353,** 1157–1161 (2016).
25. Serres, E. *et al.* Fibronectin expression in glioblastomas promotes cell cohesion, collective invasion of basement membrane in vitro and orthotopic tumor growth in mice. *Oncogene* **33,** 3451–3462 (2014).
26. Camand, E., Peglion, F., Osmani, N., Sanson, M. & Etienne-Manneville, S. N-cadherin expression level modulates integrin-mediated polarity and strongly impacts on the speed and directionality of glial cell migration. *J. Cell Sci.* **125,** 844–857 (2012).
27. Kolodkin, A. L. & Tessier-Lavigne, M. Mechanisms and molecules of neuronal wiring: a primer. *Cold Spring Harb. Perspect. Biol.* **3,** (2011).
28. Hirano, S. & Takeichi, M. Cadherins in brain morphogenesis and wiring. *Physiol. Rev.* **92,** 597–634 (2012).
29. Fujita, Y. & Yamashita, T. Axon growth inhibition by RhoA/ROCK in the central nervous system. *Front. Neurosci.* **8,** 338 (2014).
30. Hensel, N., Rademacher, S. & Claus, P. Chatting with the neighbors: crosstalk between Rho-kinase (ROCK) and other signaling pathways for treatment of neurological disorders. *Front. Neurosci.* **9,** 198 (2015).
31. Chan, C.-H. *et al.* Deciphering the transcriptional complex critical for RhoA gene expression and cancer metastasis. *Nat. Cell Biol.* **12,** 457–467 (2010).
32. Muramatsu, T. *et al.* The hypusine cascade promotes cancer progression and metastasis through the regulation of RhoA in squamous cell carcinoma. *Oncogene* **35,** 5304–5316 (2016).
33. Watkins, S. & Sontheimer, H. Hydrodynamic cellular volume changes enable glioma cell invasion. *J. Neurosci.* **31,** 17250–17259 (2011).
34. Gnanaguru, G. *et al.* Laminins containing the beta2 and gamma3 chains regulate astrocyte migration and angiogenesis in the retina. *Development* **140,** 2050–2060 (2013).
35. Weissman, T. A., Riquelme, P. A., Ivic, L., Flint, A. C. & Kriegstein, A. R. Calcium waves propagate through radial glial cells and modulate proliferation in the developing neocortex. *Neuron* **43,** 647–661 (2004).
36. Motiani, R. K. *et al.* STIM1 and Orai1 mediate CRAC channel activity and are essential for human glioblastoma invasion. *Pflugers Arch.* **465,** 1249–1260 (2013).
37. Lieberman, A. R. & Spacek, J. Filamentous contacts: the ultrastructure and three-dimensional organization of specialized non-synaptic interneuronal appositions in thalamic relay nuclei. *Cell Tissue Res.* **288,** 43–57 (1997).
38. Ireton, R. C. *et al.* A novel role for p120 catenin in E-cadherin function. *J. Cell Biol.* **159,** 465–476 (2002).
39. Ishiyama, N. *et al.* Dynamic and static interactions between p120 catenin and E-cadherin regulate the stability of cell-cell adhesion. *Cell* **141,** 117–128 (2010).
40. Elia, L. P., Yamamoto, M., Zang, K. & Reichardt, L. F. p120 catenin regulates dendritic spine and synapse development through Rho-family GTPases and cadherins. *Neuron* **51,** 43–56 (2006).
41. Schackmann, R. C. J., Tenhagen, M., van de Ven, R. A. H. & Derksen, P. W. B. p120-catenin in cancer - mechanisms, models and opportunities for intervention. *J. Cell Sci.* **126,** 3515–3525 (2013).
42. Anastasiadis, P. Z. *et al.* Inhibition of RhoA by p120 catenin. *Nat. Cell Biol.* **2,** 637–644 (2000).
43. Friedl, P. & Alexander, S. Cancer invasion and the microenvironment: plasticity and reciprocity. *Cell* **147,** 992–1009 (2011).
44. Theveneau, E. & Mayor, R. Cadherins in collective cell migration of mesenchymal cells. *Curr. Opin. Cell Biol.* **24,** 677–684 (2012).
45. Yang, X., Hou, D., Jiang, W. & Zhang, C. Intercellular protein-protein interactions at synapses. *Protein Cell* **5,** 420–444 (2014).
46. Gravendeel, L. A. M. *et al.* Intrinsic gene expression profiles of gliomas are a better predictor of survival than histology. *Cancer Res.* **69,** 9065–9072 (2009).

47. Sloan, S. A. & Barres, B. A. Mechanisms of astrocyte development and their contributions to neurodevelopmental disorders. *Curr. Opin. Neurobiol.* **27,** 75–81 (2014).
48. Osswald, M., Solecki, G., Wick, W. & Winkler, F. A malignant cellular network in gliomas: potential clinical implications. *Neuro. Oncol.* **18,** 479–485 (2016).
49. Dohn, M. R., Brown, M. V & Reynolds, A. B. An essential role for p120-catenin in Src- and Rac1-mediated anchorage-independent cell growth. *J. Cell Biol.* **184,** 437–450 (2009).
50. Johnson, E. *et al.* HER2/ErbB2-induced breast cancer cell migration and invasion require p120 catenin activation of Rac1 and Cdc42. *J. Biol. Chem.* **285,** 29491–29501 (2010).
51. van de Ven, R. A. H. *et al.* Nuclear p120-catenin regulates the anoikis resistance of mouse lobular breast cancer cells through Kaiso-dependent Wnt11 expression. *Dis. Model. Mech.* **8,** 373–384 (2015).
52. Schackmann, R. C. J. *et al.* Cytosolic p120-catenin regulates growth of metastatic lobular carcinoma through Rock1-mediated anoikis resistance. *J. Clin. Invest.* **121,** 3176–3188 (2011).
53. Te Boekhorst, V. & Friedl, P. Plasticity of Cancer Cell Invasion-Mechanisms and Implications for Therapy. *Adv. Cancer Res.* **132,** 209–264 (2016).
54. Cooper, J. A. Molecules and mechanisms that regulate multipolar migration in the intermediate zone. *Front. Cell. Neurosci.* **8,** 386 (2014).
55. Wynn, M. L., Kulesa, P. M. & Schnell, S. Computational modelling of cell chain migration reveals mechanisms that sustain follow-the-leader behaviour. *J. R. Soc. Interface* **9,** 1576–1588 (2012).
56. Barriga, E. H. & Mayor, R. Embryonic cell-cell adhesion: a key player in collective neural crest migration. *Curr. Top. Dev. Biol.* **112,** 301–323 (2015).
57. Kapitein, L. C. & Hoogenraad, C. C. Building the Neuronal Microtubule Cytoskeleton. *Neuron* **87,** 492–506 (2015).
58. Sakakibara, A. & Hatanaka, Y. Neuronal polarization in the developing cerebral cortex. *Front. Neurosci.* **9,** 116 (2015).
59. Reffay, M. *et al.* Interplay of RhoA and mechanical forces in collective cell migration driven by leader cells. *Nat. Cell Biol.* **16,** 217–223 (2014).
60. Zegers, M. M. & Friedl, P. Rho GTPases in collective cell migration. *Small GTPases* **5,** e28997 (2014).
61. Chen, C., Li, P. P., Madhavan, R. & Peng, H. B. The function of p120 catenin in filopodial growth and synaptic vesicle clustering in neurons. *Mol. Biol. Cell* **23,** 2680–2691 (2012).
62. McCrea, P. D. & Gottardi, C. J. Beyond beta-catenin: prospects for a larger catenin network in the nucleus. *Nat. Rev. Mol. Cell Biol.* **17,** 55–64 (2016).
63. Salinas, P. C. Wnt signaling in the vertebrate central nervous system: from axon guidance to synaptic function. *Cold Spring Harb. Perspect. Biol.* **4,** (2012).
64. Yam, P. T. & Charron, F. Signaling mechanisms of non-conventional axon guidance cues: the Shh, BMP and Wnt morphogens. *Curr. Opin. Neurobiol.* **23,** 965–973 (2013).
65. Kitai, R. *et al.* Nestin expression in astrocytic tumors delineates tumor infiltration. *Brain Tumor Pathol.* **27,** 17–21 (2010).
66. Wurdinger, T. *et al.* A secreted luciferase for ex vivo monitoring of in vivo processes. *Nat. Methods* **5,** 171–173 (2008).
67. Mir, S. E. *et al.* In silico analysis of kinase expression identifies WEE1 as a gatekeeper against mitotic catastrophe in glioblastoma. *Cancer Cell* **18,** 244–257 (2010).
68. Korff, T. & Augustin, H. G. Integration of endothelial cells in multicellular spheroids prevents apoptosis and induces differentiation. *J. Cell Biol.* **143,** 1341–1352 (1998).
69. Sawamiphak, S. *et al.* Ephrin-B2 regulates VEGFR2 function in developmental and tumour angiogenesis. *Nature* **465,** 487–491 (2010).
70. Wu, T. D. & Watanabe, C. K. GMAP: a genomic mapping and alignment program for mRNA and EST sequences. *Bioinformatics* **21,** 1859–1875 (2005).
71. Anders, S., Pyl, P. T. & Huber, W. HTSeq--a Python framework to work with high-throughput sequencing data. *Bioinformatics* **31,** 166–169 (2015).

72. Anders, S. & Huber, W. Differential expression analysis for sequence count data. *Genome Biol.* **11,** R106 (2010).
73. Subramanian, A. *et al.* Gene set enrichment analysis: a knowledge-based approach for interpreting genome-wide expression profiles. *Proc. Natl. Acad. Sci. U. S. A.* **102,** 15545–15550 (2005).
74. Mootha, V. K. *et al.* PGC-1alpha-responsive genes involved in oxidative phosphorylation are coordinately downregulated in human diabetes. *Nat. Genet.* **34,** 267–273 (2003).
75. Wu, Y., Siadaty, M. S., Berens, M. E., Hampton, G. M. & Theodorescu, D. Overlapping gene expression profiles of cell migration and tumor invasion in human bladder cancer identify metallothionein 1E and nicotinamide N-methyltransferase as novel regulators of cell migration. *Oncogene* **27,** 6679–6689 (2008).

CHAPTER 5

MULTIPLE ADHESION STRATEGIES MEDIATE GLIOMA CELL INVASION IN COMPLEX ENVIRONMENTS

Pavlo Gritsenko[1] and Peter Friedl[1,2,3]

[1] Microscopical Imaging of the Cell, Department of Cell Biology, Radboud Institute for Molecular Life Sciences, Radboud University Nijmegen Medical Centre
[2] David H Koch Center for Applied Research of Genitourinary Cancers, Department of Genitourinary Medical Oncology, The University of Texas, MD Anderson Cancer Center, Houston, Texas, USA
[3] Genomics Centre (CGC.nl), 3584 Utrecht, The Netherlands

ABSTRACT

Malignant gliomas represent a heterogeneous group of primary brain tumors which diffusely invade the brain parenchyma and render complete surgical resection ineffective. For their dissemination glioma cells preferentially migrate along anatomical vascular and neuronal brain structures, however the mechanotransduction underlying each invasion route remains poorly defined. To identify matrix molecules and adhesion receptor systems supporting glioma cell invasion into brain-like environments we used 2D and 3D invasion assays recapitulating different organotypic cell-cell and cell-matrix conditions and combined antibody-, small molecule- and RNA-based molecular interference. Migration of U-251 and E-98 glioma cells on reconstituted basement membrane was readily abolished by interference with β1 and αV integrins, however perivascular invasion into primary brain slices, infiltration of 3D astrocyte-based scaffolds or migration on astrocyte-deposited matrix was only partly affected and residual migration persisted with 30-50% efficacy. Laminin 511 was identified as a central mediator securing integrin-dependent glioma cell migration along astrocyte-derived matrix, however, multi-targeted interference with all integrin systems expressed by U-251 and E-98 cells, including laminin-binding β1, αV and α6 integrins, reduced glioma cell migration into astrocyte scaffolds and on laminin 511 by 50-80%, but failed to induce complete migration arrest. These data implicate integrin/laminin 511 interactions as important adhesion system in glioma cell invasion, in cooperation with additional, yet unidentified mechanocoupling strategies.

INTRODUCTION

Gliomas originate from transformed brain cell progenitors replicating abnormal brain development programs with local growth and diffuse infiltration into the brain stroma as fatal outcomes[1–4]. Glioblastoma multiforme is the most detrimental form of gliomas in humans due to rapidly progressing diffuse infiltration into any brain region, which renders curative surgery impossible[5].

Glioma invasion into the healthy brain occurs along structures of the brain parenchyma, including white matter tracks comprising myelinated axons, astrocyte processes and/or the basement membranes of blood vessels and the meninges[5,6]. Astrocytes, as the most abundant cell population in the brain, are ubiquitously present in the neuropil and, together with myelinated fibers, form complex cellular networks filled with relatively soft extracellular matrix (ECM), including hyaluronan, the main ECM component in brain[6,7]. Glioma cell invasion along brain blood vessels follows a particularly permissive niche, where brain stroma and vascular basement membranes interface to support molecularly and physically complex types of invasion along confined space[5,6,8]. Brain blood vessels are ensheathed with basement membranes jointly formed by endothelium, pericytes and astrocytes, and are tightly enveloped with glia limitans formed by astrocytic endfeet from the parenchymal side[9–13]. Glioma cells in the perivascular niche either migrate along basement membrane of glia limitans, by displacing astrocytes, or along basement membrane underlying the endothelium in perivascular space[8,14,15]. Glioma cell migration along basement membrane proteins including laminin isoforms and type IV collagen has been reported[16,17], yet the molecular guidance mechanisms of glioma cell invasion in the neuropil, along astrocytic and axonal networks, are likely distinct and remain unexplored.

The interaction of moving cells, including glioma cells, to basement membranes predominantly depends upon integrin adhesion receptors[18,17]. Laminin-binding integrins include α3β1, α6β1, α6β4, and α7β1; type-IV collagen is bound by α1β1, α2β1 integrins[19,20]. αVβ3 and αVβ5 integrins mediate adhesion to both laminin and type-IV collagen[21–23]. Invading glioma cells upregulate multiple integrins in human gliomas, including α3β1 and αVβ3 integrins[24–26], and engage with a range of basement membrane and other stromal proteins in in vitro assays[16,17,27–32].

To address glioma invasion functionally, diverse in vitro assays have been developed to model brain stroma[33]. 3D collagen scaffolds, broadly used in cancer research, are effectively invaded by glioma cells[34–36], however the relevance of fibrillar collagen for largely collagen-free brain parenchyma remains disputed[33]. Reconstituted basement membranes (rBM) or cross-linked hyaluronan partially mimic brain ECM were used for probing glioma cell migration[37,38], but these substrates lack cellular and structural components of the brain tissue, such as astrocytes and myelinated axons, which provide additional ligands and guidance[5,6]. Astrocytes cultured as 2D monolayers provide gap-junction communication and paracrine secretion of migration-enhancing molecules to glioma cells[39–41]. As most

complex system, brain slice assays provide in vivo-like substrate topologies to reproduce glioma cell invasion including radial migration along blood vessels[42,43].

The role of integrin subsets in glioma cell migration was demonstrated for 2D surfaces coated with matrix molecules related to basement membranes, including α3β1, α6β1, α1β1 integrins binding to laminins, type IV collagen[16,17,27–32] and fibrillar collagen[44], however the role of integrins in mediating invasion into organotypic brain-like 3D environments remains unclear. We applied complementary 2D and 3D organotypic migration assays representing defined both ECM and cell-derived structures for in vitro modelling of glioma cell invasion in the brain tissue. With a focus on astrocyte-derived matrix and basement membrane of blood vessels, we tested which ECM molecules and integrin subunits mediate glioma cell invasion, and identify β1 integrin/laminin 511 interactions as dominant interaction system driving glioma cell invasion. However, using multi-inhibitor integrin targeting strategies, we further identify residual invasion activity implicating alternative, yet unexplored compensatory mechanisms maintaining this pathological process.

MATERIALS AND METHODS

Antibodies and reagents

The following antibodies and concentrations were used: adhesion-perturbing anti-human β1 integrin (mouse monoclonal, clone 4B4, human-specific; 15 µg/ml, BD Biosciences); adhesion-perturbing anti-mouse α6-integrin (rat monoclonal, clone GOH3, 10 µg/ml, BD Biosciences); adhesion-perturbing anti-human αV-integrin (mouse monoclonal, human-specific, clone 17E6, 10 µg/ml, Abcam); anti human α3-integrin (mouse monoclonal, clone 17C6, 10 µg/ml, AbD Serotec); anti human β3-integrin (mouse monoclonal, clone Y2/51, 10 µg/ml, AbD Serotec); anti-human β4-integrin (mouse monoclonal, clone ASC-3, 10 µg/ml, Abcam); anti human α1-integrin (mouse monoclonal, FITC labelled, clone TS2/7, 1:10, Abcam), human α2-integrin (mouse monoclonal, FITC labelled, clone AK-7, 1:10, BD Biosciences); anti-mouse laminin (rabbit polyclonal, 1:100, Sigma); anti-human collagen-IV (mouse, clone Col-94, 1:300, Sigma); anti-human vimentin (rabbit, SP20 clone, human specific,1:300, Thermo Scientific).

Cyclic cRGDFV and control cRADFV peptides (Biochem) were used to interfere with αV/α5 integrins in migration assays. Growth factor reduced rBM (matrigel; BD Biosciences) was used in migration assays as undiluted solution (» 9.8 mg/ml) or for coating culture plastic (30 µg/ml in PBS). Recombinant human laminin 511 and laminin 211 (BioLamina) and human placenta-derived type IV collagen (Advanced Bio Matrix) were used for coating culture plastic (10 µg/ml in PBS).

Cell lines and culture

Human glioblastoma U-251MG cells (kind gift from Dr. J. Schalkwijk, Nijmegen) and E-98 cells[45] were propagated in vitro in flasks for up to passage 35. H2B/eGFP-expressing U-251 and E-98 cells were generated by lentiviral transduction with pLenti6.2/V5-DEST™ Gateway (Invitrogen) containing histone2B/eGFP. Primary mouse astrocytes were immortalized with SV40 large T-antigen and additionally transformed with retrovirus pBabe puro H-Ras V12, as described[46] (kindly provided by Prof. Amparo Acker-Palmer, Frankfurt). Primary human astrocytes were immortalized with SV40 large T-antigen only (ABM).

Glioma cells and astrocytes were cultured in complete Dulbecco's Modified Eagle's Medium (DMEM; Invitrogen) supplemented with 10% fetal bovine serum (Sigma-Aldrich), penicillin (100 U/ml) and streptomycin (100 µg/ml; both PAA), L-glutamine (2 mM, Invitrogen) and sodium pyruvate (1 mM; Invitrogen).

Generation of glioma cell spheroids

U-251 and E-98 cell spheroids were generated using the hanging drop method. Cells were cultured in DMEM until subconfluency, detached with 1 mM EDTA/0.075% trypsin, washed with PBS, and maintained for 24h in complete DMEM /methylcellulose (2.4%; Sigma) as hanging droplets (25 µL) containing 1000 (U-251) or 2000 cells (E-98).

Interference with integrin function

Integrin function was perturbed by subunit-specific mouse-anti-human mAb targeting β1 (4B4; 15 µg/mlL, α6 (GOH3; 10 µg/mL), αV (17E6; 10 µg/ml), and cyclic peptide cRGDFV (50 µM) targeting RGD-binding αV and α5 integrins. As negative controls, isotypic IgG1 (10-15 µg/ml) or not-functional cRADFV peptide (50 µM) were used. Antibodies and peptides were added to the culture medium 2 - 4 h after seeding to secure initial spheroid engagement with the substrate.

Reconstituted basement membrane migration assays

Glioma cell spheroids were placed on 96-well-plates coated with growth factor reduced rBM (30 µg/ml) and overlaid with medium. 3D Matrigel-hyaluronan interface cultures were generated by polymerizing Matrigel on a culture dish (30 min, 37°C), addition of glioma spheroids (2h, 37°C), followed by addition of complete DMEM supplemented with hyaluronan (10 mg/ml; Sigma) as described[47]. For analysis of migration efficacy after 24h, samples were fixed (4% PFA) and analysed by bright-field or confocal microscopy.

Invasion into murine brain-slices

Glioma cell invasion from multicellular spheroids was probed using 3D murine brain slice culture, as described[47]. In brief, brains were dissected from female mice (5-6 weeks old, from Charles River or Jackson laboratories) C57BL/6-Tg(TcraTcrb)1100Mjb/Crl (OT1) crossed with B6.Cg-Tg(CAG-DsRed*MST)1Nagy/J (dsRed) in our laboratory. 400 µm-thick tissue slices were freshly sectioned using a vibratome (Leica, VT100s) and maintained on transwell insert membranes (Costar, 12-well plate; 8 µm pore diameter) in complete

DMEM (37°C, 5% CO_2) for 1h. Glioma cell spheroids expressing H2B/eGFP were added (8-10 spheroids per slice), allowed to initially adhere to the substrate (3h), and antibodies and peptides were added. During culture, medium and inhibitors were refreshed after 24h and migration efficacy was assessed after 48 h. Brain slices were fixed (4% PFA, 1h, RT), washed and stained with human-specific anti-vimentin antibody to discriminate glioma cells from DsRed-expressing blood vessels.

3D astrocyte scaffold invasion assay

3D astrocyte-derived scaffolds were generated by immortalized murine astrocytes maintained at high cell density in 96-well plates (20,000 cells/well, coated with growth factor-reduced rBM) for 2 days resulting in consolidated scaffolds of up to 3 cell layers in thickness (~50 µm), as described[47]. Glioma cell spheroids expressing H2B/eGFP were cultured on top of astrocyte scaffolds for 2 d, fixed (30 min, 4%PFA), stained to visualize glioma cells, astrocytes and ECM proteins. Primary antibodies were visualized with secondary AlexaFluor-conjugated goat-anti-mouse or goat-anti-rabbit polyclonal antibody to (Invitrogen; 5 µg/ml). Cell nuclei were stained with 4',6-diamidino-2-phenylindole (DAPI; 2.5 µg/ml).

Confocal microscopy and quantification of glioma cell migration

Confocal microscopy (Olympus FV1000) was performed using long working distance 20× NA 0.50 and 40× NA 0.80 objectives at a step size of 2-3 µm. Imaris V.6.1.5 software (Bitplane) was used for 3D reconstruction of Z-stacks.

For quantitative image analysis, operator-assisted image segmentation of bright-field or confocal 3D stacks was performed (Fiji software, V.1.49g[48]). The average cell migration distance representing radial migration of glioma cells from spheroids was calculated according to the following formula:

$$\text{Average distance of cell migration} = \sqrt{\text{Total cell area} / \pi} - \sqrt{\text{spheroid area} / \pi}$$

Mass-spectrometry

To identify proteins deposited by the astrocytes on culture plastic dishes murine and human astrocytes were cultured for 3 and 7 days, respectively, detached (2 mM EDTA/PBS), remnants of cells solubilized (0.25% Triton X100/0.25% sodium deoxycholate/PBS), and adsorbed proteins were harvested by scraping (disposable cell scraper, Greiner bio-one). The resulting protein fraction was centrifuged (4,250 x G, 45 min), the sediment dissolved (8 M urea, 3% SDS, 5% β-mercaptoethanol), cleaned and trypsin digested in a 12% polyacrylamide gel (TGX, BioRad), concentrated and desalted using STAGE tips (Thermo Scientific). The protein digest was separated on a nanoLC system using a reversed phase C18 column coupled to a LTQ FT Ultra mass spectrometer (Thermo Fisher Scientific; Radboud Proteomics Centre, Radboudumc, Nijmegen). Peptide analysis was performed using a customized database consisting of the RefSeq protein database with Mus musculus, together with Bos taurus taxonomies to identify possible contaminating proteins originating from fetal bovine serum used for culture. Validation of peptide and protein identifications was carried out by applying score thresholds to minimize false positive identification of emPAI values and number of peptides identified per protein. emPAI values were calculated as follows emPAI = $10^{N\ observed/N\ observable} - 1$, where $N_{observed}$ is the number of experimentally observed peptides and $N_{observable}$ is the calculated number of observable peptides for each protein[49].

Transient down-regulation of β1 integrin expression

Glioma cells were incubated with β1 integrin- or non-targeting smart-pool siRNA (Dharmacon; 50 nM) in the presence of Lipofectamine-2000 (1:1000, Dharmacon) for 20h, washed with growth media, cultured for 24h, aggregated for glioma cell spheroid generation (hanging drop assay) and monitored in migration assays for additional 24-28h. Efficiency of β1 integrin downregulaton was assessed by flow cytometry of single cells after detachment with EDTA (2 mM) 3 and 4d after transfection.

RESULTS

U-251 and E-98 glioma cell lines abundantly expressed α3 and β1 integrin subunits, moderate levels of α6, αV, β3, and negligible levels of α1, α2 and β4 integrins (Suppl. Fig. 1). Based on known subunit combinations, both cell lines thus predominantly expressed α3β1 and α6β1 integrin heterodimers, with predicted combined ligand preference for laminins[50,51]. Compared to E-98 cells, U-251 expressed higher levels of αVβ3, a RGD dependent integrin with broad substrate specificity[52,53].

As reference to published work[54], the role of integrins for emigration from U-251 and E-98 spheroids on reconstituted basement membrane (rBM) was tested. Combined, but not individual interference with antibody and peptide targeting β1 and αV integrins abrogated migration of U-251 cells in this assay, confirming a role of both integrin subsets for U-251 cells (Fig. 1a, b). E-98 cells migrating on rBM were more sensitive to mono-targeted β1 integrin interference than U-251 cells (Fig. 1a, b), indicating more limited substrate repertoire based on comparably low αVβ3 integrin surface levels (Suppl. Fig. 1). Similarly, a prominent pro-migratory function of b1 integrins in both cell types was confirmed using a 3D rBM/hyaluronan interface assay (Suppl. Fig. 2a, b), confirming the importance of b1 integrins for a 3D model.

When cultured on 3D organotypic brain slices, U-251 and E-98 cells invaded preferentially along blood vessels (Fig. 2a, d), and combined interference with β1 and αV integrin subunits decreased their distance migrated by 50 % (Fig. 2a, b). Despite abundant presence of adhesion-perturbing antibody 4B4 at the cell surface, detected

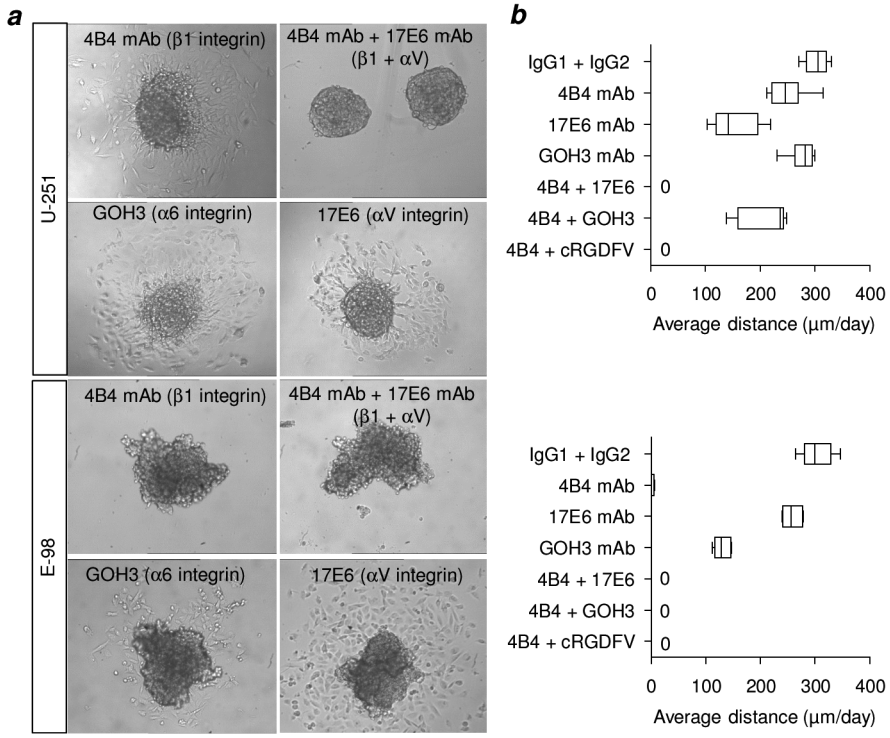

Figure 1. Migration of glioma cells on rBM coated surface is dependent on β1, αV and α6 integrin subunits. **a**. Radial migration of U-251 and E-98 cells from spheroids on plastic surface coated with rBM molecules (Matrigel) in media with control isotype IgG1, IgG2, adhesion-perturbing anti-integrin mAbs - anti β1 (4B4), anti aV (17E6), anti a6 (GOH3), and anti aV integrin cRGDFV peptide. **b**. Average migration distance of U-251 and E-98 cell on rBM. Values display median (black line), 25/75 percentiles (boxes) and maximum/minimum (whiskers). P values, Mann Whitney test.

by post-fixation confocal microscopy using secondary antibody only, glioma cells effectively interacted with capillary basement membranes and developed elongation and front-rear polarity during persistent migration (Fig. 2c, arrowheads). Moreover, the fraction of migrating glioma cells associated with blood vessels increased significantly in response to integrin inhibition, whereas interstitial movement was strongly reduced (Fig. 2d). This indicates differential adhesion requirements in perivascular versus interstitial tissue invasion.

To address the role of interstitial astrocyte-rich stroma in glioma cell invasion directly, an astrocyte-generated 3D scaffold was developed and used as migration substrate[47]. After 3-day culture, immortalized murine astrocytes formed multicellular networks in locally varying random or aligned order, with extracellular deposition of laminin and type IV collagen along cell-cell junctions (Suppl. Fig. 3a). After addition of glioma cell spheroids, glioma cells invaded into the astrocyte scaffolds along the boundaries between astrocytes (Fig. 3a). Similarly, to the brain slice assay U-251 and E-98 cell invasion into

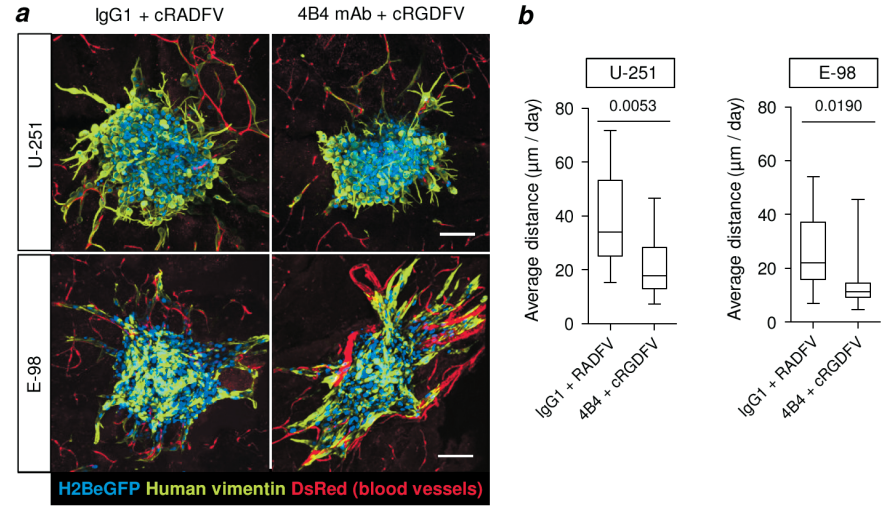

Figure 2. Glioma cells effectively invade along blood vessels in mouse brain slices in the presence of β1 and αV integrin inhibitors. **a.** Invasion of U-251 and E-98 cells from spheroids (for 2 days) in media with control isotype IgG1 + cRADFV peptide or with adhesion-perturbing anti β1 integrin 4B4 mAb + anti aV integrin cRGDFV peptide. Red signal originates from the DsRed mouse background, as contrast of vessels (bright signals) and stromal cells (dim signal). **b**. Average invasion distance of glioma cells in mouse brain slices. Values display median (black line), 25/75 percentiles (boxes) and maximum/minimum (whiskers) from 3 independent experiments. P values, Mann Whitney test. **c**. Glioma cells invasion along capillaries in the presence of anti β1 and aV integrin inhibitors. Anti β1 integrin 4B4 mAb was visualized with secondary AlexaFluor-conjugated goat-anti-mouse polyclonal antibody. Basement membranes were stained with anti-laminin or collagen IV antibodies. Arrowheads point to elongated glioma cells and their protrusions interacting to basement membrane of capillaries. **d**. Glioma cell distribution in the brain slices. % of blood vessels associated cells with or without β1+aV integrin interference. Data represent 3 independent experiments. P values, Mann Whitney test. Scale bars, 100 μm (**a**), 20 μm (**c**).

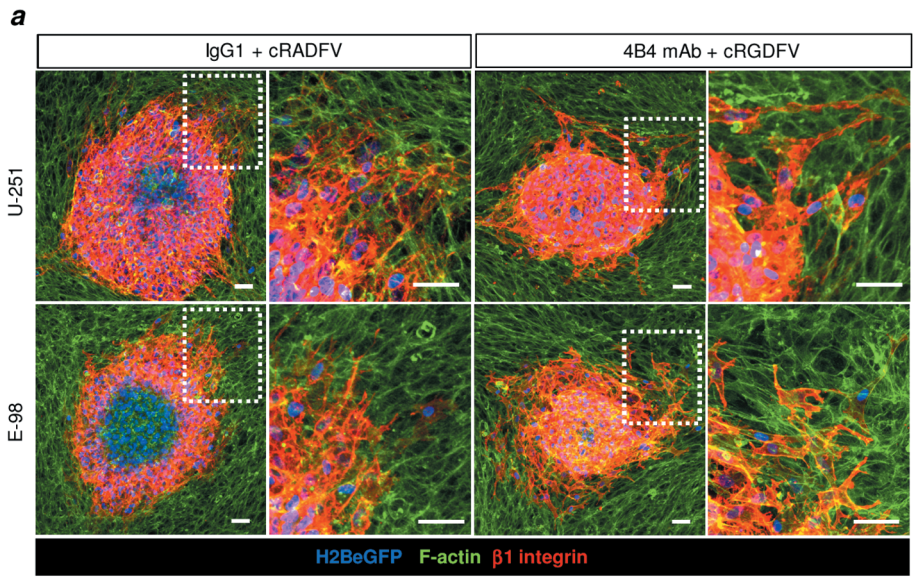

Figure 3. Glioma cells effectively invade in 3D astrocyte scaffolds in the presence of β1 and αV integrin inhibitors. **a**. Invasion of U-251 and E-98 cells from spheroids in 3D astrocyte scaffolds in media with control isotype IgG1 + cRADFV peptide or adhesion-perturbing anti β1 integrin 4B4 mAb + anti aV integrin cRGDFV peptide. **b**. Average invasion distance of U-251 and E-98 in 3D astrocytes scaffolds. Values display median (black line), 25/75 percentiles (boxes) and maximum/minimum (whiskers) from 3 independent experiments. P values, Mann Whitney test. Scale bar, 50 µm.

astrocyte scaffolds was reduced by 50% to 60% after interference with β1 and αV integrins (Fig. 3a, b). To discern the matrix components which supported glioma cell invasion in this assay, astrocyte-deposited matrix was decellularized and used as migration substrate (Suppl. Fig. 3b). Interference with β1 and αV integrin subunits inhibited glioma migration on astrocyte-derived matrix by up to 95% and 60% for U-251 and E-98 cells, respectively (Fig. 4a-c). Similar inhibition was obtained by interference with β1 and αV integrins when matrix deposited by human astrocytes after 3 and 7 days of culture was

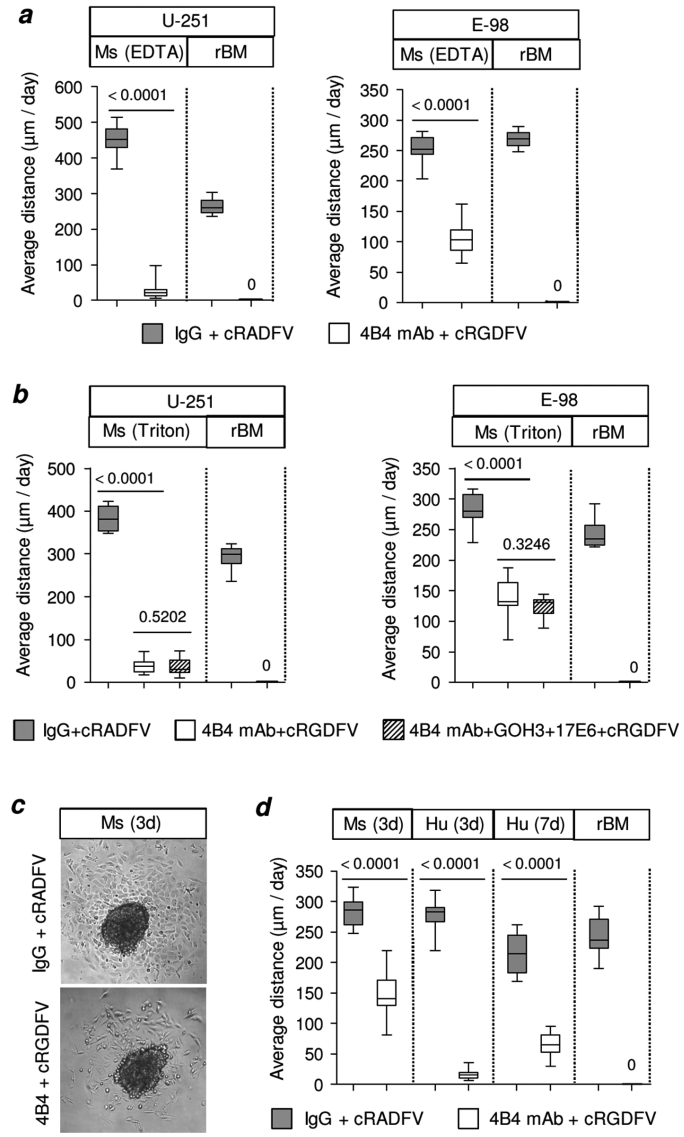

Figure 4. β1 and αV integrin interference abolishes migration of glioma cells on rBM but not on astrocyte-deposited matrix. **a, b.** Average migration distance of U-251 and E-98 cells from spheroids on mouse (**Ms**) astrocyte-deposited matrix or **rBM** (matrigel coated surface) in media with control isotype IgG, IgG2, adhesion-perturbing anti-integrin mAbs - anti β1 (4B4), anti aV (17E6), anti a6 (GOH3), and anti aV cRGDFV peptide and control cRADFV peptide. Mouse astrocytes were removed from culture surface with 0.002 M EDTA only (**a**), or (**b**) the culture surface was additionally treated 0.25% Triton X100 + 0.25% sodium deoxycholate/PBS. **c, d**. Overviews and average migration distance of E-98 cells from spheroids on mouse (**Ms**) or human (**Hu**) astrocyte deposited matrix. Astrocytes were cultured for 3 (**3d)** or 7 (**7d**) days and removed with 0.002 M EDTA followed by treatment of culture surface with 0.25% Triton X100 + 0.25% sodium deoxycholate/PBS. Values display median (black line), 25/75 percentiles (boxes) and maximum/minimum (whiskers) from 3 independent experiments. P values, Mann Whitney test.

used as migration substrate for E-98 cells (Fig. 4d; minus 95 and 69%, respectively). Thus, in contrast to glioma cell migration along rBM, invasion into complex brain stroma, 3D astrocyte scaffolds or astrocyte-deposited matrix was incompletely inhibited by antibody and small molecule based interference with integrins.

To identify their protein repertoire, astrocyte-deposited matrices were analyzed by mass-spectrometry analysis. 9 and 22 ECM proteins were identified in mouse and human astrocyte-derived matrix, respectively (Fig. 5b, c; Suppl. Tables 1 and 2). Laminin α5 was present in both murine- and human-derived samples, but largely absent in rBM, where laminin 111 dominates[55]. Laminin α5 contributes to laminin 511, the predominant isoform in basement membranes of brain blood vessels[12,13].

To test whether laminin 511 accounts for integrin-dependent or integrin-independent glioma cell-matrix interactions, human recombinant laminin 511 coated on the culture surface was used as migration substrate. Combined β1/αV integrin interference decreased U-251 cell migration on laminin 511 by 28%, while E-98 cell migration was not affected (Fig. 6a, b). Conversely, migration of U-251 and E-98 cells on laminin 211, type IV collagen and rBM (containing predominantly laminin 111[55]) was ablated by dual-integrin targeting (Fig. 6a, b). This verifies the technical stringency of the interference strategy and reveals particular pro-migratory properties of laminin 511 beyond β1 and αV integrins.

The main cell receptors for adhesion to laminin 511 are α3β1, α6β1 and α6β4 integrins[50,51]. To address whether glioma cells moving on laminin 511 after dual-integrin targeting still develop focal substrate interactions, samples were stained for paxillin, a structural protein central to integrin-dependent focal adhesions[56]. E-98 and U-251 cells with and without β1/αV integrin inhibitors formed string-like focalized enrichments corresponding to focal adhesions (Fig. 6c). This finding indicates the presence of either residual adhesion by β1/αV integrins or alternative laminin 511 binding integrin subsets.

To address the role of residual β1 integrin subunits in glioma cell migration on laminin 511 and in astrocyte scaffolds, siRNA knock-down was combined with antibody and peptide-based β1/αV integrin interference. Transient down-regulation of β1 integrin reached 73 - 88% reduction of cell surface levels in the majority of cells detected by flow cytometry (Fig. 7a1) or confocal microscopy (Fig. 7a2). This triple-interference caused additional reduction of migration efficiency of U-251 and E-98 cells on laminin 511 by respective 34% and 59%, compared to non-targeting siRNA (Fig. 7b, c). Likewise, triple-interference was effective for U-251 and E-98 cell invasion in 3D astrocyte scaffolds resulting in additionally reduction of migration distance by ~30% (Fig. 7b, c). Despite significant further reduction of migration ability after combinatorial integrin targeting, residual activity indicated the engagement of additional adhesion mechanisms, such as via α6β4, which is expressed in U-251 but not E-98 cells (Suppl. Fig. 1). To address whether α6β4 integrin supports U-251 cell migration, adhesion-perturbing anti-α6 integrin GoH3 monoclonal antibody[57] was combined with anti-β1 antibody, cRGDFV peptide and transient β1 integrin RNA interference reaching downregulation of 93% (Suppl. Fig. 4a). No additional inhibition was achieved by GoH3 antibody for U-251 cell invasion in 3D astrocyte scaffolds or migration on laminin 511 coated surface (Suppl. Fig. 4b-d).

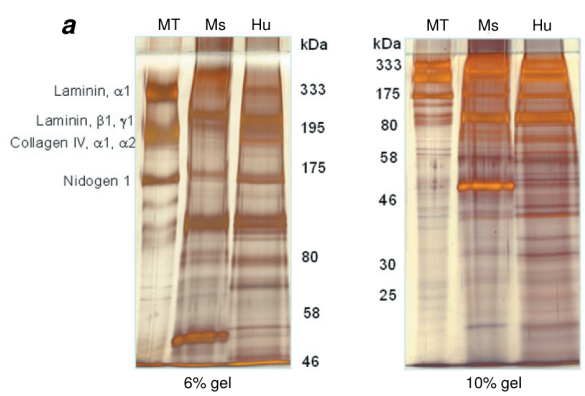

c

Matrix proteins identified both in mouse and human astrocyte matrixes
nidogen-1
laminin subunit alpha-1
laminin subunit beta-1
laminin subunit gamma-1
perlecan
fibronectin
vitronectin *
collagen alpha-1(XVIII) *
laminin subunit alpha-5 *
* Proteins present in Matrigel in trace amounts

b

Proteins deposited by mouse astrocytes

PROTEIN	emPAI Sample 1	NR-PEPS Sample 1
serine protease HTRA1 precursor [Mus musculus]	2.26	17
tubulointerstitial nephritis antigen-like precursor [Mus musculus]	0.60	7
nidogen-1 precursor [Mus musculus]	0.54	16
cathelicidin-7 precursor [Bos taurus]	0.47	2
keratin 9 [Homo sapiens]	0.40	6
plasminogen activator inhibitor 1 precursor [Mus musculus]	0.39	6
vimentin [Mus musculus]	0.36	7
lysyl oxidase homolog 2 precursor [Mus musculus]	0.31	7
alpha-2-HS-glycoprotein precursor [Bos taurus]	0.28	3
keratin, type I cytoskeletal 14 [Bos taurus]	0.26	5
nidogen-1 precursor [Bos taurus]	0.25	10
PREDICTED: hemoglobin subunit beta-like [Bos taurus]	0.25	2
PREDICTED: keratin, type I cytoskeletal 10-like [Bos taurus]	0.23	4
actin, cytoplasmic 1 [Mus musculus]	0.21	3
keratin, type II cytoskeletal 1 [Mus musculus]	0.20	3
keratin, type I cytoskeletal 10 [Mus musculus]	0.17	3
laminin subunit beta-1 [Mus musculus]	0.17	9
vitronectin precursor [Bos taurus]	0.17	2
fibronectin precursor [Mus musculus]	0.16	11
keratin, type II cytoskeletal 6A [Bos taurus]	0.15	3
von Willebrand factor A domain-containing protein 1 precursor [Mus musculus]	0.15	2
PREDICTED: keratin, type II cytoskeletal 1 [Bos taurus]	0.14	3
laminin subunit gamma-1 precursor [Mus musculus]	0.13	7
PREDICTED: keratin, type I cytoskeletal 25-like [Bos taurus]	0.13	2
PREDICTED: keratin, type II cytoskeletal 2 epidermal [Bos taurus]	0.12	3
PREDICTED: keratin, type II cytoskeletal 3 [Bos taurus]	0.11	2
basement membrane-specific heparan sulfate proteoglycan core protein precursor [Mus musculus]	0.11	14
laminin subunit alpha-1 precursor [Mus musculus]	0.11	11
PREDICTED: keratin, type I cytoskeletal 13 [Bos taurus]	0.11	2
keratin, type II cytoskeletal 2 epidermal [Mus musculus]	0.10	3
collagen alpha-1(XVIII) chain isoform 2 precursor [Mus musculus]	0.10	4
lysyl oxidase homolog 4 isoform 1 precursor [Mus musculus]	0.10	3
keratin, type II cytoskeletal 7 [Bos taurus]	0.09	2
A disintegrin and metalloproteinase with thrombospondin motifs 1 precursor [Mus musculus]	0.06	2
prelamin-A/C isoform A [Mus musculus]	0.03	1
laminin subunit alpha-5 precursor [Mus musculus]	0.02	3

Figure 5. Differences in ECM composition of astrocyte-deposited matrix and Matrigel. **a**. PAAG electrophoresis of Matrigel (**MT**), mouse (**Ms**) and human (**Hu**) astrocyte deposited matrixes (silver staining). **b**. Matrix proteins identified both in mouse and human astrocyte matrixes and which are minor in growth factor reduced Matrigel based on published mass-spectrometry data[55]. **c**. Proteins identified by mass-spectrometry in mouse deposited matrix.

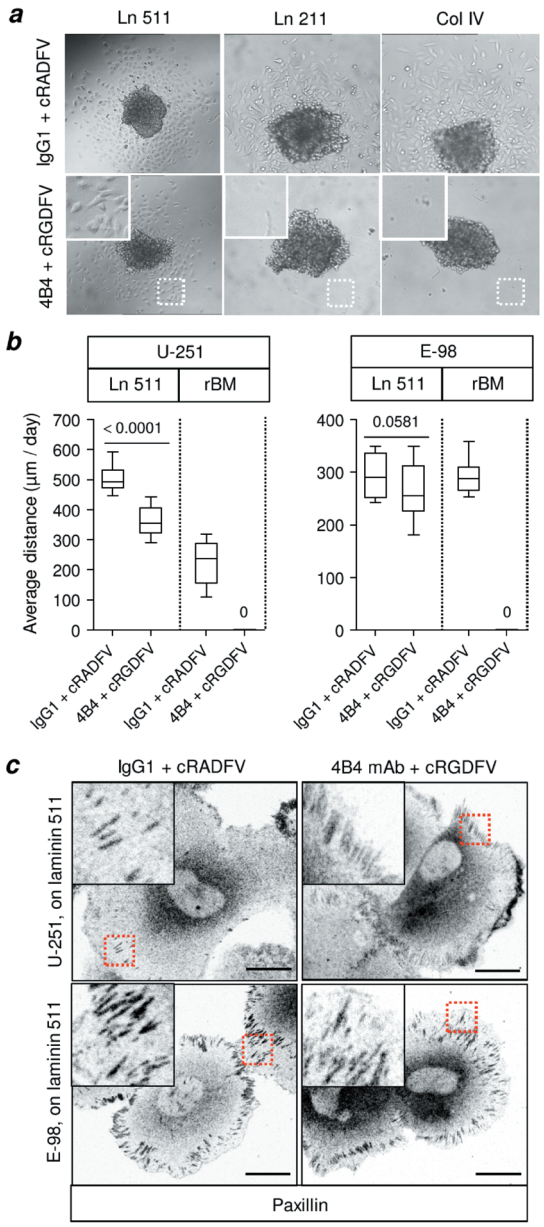

Figure 6. Glioma cells effectively migrate and form focal adhesions on laminin 511 in the presence of β1 and αV integrin inhibitors. **a**. Migration of U-251 and E-98 cells from spheroids on a plastic surface coated with laminin 511, laminin 211 or collagen IV, in media with control isotype IgG1 + cRADFV peptide or with adhesion-perturbing anti β1 integrin 4B4 mAb + anti αV integrin cRGDFV peptide. **b**. Average migration distance of U-251 and E-98 cells on the plastic surface coated with laminin 511. Values display median (black line), 25/75 percentiles (boxes) and maximum/minimum (whiskers) from 3 independent experiments. P values, Mann Whitney test. **c**. Paxillin staining in E-98 and U-251 cells radially migrated from spheroids on astrocyte deposited matrix or laminin 511 coated surface. Scale bar, 25 µm.

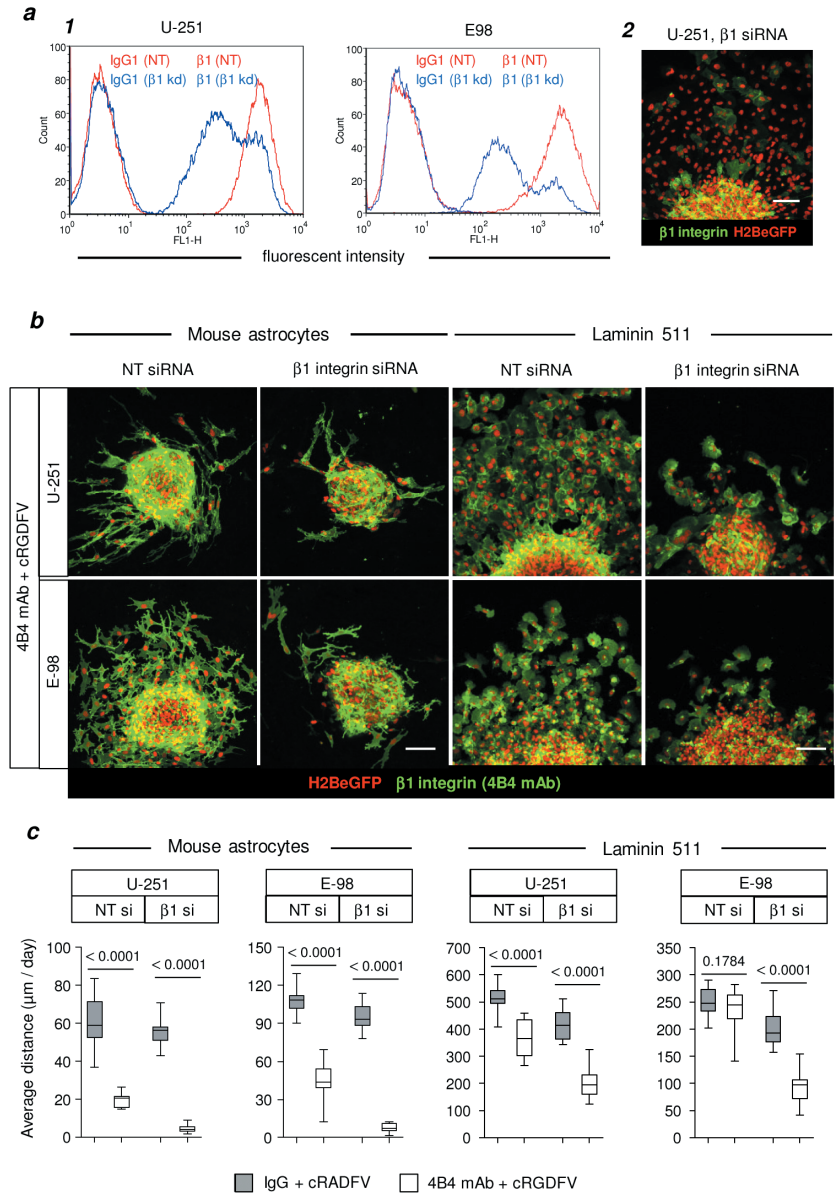

Figure 7. β1 integrin subunits mediate glioma cell migration on laminin 511 and invasion in 3D astrocyte scaffolds. **a**. Expression of β1 integrin subunit in U-251 and E-98 cells in 3 days after their transfection with either NT siRNA or anti β1 integrin siRNA based on flow cytometry (**1**) or confocal microscopy (**2**). **b**. Migration of U-251 and E-98 cells transfected with NT siRNA or anti β1 integrin siRNA from spheroids on laminin 511 coated culture surface and the cell invasion in 3D astrocyte scaffolds, in media with adhesion-perturbing anti β1 integrin 4B4 mAb + anti αV integrin cRGDFV peptide. **c**. Average migration distance of U-251 and E-98 cells on the plastic surface coated with laminin 511 and the cell invasion in 3D astrocyte scaffolds. Values display median (black line), 25/75 percentiles (boxes) and maximum/minimum (whiskers) from 3 independent experiments. P values, Mann Whitney test. Scale bars, 100 µm.

In aggregate, these data suggest that in complex brain-like environments β1 integrin represent the primary adhesion system for glioma cell migration, with laminin 511 present in basement membrane and interstitial astrocyte-derived stroma as key ligand. The differential interference efficacy across migration models further indicates that adhesion requirements are strongly assay dependent, whereby compensation by integrin-dependent and, likely, integrin-independent interaction strategies increases with the dimensionality and topologic complexity of the substrate.

Discussion

By using brain-like culture models to quantify glioma cell invasion, we identified β1 integrins as the central adhesion system driving glioma cell invasion, predominantly through interaction with laminin 511. By comparing 2D and 3D models which represent the heterogeneity of cell-matrix and cell-cell interfaces present in the neuropil, the data reveal significant resilience of glioma cell migration in complex environments despite stringent molecular interference. Thus, adhesion targeting may delay but not abrogate invasive progression of gliomas in vivo.

Major constituents of brain basement membranes include type IV collagen and predominant laminin isoforms 511, 211, 411, 332, 111[18,20,58]. rBM (Matrigel) is broadly used in cell invasion assays as an extracellular matrix to reproduce aspects of basement membranes in vitro, based on its content of laminin 111 and type IV collagen[55]. However, rBM lacks most other brain-related laminin isoforms, and thus lacks the ligand heterogeneity of brain ECM deposited by astrocytes, endothelium and pericytes[12,13,17]. Accordingly glioma cell migration on rBM was abolished with β1 and αV integrin interference, while invasion along basement membranes in brain slices and in 3D astrocyte scaffolds was reduced by only half, suggesting alternative integrin-ECM interactions available in a complex brain-like models.

By mass-spectrometry analysis of the astrocyte deposited matrixes we identified laminin 511 as a molecule guiding glioma cell migration and focalized adhesion formation in control cells and cells after β1 and αV integrin interference. Laminin 511 is a multifunctional adhesion protein ubiquitously expressed in basement membranes of different tissue structures including brain blood vessels[12,59,60]. Integrins α3β1, α6β1, α6β4 and α7β1 are the major receptors ensuring cell adhesion and migration on laminin 511[50,51], and αVβ3 integrin can additionally provide interactions to laminin 511[21]. Notably, laminin 511 contains two binding sites for α3β1 (in the LG1-3 and LN domains) and one further site for αVβ3 integrins (in the L4a domain)[21,61–63], and thereby can act as multi-domain interaction scaffold to engage multiple integrin subtypes simultaneously and in a non-competitive manner. Accordingly, multi-targeted interference with β1 integrin, the predominant subunit expressed by U-251 and E-98 cells and other glioma models[17], revealed its dominant role in mediating migration along laminin 511.

Several mechanisms may mediate residual migration retained in both cell types despite interference with adhesion-perturbing anti-b1 integrin antibody 4B4 and anti αV-integrin cRGD peptide. β1 integrins interact with laminin 511 with high affinity[50,51]; moreover, clustering of integrin molecules in the plasma membrane additionally increases the avidity of cell-matrix interactions[64,65]. Therefore the natural integrin-ligand interaction may outcompete the used competitive (cRGD) and allosteric (mAb 4B4) integrin inhibitors[66–68]. Laminin 511 may further provide binding sites for non-integrin receptors, including Lu/B-CAM, a-dystroglycan and syndecan-4[62,69–71].

Laminin 511 is present in quiescent and reactive brain stroma, including basement membranes along capillaries and larger brain vessels, and diffusely in tumor associated stroma released by astrocytes[12,13,41,72–76]. Moving glioma cells themselves may secrete laminins, including laminin 511[17], in an autocrine manner and thereby support migration in laminin deficient environments or when integrin functions are antagonized.

Our and other data[17] suggest β1 integrin – laminin 511 interactions as a major driver of glioma cell invasion along blood vessels and possibly in astrocyte reach stroma. Consequently, integrins may be considered as a therapeutic target to combat glioma cell dissemination in the brain tissue. Clinically relevant integrin targeting in glioma patients using the αVβ3/αVβ5 integrin inhibitor cilengitide, a RGD mimicking cyclic peptide[66], significantly reduced diffuse glioma cell invasion in mouse brain[77,78]. However, recent phase II clinical trials in late-stage glioblastoma patients did not confirm efficiency of cilengitide to improve overall survival[79–82]. In a pilot study, humanized anti β1-integrin neutralizing antibody OS2966 was injected intracranially for 28 days in mouse brain, and this treatment significantly inhibited the invasion of human glioma xenografts[28]. Beyond a direct antiinvasive effect, targeting β1 integrins may further reduce tumor growth and sensitize glioma cells to radio-, chemo, anti-angiogenesis therapies[28,83]. Yet, the benefit of the combination of anti-β1 to further integrin-targeting strategies or other adhesion systems will require exploration. Thus, in line with these limited preclinical and clinical data, our findings suggest that overlapping integrin-dependent and, possibly, integrin-independent adhesion systems support glioma cell invasion. Targeted approaches to interfere with glioma cell invasion will thus require combinatorial strategies designed to prevent adhesion plasticity of glioma cell dissemination and/or escape to alternative ECM systems and invasion routes in the brain tissue.

REFERENCES

1. Wen, P. Y. & Reardon, D. A. Neuro-oncology in 2015: Progress in glioma diagnosis, classification and treatment. *Nat. Rev. Neurol.* **12,** 69–70 (2016).
2. Brat, D. J. *et al.* Comprehensive, Integrative Genomic Analysis of Diffuse Lower-Grade Gliomas. *N. Engl. J. Med.* **372,** 2481–2498 (2015).
3. Patel, A. P. *et al.* Single-cell RNA-seq highlights intratumoral heterogeneity in primary glioblastoma. **344,** 1396–1401 (2014).
4. Capdevila, C., Rodriguez Vazquez, L. & Marti, J. Glioblastoma Multiforme and Adult Neurogenesis in the Ventricular-Subventricular Zone: A Review. *J. Cell. Physiol.* (2016). doi:10.1002/jcp.25502
5. Cuddapah, V. A., Robel, S., Watkins, S. & Sontheimer, H. A neurocentric perspective on glioma invasion. *Nat. Rev. Neurosci.* **15,** 455–465 (2014).
6. Gritsenko, P. G., Ilina, O. & Friedl, P. Interstitial guidance of cancer invasion. *J. Pathol.* **226,** 185–199 (2012).
7. Zimmermann, D. R. & Dours-Zimmermann, M. T. Extracellular matrix of the central nervous system: from neglect to challenge. *Histochem Cell Biol* **130,** 635–653 (2008).
8. Farin, A. *et al.* Transplanted glioma cells migrate and proliferate on host brain vasculature: a dynamic analysis. *Glia* **53,** 799–808 (2006).
9. Krueger, M. & Bechmann, I. CNS pericytes: concepts, misconceptions, and a way out. *Glia* **58,** 1–10 (2010).
10. Zhang, E. T., Inman, C. B. & Weller, R. O. Interrelationships of the pia mater and the perivascular (Virchow-Robin) spaces in the human cerebrum. *J Anat* **170,** 111–123 (1990).
11. Mathiisen, T. M., Lehre, K. P., Danbolt, N. C. & Ottersen, O. L. E. P. The Perivascular Astroglial Sheath Provides a Complete Covering of the Brain Microvessels: An Electron Microscopic 3D Reconstruction. **1103,** 1094–1103 (2010).
12. Yousif, L. F., Di Russo, J. & Sorokin, L. Laminin isoforms in endothelial and perivascular basement membranes. *Cell Adh. Migr.* **7,** 101–110 (2013).
13. Di Russo, J. *et al.* Vascular laminins in physiology and pathology. *Matrix Biol.* (2016). doi:10.1016/j.matbio.2016.06.008
14. Arita, N., Taneda, M. & Hayakawa, T. Leptomeningeal dissemination of malignant gliomas. Incidence, diagnosis and outcome. *Acta Neurochir* **126,** 84–92 (1994).
15. Watkins, S. *et al.* Disruption of astrocyte-vascular coupling and the blood-brain barrier by invading glioma cells. *Nat. Commun.* **5,** 4196 (2014).
16. Haugland, H. K., Tysnes, B. B. & Tysnes, O. B. Adhesion and migration of human glioma cells are differently dependent on extracellular matrix molecules. *Anticancer Res.* **17,** 1035–1042 (1997).
17. Kawataki, T. *et al.* Laminin isoforms and their integrin receptors in glioma cell migration and invasiveness: Evidence for a role of alpha5-laminin(s) and alpha3beta1 integrin. *Exp Cell Res* **313,** 3819–3831 (2007).
18. Yurchenco, P. D. Basement membranes: cell scaffoldings and signaling platforms. *Cold Spring Harb. Perspect. Biol.* **3,** (2011).
19. Khoshnoodi, J., Pedchenko, V. & Hudson, B. G. Mammalian collagen IV. *Microsc Res Tech* **71,** 357–370 (2008).
20. Yurchenco, P. D. Integrating Activities of Laminins that Drive Basement Membrane Assembly and Function. *Curr. Top. Membr.* **76,** 1–30 (2015).
21. Sasaki, T. & Timpl, R. Domain IVa of laminin alpha5 chain is cell-adhesive and binds beta1 and alphaVbeta3 integrins through Arg-Gly-Asp. *FEBS Lett.* **509,** 181–185 (2001).
22. Xu, J. *et al.* Proteolytic exposure of a cryptic site within collagen type IV is required for angiogenesis and tumor growth in vivo. *J. Cell Biol.* **154,** 1069–1079 (2001).
23. Pedchenko, V., Zent, R. & Hudson, B. G. Alpha(v)beta3 and alpha(v)beta5 integrins bind both the proximal RGD site and non-RGD motifs within noncollagenous (NC1) domain of the alpha3 chain of type IV collagen: implication for the mechanism of endothelia cell adhesion. *J. Biol. Chem.* **279,** 2772–2780 (2004).
24. Paulus, W., Baur, I., Schuppan, D. & Roggendorf, W. Characterization of integrin receptors in normal and neoplastic human brain. *Am J Pathol* **143,** 154–163 (1993).
25. Schittenhelm, J. *et al.* Longitudinal expression analysis of αv integrins in human gliomas reveals upregulation of integrin αvβ3 as a negative prognostic factor. *J. Neuropathol. Exp. Neurol.* **72,** 194–210 (2013).
26. Bello, L. *et al.* avb3 and avb5 Integrin Expression in Glioma Periphery. *Neurosurgery* **49,** 380–390 (2001).
27. Nakada, M. *et al.* Integrin α3 is overexpressed in glioma stem-like cells and promotes invasion. *Br. J. Cancer* **108,** 2516–24 (2013).
28. Carbonell, W. S., Delay, M., Jahangiri, A., Park, C. C. & Aghi, M. K. Beta1 Integrin Targeting Potentiates Antiangiogenic Therapy and Inhibits the Growth of Bevacizumab-Resistant Glioblastoma. *Cancer Res.* **73,** 3145–3154 (2013).
29. Delamarre, E. *et al.* Expression of Integrin alpha6 beta1 Enhances Tumorigenesis in Glioma Cells. **175,** 844–855 (2009).
30. Lathia, J. D. *et al.* Integrin alpha 6 regulates glioblastoma stem cells. *Cell Stem Cell* **6,** 421–432 (2011).
31. Fukushima, Y., Ohnishi, T., Arita, N., Hayakawa, T. & Sekiguchi, K. Integrin alpha3beta1-mediated interaction with laminin-5 stimulates adhesion, migration and invasion of malignant glioma cells. *Int. J. cancer* **76,** 63–72 (1998).
32. Rooprai, H. K. *et al.* The role of integrin receptors in aspects of glioma invasion in vitro. *Int. J. Dev. Neurosci.* **17,** 613–623 (1999).
33. Rape, A., Ananthanarayanan, B. & Kumar, S. Engineering strategies to mimic the glioblastoma microenvironment. *Adv. Drug Deliv. Rev.* **79–80,** 172–183 (2014).
34. Frolov, A. *et al.* Imatinib and Nilotinib increase glioblastoma cell invasion via Abl-independent stimulation of p130Cas and FAK signalling. *Sci. Rep.* **6,** 27378 (2016).
35. Kaufman, L. J. *et al.* Glioma expansion in collagen I matrices: analyzing collagen concentration-dependent growth and motility patterns. *Biophys. J.* **89,** 635–650 (2005).
36. Yang, Y., Motte, S. & Kaufman, L. J. Pore size variable type I collagen gels and their interaction with glioma cells. *Biomaterials* **31,** 5678–5688 (2010).
37. Gordon, V. D. *et al.* Measuring the mechanical stress induced by an expanding multicellular tumor system: a case study. *Exp. Cell Res.* **289,** 58–66 (2003).
38. Ananthanarayanan, B., Kim, Y. & Kumar, S. Elucidating the mechanobiology of malignant brain tumors using a brain matrix-mimetic hyaluronic acid hydrogel platform. *Biomaterials* **32,** 7913–7923 (2011).
39. Hong, X., Sin, W. C., Harris, A. L. & Naus, C. C. Gap junctions modulate glioma invasion by direct transfer of microRNA. *Oncotarget* **6,** 15566–15577 (2015).
40. Oliveira, R. *et al.* Contribution of gap junctional communication between tumor cells and astroglia to the invasion of the brain parenchyma by human glioblastomas. *BMC Cell Biol.* **6,** 1–17 (2005).
41. Rath, B. H., Fair, J. M., Jamal, M., Camphausen, K. & Tofilon, P. J. Astrocytes enhance the invasion potential of glioblastoma stem-like cells. *PLoS One* **8,** e54752 (2013).
42. Alfi, S. T. P., Eguerinel, C. A. L. & Asset, M. I. M. Invasion of human glioma biopsy specimens in cultures of rodent brain slices: a quantitative analysis. *J Neurosurg* **97,** 169–176 (2002).
43. Fayzullin, A. *et al.* Time-lapse phenotyping of invasive glioma cells ex vivo reveals subtype-specific movement patterns guided by tumor core signaling. *Exp. Cell Res.* **349,** 199–213 (2016).
44. O'Rourke, C., Drake, R. A. L., Cameron, G. W. W., Loughlin, A. J. & Phillips, J. B. Optimising contraction and alignment of cellular collagen hydrogels to achieve reliable and consistent engineered anisotropic tissue. *J. Biomater. Appl.* **30,** 599–607 (2015).
45. Claes, A. *et al.* Phenotypic and Genotypic Characterization of Orthotopic Human Glioma Models and Its Relevance for the Study of Anti-glioma Therapy. *Brain Pathol.* **18,** 423–433 (2008).
46. Sawamiphak, S. *et al.* Ephrin-B2 regulates VEGFR2 function in developmental and tumour angiogenesis. *Nature* **465,** 487–491 (2010).

47. Gritsenko, P., Leenders, W. & Friedl, P. Recapitulating in vivo-like plasticity of glioma cell invasion along blood vessels and in astrocyte-rich stroma. *Histochem. Cell Biol.* **148,** 395–406 (2017).
48. Schindelin, J. *et al.* Fiji: an open-source platform for biological-image analysis. *Nat. Methods* **9,** 676–682 (2012).
49. Ishihama, Y. *et al.* Exponentially modified protein abundance index (emPAI) for estimation of absolute protein amount in proteomics by the number of sequenced peptides per protein. *Mol. Cell. Proteomics* **4,** 1265–1272 (2005).
50. Nishiuchi, R. *et al.* Characterization of the ligand-binding specificities of integrin alpha3beta1 and alpha6beta1 using a panel of purified laminin isoforms containing distinct alpha chains. *J. Biochem.* **134,** 497–504 (2003).
51. Nishiuchi, R. *et al.* Ligand-binding specificities of laminin-binding integrins: a comprehensive survey of laminin-integrin interactions using recombinant alpha3beta1, alpha6beta1, alpha7beta1 and alpha6beta4 integrins. *Matrix Biol.* **25,** 189–197 (2006).
52. Goodman, S. L. & Picard, M. Integrins as therapeutic targets. *Trends Pharmacol. Sci.* **33,** 405–412 (2012).
53. Demircioglu, F. & Hodivala-Dilke, K. alphavbeta3 Integrin and tumour blood vessels-learning from the past to shape the future. *Curr. Opin. Cell Biol.* **42,** 121–127 (2016).
54. Benton, G., Arnaoutova, I., George, J., Kleinman, H. K. & Koblinski, J. Matrigel: from discovery and ECM mimicry to assays and models for cancer research. *Adv. Drug Deliv. Rev.* **79–80,** 3–18 (2014).
55. Hughes, C. S., Postovit, L. M. & Lajoie, G. A. Matrigel : A complex protein mixture required for optimal growth of cell culture. *Proteomics* **10,** 1886–1890 (2010).
56. Schaller, M. D. Paxillin: a focal adhesion-associated adaptor protein. *Oncogene* **20,** 6459–6472 (2001).
57. Lee, E. C., Lotz, M. M., Steele, G. D. J. & Mercurio, A. M. The integrin alpha 6 beta 4 is a laminin receptor. *J. Cell Biol.* **117,** 671–678 (1992).
58. Halfter, W. *et al.* New concepts in basement membrane biology. *FEBS J.* **282,** 4466–79 (2015).
59. Pouliot, N. & Kusuma, N. Laminin-511 A multi-functional adhesion protein regulating cell migration , tumor invasion and metastasis. *Cell Adh. Migr.* **7,** 142–149 (2013).
60. Spenlé, C., Simon-assmann, P., Orend, G. & Miner, J. H. Laminin a 5 guides tissue patterning and organogenesis. *Cell Adh. Migr.* **7,** 90–100 (2013).
61. Ido, H. *et al.* Molecular dissection of the alpha-dystroglycan- and integrin-binding sites within the globular domain of human laminin-10. *J. Biol. Chem.* **279,** 10946–10954 (2004).
62. Kikkawa, Y. *et al.* The LG1-3 tandem of laminin alpha5 harbors the binding sites of Lutheran/basal cell adhesion molecule and alpha3beta1/alpha6beta1 integrins. *J. Biol. Chem.* **282,** 14853–14860 (2007).
63. Nielsen, P. K. & Yamada, Y. Identification of cell-binding sites on the Laminin alpha 5 N-terminal domain by site-directed mutagenesis. *J. Biol. Chem.* **276,** 10906–10912 (2001).
64. Laplantine, E. *et al.* The integrin beta1 subunit cytoplasmic tail forms oligomers: a potential role in beta1 integrin clustering. *Biol. Cell* **94,** 375–387 (2002).
65. Wiseman, P. W. *et al.* Spatial mapping of integrin interactions and dynamics during cell migration by image correlation microscopy. *J. Cell Sci.* **117,** 5521–5534 (2004).
66. Mas-Moruno, C., Rechenmacher, F. & Kessler, H. Cilengitide: the first anti-angiogenic small molecule drug candidate design, synthesis and clinical evaluation. *Anticancer. Agents Med. Chem.* **10,** 753–768 (2010).
67. Mould, A. P. *et al.* Ligand-induced epitope masking. Dissociation of integrin alpha5beta1-fibronectin complexes only by monoclonal antibodies with an allosteric mode of action. *J. Biol. Chem.* (2016). doi:10.1074/jbc.M116.736942
68. Takada, Y. & Puzon, W. Identification of a regulatory region of integrin beta 1 subunit using activating and inhibiting antibodies. *J. Biol. Chem.* **268,** 17597–17601 (1993).
69. Lin, L. & Kurpakus-Wheater, M. Laminin alpha5 chain adhesion and signaling in conjunctival epithelial cells. *Invest. Ophthalmol. Vis. Sci.* **43,** 2615–2621 (2002).
70. Shimizu, H., Hosokawa, H., Ninomiya, H., Miner, J. H. & Masaki, T. Adhesion of cultured bovine aortic endothelial cells to laminin-1 mediated by dystroglycan. *J. Biol. Chem.* **274,** 11995–12000 (1999).
71. Kikkawa, Y. *et al.* The lutheran/basal cell adhesion molecule promotes tumor cell migration by modulating integrin-mediated cell attachment to laminin-511 protein. *J. Biol. Chem.* **288,** 30990–31001 (2013).
72. Access, N. A. *et al.* Reactive astrocytes potentiate tumor aggressiveness in a murine glioma resection and recurrence model. *Neuro. Oncol.* 1–12 (2016). doi:10.1093/neuonc/now117
73. Placone, A. L., Quiñones-hinojosa, A. & Searson, P. C. The role of astrocytes in the progression of brain cancer : complicating the picture of the tumor microenvironment. *Tumor Biol* **37,** 61–69 (2016).
74. Knott, J. C. *et al.* Stimulation of extracellular matrix components in the normal brain by invading glioma cells. *Int. J. cancer* **75,** 864–872 (1998).
75. Mahesparan, R. *et al.* Expression of extracellular matrix components in a highly infiltrative in vivo glioma model. *Acta Neuropathol.* **105,** 49–57 (2003).
76. Keene, S. D. *et al.* Mass spectrometric and computational analysis of cytokine-induced alterations in the astrocyte secretome. *Proteomics* **9,** 768–782 (2009).
77. Onishi, M. *et al.* Bimodal anti-glioma mechanisms of cilengitide demonstrated by novel invasive glioma models. *Neuropathology* **33,** 162–174 (2013).
78. Ishida, J. *et al.* Integrin inhibitor suppresses bevacizumab-induced glioma invasion. *Transl. Oncol.* **7,** 292–302.e1 (2014).
79. Nabors, L. B. *et al.* Two cilengitide regimens in combination with standard treatment for patients with newly diagnosed glioblastoma and unmethylated MGMT gene promoter: results of the open-label, controlled, randomized phase II CORE study. *Neuro. Oncol.* **17,** 708–717 (2015).
80. Mason, W. P. End of the road: confounding results of the CORE trial terminate the arduous journey of cilengitide for glioblastoma. *Neuro. Oncol.* **17,** 634–635 (2015).
81. Eisele, G. *et al.* Cilengitide treatment of newly diagnosed glioblastoma patients does not alter patterns of progression. *J. Neurooncol.* **117,** 141–145 (2014).
82. Khasraw, M. *et al.* Cilengitide with metronomic temozolomide, procarbazine, and standard radiotherapy in patients with glioblastoma and unmethylated MGMT gene promoter in ExCentric, an open-label phase II trial. *J. Neurooncol.* **128,** 163–171 (2016).
83. Blandin, A.-F. *et al.* beta1 Integrins as Therapeutic Targets to Disrupt Hallmarks of Cancer. *Front. Pharmacol.* **6,** 279 (2015).

SUPPLEMENTARY INFORMATION

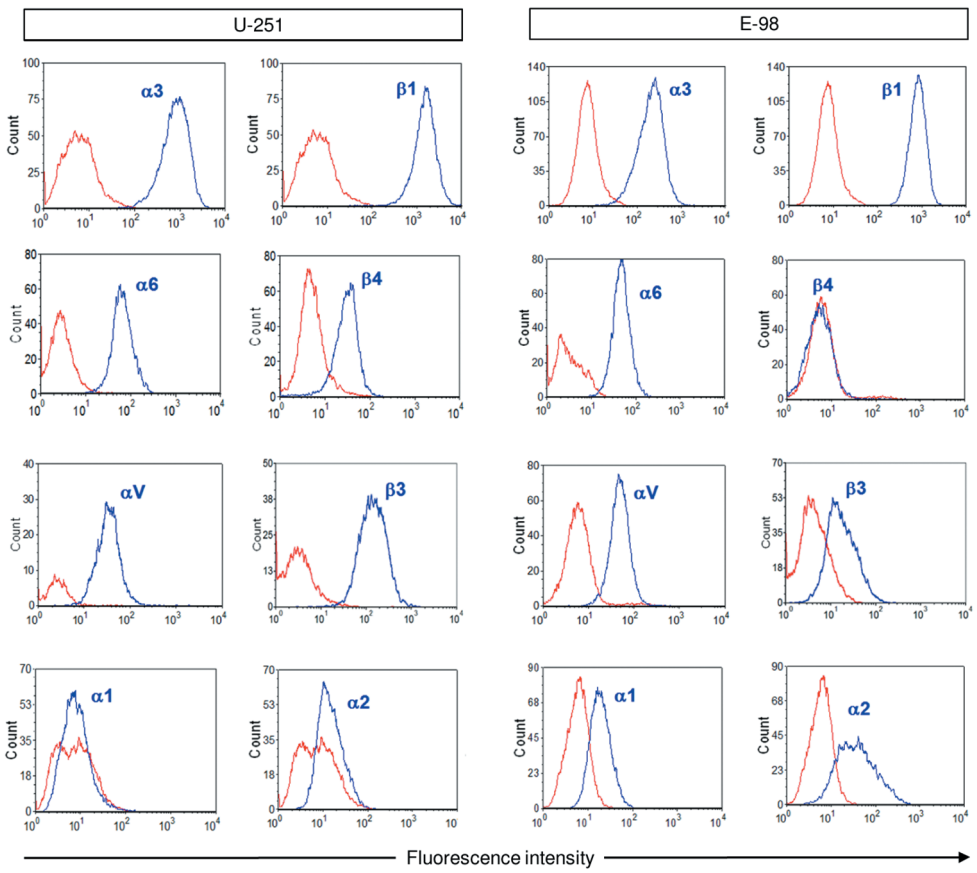

Supplementary Figure 1. Expression of integrin subunits in U-251 and E-98 cells measured with flow cytometry.

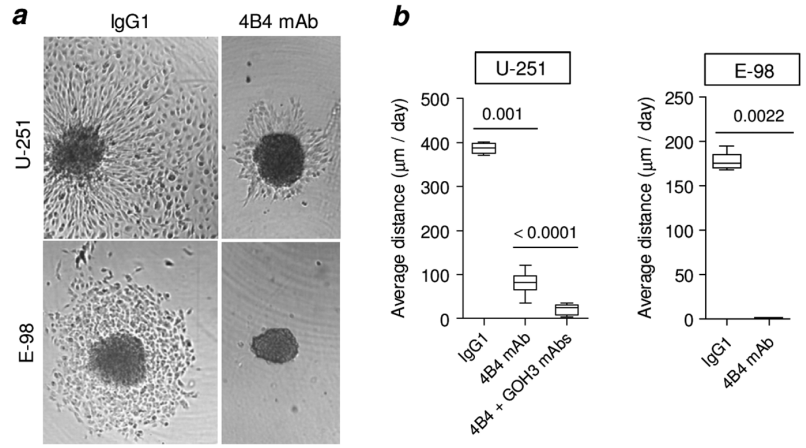

Supplementary Figure 2. Migration of glioma cells along hyaluronan-rBM interface is dependent on β1 and α6 integrin subunits. **a**. Migration of U-251 and E-98 cells from spheroids along hyaluronan-rBM interface in media with control isotype IgG1 or with adhesion-perturbing anti β1 integrin 4B4 mAb or anti α6 GOH3 mAb. **b**. Average migration distance of U-251 and E-98 cells along hyaluronan-rBM interface. Values display median (black line), 25/75 percentiles (boxes) and maximum/minimum (whiskers). P value, Mann Whitney test.

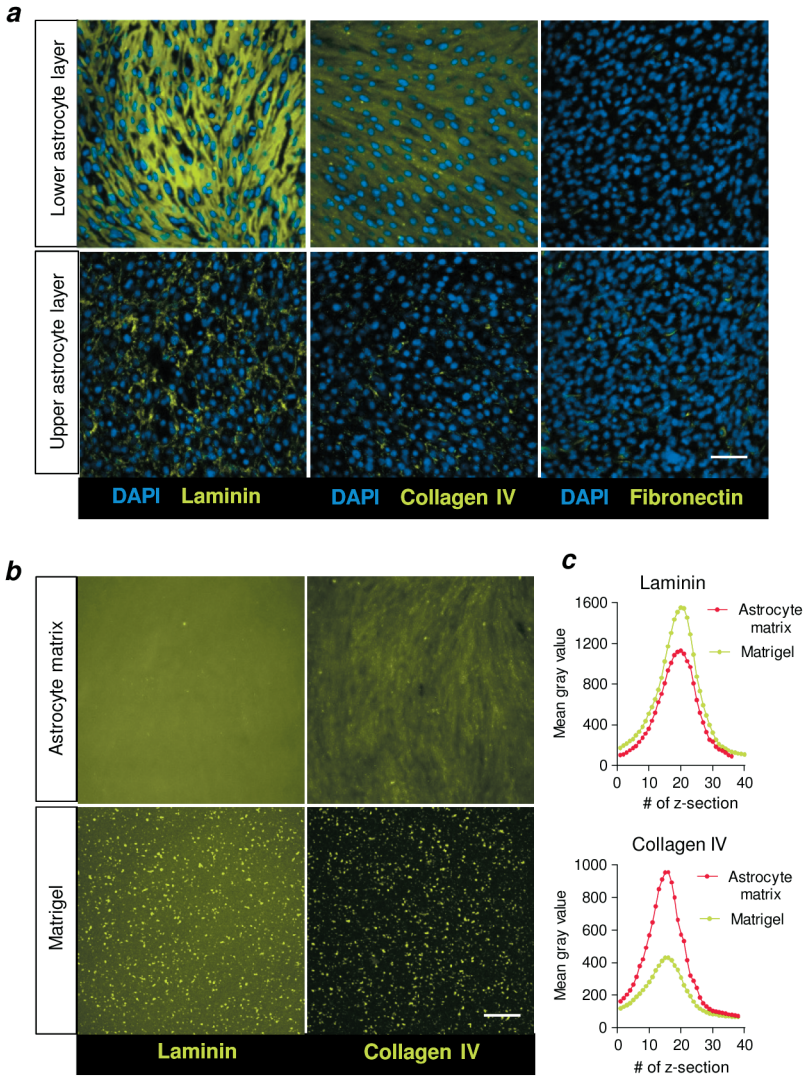

Supplementary Figure 3. Mouse astrocytes deposit matrix molecules related to basement membrane. **a**. Confocal images of mouse astrocytes cultured for 3 days and stained for laminin, collagen IV and fibronectin. **b**. Confocal images of mouse astrocyte deposited matrix. Astrocytes were cultured for 3 days and removed with 0.002M EDTA/PBS followed by treatment of culture surface with 0.25% Triton X100 + 0.25% sodium deoxycholate/PBS. **c**. Mean grey values in confocal images (Z-stack) of astrocyte deposited matrix and plastic surface coated with Matrigel. Scale bars, 50 µm.

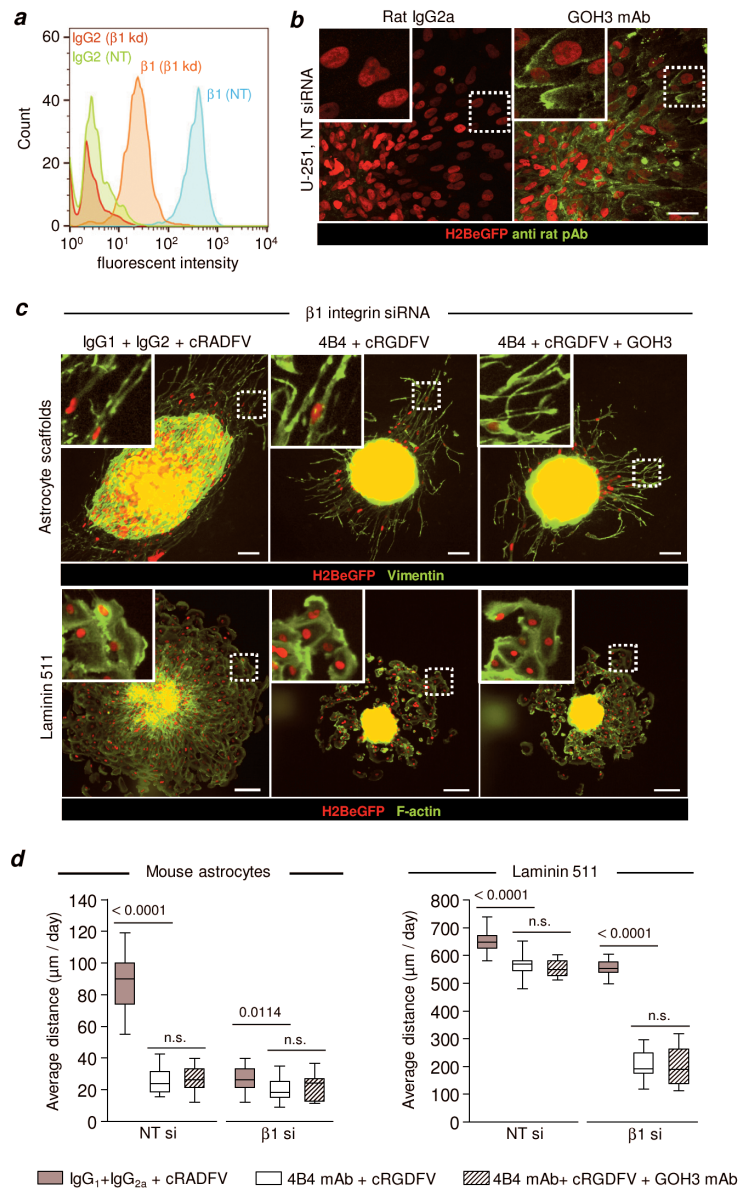

Supplementary Figure 4. Residual migration of U-251 cells after β1, αV and α6 integrin interference. **a**. Surface levels of β1 integrin in U-251 cells 3 days after transfection with either NT or β1 integrin siRNA detected by flow cytometry. **b**. Binding of anti-α6 integrin mAb GoH3 but not isotypic IgG by migrating U-251 cells in spheroid culture on laminin 511. **c.** Migration of U-251 cells from spheroids on laminin 511 or in 3D astrocyte scaffold culture after multi-targeted interference, as indicated. Glioma cells invading astrocyte scaffolds were identified by human-specific vimentin staining and nuclear H2BeGFP. **c**. Migration distance of U-251 and E-98 cells on laminin 511 or into 3D astrocyte scaffolds. Values display median (black line), 25/75 percentiles (boxes) and maximum/minimum (whiskers) from 3 independent experiments. P values, Mann Whitney test. Scale bars, 50 µm (**b**) and 100 µm (**c**).

CHAPTER 6

GENERAL DISCUSSION, FUTURE DIRECTIONS AND CLINICALLY RELEVANT IMPLICATIONS

Gliomas are malignant tumours of the central nervous system originating from transformed brain cells as a result of serial mutations and selections of the cancer cells with the highest resistance and proliferative potential[1–6]. In this thesis, using innovative 3D models for glioma cell invasion (Chapter 3) and in vivo strategies, new mechanisms of glioma cell dissemination in the brain parenchyma have been established: diffuse multicellular network invasion ensured by p120 catenin (Chapter 4) and perivascular glioma cell invasion driven by β1 integrin - laminin 511 interactions (Chapter 5). The data support the concept that glioma cells reproduce abnormal brain development programs, diffusely invade brain parenchyma along different anatomical structures, proliferate and ultimately disintegrate the brain.

HYPOTHESES OF GLIOMA CELL DISSEMINATION IN THE BRAIN TISSUE

Recent data demonstrated that diffuse astrocytomas, comprise extensive multicellular networks structurally and functionally resembling astrocytic or neuronal syncytium[7] (Chapter 4). These findings challenged the single-cell dissemination concept, which predicts that glioma cells invade the brain tissue individually similarly to the migration of normal glial and neuronal progenitors[8–10]. However, both views can come to an agreement when considered in the context of normal brain development where non-migratory neural stem cells produce neuronal and glial cell progenitors migrating individually throughout the brain parenchyma, differentiate into neurons, astrocytes and oligodendrocytes which finally form multicellular networks[11–14]. Similarly, tumor-initiating stem-like glioma cells can undergo neuronal and astrocytic differentiation-like transitions[4,15,16], and multicellular glioma networks possibly are pathological counterparts of normal brain cell networks[17]. Both in vitro and in vivo, single glioma cells with uni- or bi-polar morphology are consistently present at the invasion front of glioma networks[17,18] (Fig. 1a and Chapter 4). These individual "forerunner" cells resemble transformed glial cell progenitors migrating and proliferating *en route* in rodent brain tissue[18,19]. Single glioma cells can divide and undergo differentiation-like transitions establishing intercellular filamentous connections (Fig. 1a, b). Such individual glioma cells could create a pool of tumor cells possibly ensuring glioma network growth at the invasion front. Due to their deregulated cell cycle, glioma cells also proliferate within multicellular networks, and the cell proliferation likely contributes to network expansion in the brain tissue (Fig. 1b).

Glioma networks, unlike quiescent astrocytic or neuronal syncytia, are not static but enable glioma cell migration through the surrounding environment by disconnecting and reconnecting filamentous junctions, a unique invasion mode in the brain, which contributes to glioma network expansion in addition to the cell proliferation (Chapter 4).

This graded network topology indicates that glioma cell dissemination leads to the formation of glioma networks based on a gradient of cell density, with regions of high density and high connectivity near the tumor core and loosely connected or individualized cells located at the invasion front (Fig. 2).

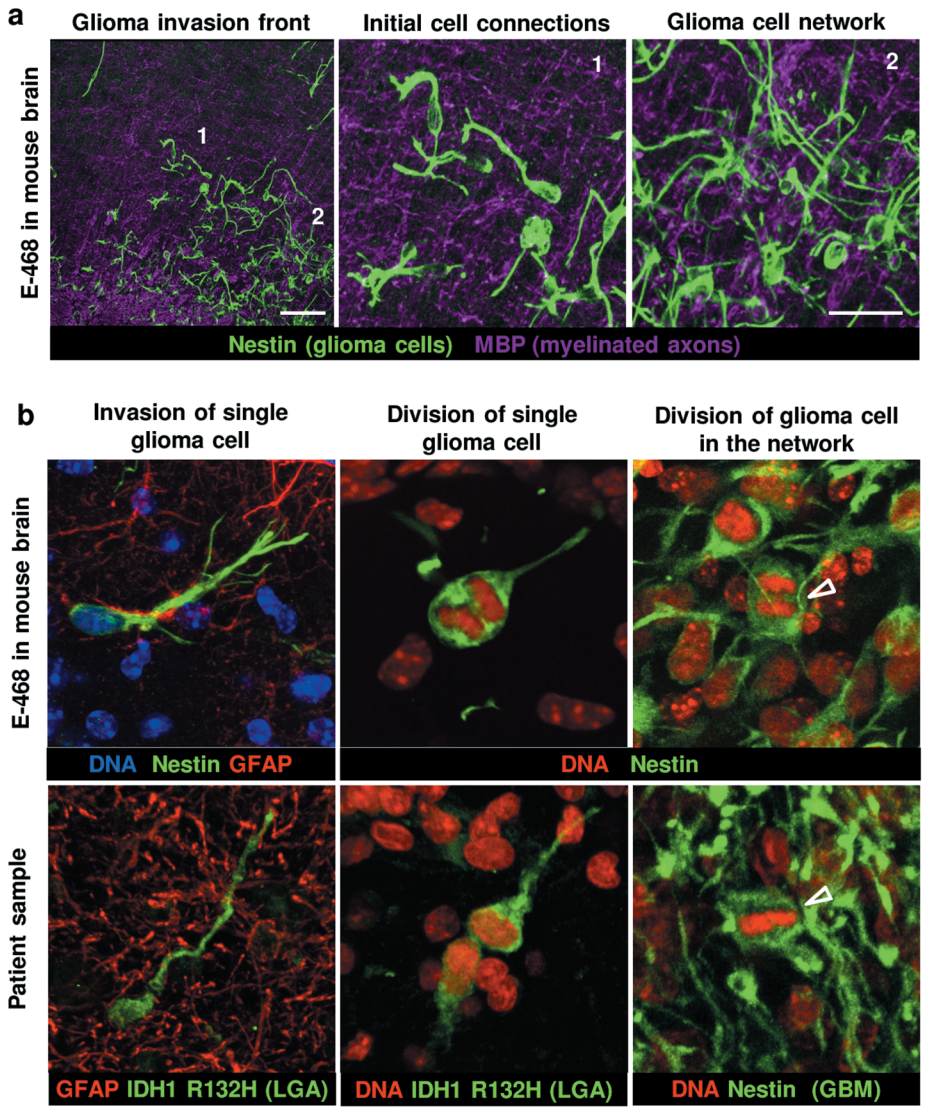

Figure 1. Different modes of glioma cell dissemination and growth in the brain. **a**. Multicellular glioma networks invade in the brain parenchyma forming and resolving intercellular filamentous connections during their migration (1) as described in Chapter 4, and possibly via incorporation of individual glioma cells at the invasion front (2). **b**. Single glioma cells migrate in the brain tissue and divide *en route* creating a pool of tumor cells, which potentially can be incorporated in the glioma network. Glioma cells also divide within the network ensuring glioma network expansion. Arrowheads point to mitotic events. Glioma cells in low grade diffuse astrocytoma (LGA) sample are visualized with monoclonal antibody (clone H09) that recognizes IDH1 R132H mutant protein and does not cross-react with wild type IDH1; glioma cells in glioblastoma multiforme (GBM) sample or in xenograft mouse brain tissue are stained with human specific anti-nestin polyclonal antibody. Non-neoplastic astrocytes are visualized with anti GFAP antibody. Scale bars: 100 μm (overview), 50 μm (details).

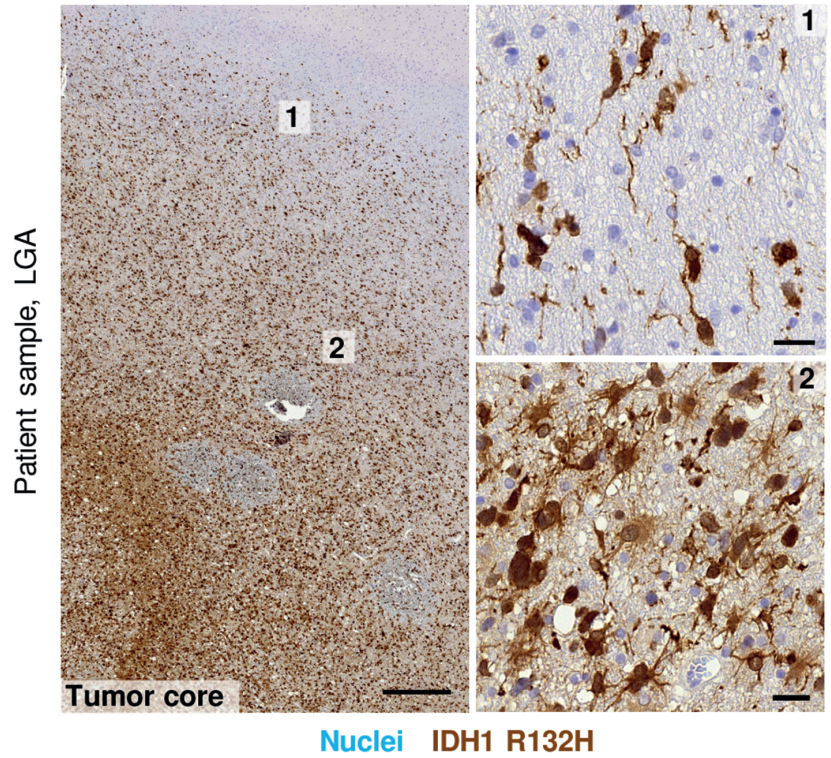

Figure 2. Gradient of cell density from glioma tumor core toward invasion front. At the invasion front, unipolar glioma cells invade either individually or form filamentous connections with adjacent glioma cells (1). Closer to tumor core multipolar glioma cells establish multiple filament connections similar to astrocytic networks (2). Glioma cells in low grade diffuse astrocytoma (LGA) are visualized with a monoclonal antibody (clone H09) that recognizes IDH1 R132H mutant protein and does not cross-react with wild type IDH1. Filamentous connections between glioma cells are underrepresented in thin (5 μm) histological sections. Scale bars: 500 μm (overview), 25 μm (details).

CELL-CELL AND CELL-MATRIX INTERACTIONS IN GLIOMA CELL INVASION

There are two major routes of glioma cell dissemination in the brain tissue, (1) along the extravascular interface of blood vessels and (2) through neuronal and astrocytic networks guided by myelinated axons and astrocyte processes[9,20]. During migration along blood vessels glioma cells interact with, and are guided by, the basement membrane with β1 integrin/laminin 511 interactions as important force-generating cell-matrix adhesion (Chapter 5). In the confined perivascular space glioma cells invade cohesively, by forming epithelial-like adherens junctions in contrast to diffuse glioma cell networks infiltrating the neuropil (Chapter 4), indicating that glioma cell-cell junctions are very plastic and modulated by geometry of the brain tissue. The mechanical and molecular adhesion mechanisms of single-cell and multicellular glioma invasion through the brain interstitium

are still largely obscure. It is not known which cell receptors and matrix molecules are involved in the generation of traction forces to ensure cell body movement in confined microchannels formed by myelinated axons and astrocytic processes[20]. Our data suggest that astrocytes secrete laminin 511, which is engaged by β1 integrins on glioma cells (Chapter 5). In addition to laminin 511, β1 and other integrin subunits expressed by glioma cells potentially could interact with various multivalent extracellular matrix molecules present in normal brain tissue (tenascin R) or de-novo synthetized by glioma and stromal cells (tenascin C, fibronectin, vitronectin, various isoforms of laminins and collagens). These molecules may decorate the surface of astrocytic filaments or myelinated axons and could provide a permissive multi-ligand substrate for glioma cell invasion[20]. Beyond integrins, additional adhesion systems may be involved in mediating glioma cell migration. Hyaluronan is the major extracellular matrix molecule in the brain tissue and its receptor CD44 is highly expressed in glioma cells[21], however, the role of CD44-hyaluronan interactions for glioma invasion in astrocytic/neuronal networks was not addressed in vivo. Recent data implicated connexin 43 mediated heterotypic interactions between glioma cells and astrocytes in the brain tissue independent of channel function of gap-junctions[22], a cell adhesion mechanism which may generate traction force and migration, similar to neuroblast migration along radial glial cells during brain development[23,24]. Another molecule which can potentially be involved in heterotypic glioma-astrocyte interactions is N-cadherin, which is the main cadherin receptor in glioma cells[25]. Whether glioma cells establish connections to non-neoplastic astrocytes and generate force via cadherin -cytoskeleton linkages, similar to moving cells in morphogenesis[26,27], awaits further investigations. Additionally, glioma cell invasion in extremely confided microchannels formed by myelinated axons or perivascular space with (sub)micrometer pore dimension, may be supported by non-adhesive, physical mechanisms, e.g. ensured by tubulin polymerization, myosin II contraction and ion channel mediated alterations of cytoplasmic volume[28–33].

P120 CATENIN IS INDISPENSABLE FOR GLIOMA NETWORK INVASION AND TUMOR GROWTH

P120 catenin (*CTNND1*) is a multifunctional protein, which directly or indirectly regulates activity of various molecular targets in different cell compartments[34,35] (Fig. 3). At the plasma membrane p120 catenin stabilizes classical cadherins, preventing their endocytosis[36]. P120 catenin modulates activity of Rho GTPases in cadherin associated or unbound states[34,35,37]. Diminishing RhoA and engaging Rac1 activities p120 promotes extension of filaments in neuronal and glioma cells[38,39]. Moreover, p120 catenin can translocate to the nucleus and inhibit activity of transcriptional repressors REST, GLIS2 and Kaiso, which modulate transcription of genes implicated in neuronal differentiation and Wnt signalling pathways[40,41].

The dynamics of multicellular glioma networks is a unique, specialized mode of collective cell invasion within discontinuous environments. We identified p120 catenin as a key molecule, which involved not only in the stabilization of cadherin cell-cell interactions but also in the formation of dendritic-like filaments connecting glioma cells within the networks, modulating RhoA/ROCK activity and axonogenesis pathways (Chapter 4). Stabilizing adherens junctions p120 catenin promotes also gap-junction commutation between glioma cells (Chapter 4), which increases resistance of glioma cells after radiotherapy[7]. Moreover, p120 catenin regulates proliferation of glioma cells and down-regulation of this protein induces dramatic growth deficit in vitro and in vivo via de-regulation of cellular pathways related to mitosis (Chapter 4). The crucial role of p120 catenin in glioma cell invasion and proliferation suggests it as a promising target for the future combinatory therapies of glioma patients.

P120 CATENIN AS A TARGET FOR ANTI-GLIOMA THERAPIES

Different amino acid sequences in p120 catenin molecule are involved in the binding and regulation of cadherins, RhoA and transcriptional repressors. To discern up- and down- stream pathways mediating p120 functions in glioma cells, different molecular approaches can be used. Established genetical constructs encoding p120 proteins with mutations or deletions in p120 functional domains will be useful to distinguish

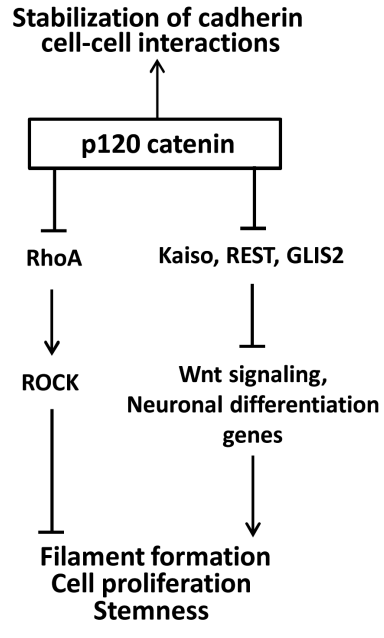

Figure 3. Up- and down- stream targets regulated by p120 catenin. Positive regulation is indicated with arrows, negative regulation - by a transverse bar at the end of the line.

the contribution of cadherin junctions, RhoA/ROCK activity and transcriptional repressors in (i) formation and elongation of glioma cell filaments, (ii) multicellular network dynamics, and (iii) cell proliferation and tumor growth. The identification of functionally important sites in the p120 molecule will provide information for the design of low-molecular compounds inhibiting glioma cell invasion and proliferation. So far, p120 catenin was not considered as a target for anti-glioma therapies. Interestingly, another member of p120 protein family – delta catenin (*CTNND2*) is often down-regulated or inactivated in glioblastoma patients because of gene deletions or point mutations, and patients with reduced delta catenin levels have poor clinical outcome especially with mesenchymal gene expression signature of the tumors[42]. It is not clear why glioma cells prefer p120 but not delta catenin. The functions of p120 and delta catenins are partially overlapping; both stabilize cadherins at the plasma membrane, binding to the same site in juxtamembrane cadherin domain, inhibit RhoA activities and promote dendritic formation in neurons[43–47]. However the mechanisms of regulation of Rho GTP-ases by delta catenin are likely cell type/cell compartment specific, and may not be universal compared to p120 catenin[43]. Moreover, in contrast to p120, delta-catenin contains a carboxyl-terminal motif, which binds to PDZ-domain containing proteins[46,48], and after cleavage with caspase-3 can regulate the activity of ZIFCAT, a transcriptional repressor with unknown gene regulatory effects[49]. Delta-catenin plays a critical role in neuronal development and in the brain tissue of adults it is expressed primarily in neurons. Since classical cadherins are crucial for synaptic activity[44,50] in the brain, it can be expected that anti p120 therapies would cause neurotoxicity as a side effect. In addition, whether delta catenin could compensate the loss of p120 function in neurons requires further analysis.

RHOA/ROCK AS POSSIBLE ANTI-GLIOMA TARGETS

Beyond p120 catenin, its down-stream effectors may be suitable for anti-glioma targeting. We demonstrated that elevated RhoA/ROCK signalling, as a consequence of p120 catenin down-regulation, restricts filament formation in glioma cells and inhibits multicellular glioma network invasion (Chapter 4). Moreover, constitutively active RhoA inhibits proliferation by retarding G1 to S phase cell cycle progression[51]. Thus, the activation of RhoA/ROCK signalling in glioma cells, for instance via inhibition of Ras or Rac1, could be a promising strategy to inhibit both glioma invasion and cell proliferation[52]. In vivo experiments using xenograft patient derived glioma cells are required to test this hypothesis.

NUCLEAR TARGETS OF P120 CATENIN

Besides regulating adherens junctions stability and Rho GTP-ase activity, p120 catenin after translocating to the nucleus, can regulate gene transcription, including genes involved in neuronal differentiation[40,53], some of which are replicated/ reproduced in glioma cells (RNA seq data, Chapter 4). In the nucleus p120 catenin can bind to and inhibit function of transcriptional repressors REST, GLIS2 and Kaiso[40,54], however the nuclear role of p120 catenin in gliomagenesis is not known. The nuclear activity of p120 is tightly regulated: at low Wnt signalling and high cadherin expression levels catenins typically do not enter the nucleus[40]. As a particular interest, REST (RE1 silencing transcription factor), an established repressor of neuronal differentiation, recently was shown as an important regulator of self-renewal of glioblastoma stem-like cells[55–57].

P120 CATENIN REGULATES STEMNESS OF GLIOMA CELLS

Of note, after p120 catenin knock-down in patient-derived glioblastoma cells established markers of glioma stem-like cells (GSC)[4] were down-regulated at the mRNA level in our datasets (Fig. 4a). Moreover, out of 30 gene signature highly over-expressed in GSC and positively correlated with poor clinical outcome[58], 26 genes are significantly down-regulated in p120 knock-down cells (Fig. 4b). Thus, p120 catenin regulated signalling may support stemness programs in glioma, including stemness-associated chemo- and radiation resistance. Moreover, we found significant down-regulation of β-catenin at the protein level in glioma cells with p120 knock-down. Since Wnt/β-catenin signalling is implicated in the proliferation and therapy resistance of GSC[59,60], the interconnection between p120 catenin and Wnt signalling warrants further investigation.

INTEGRIN-LAMININ INTERACTIONS AS A TARGET FOR ANTI-GLIOMA THERAPIES

It has been suggested that GSC reside in the perivascular niche where they interact with basement membranes[61–63]. β1 integrin-laminin 511 adhesions drive glioma cell invasion along basement membranes surrounding blood vessel (Chapter 5). α3β1/α6β1 integrins are overexpressed in GSC and the role of integrin-laminin 511 interactions in proliferation of GSC and their chemo- and radio-resistance remains subjects to future investigation[62,63]. Consequently targeting of β1 integrins could be a promising strategy to retard glioma invasion and proliferation[64]. However, high avidity interactions between β1 integrins and laminin 511, which cannot be abolished completely even by adhesion-perturbing monoclonal antibodies (Chapter 5), might still suffice to mediate glioma cell invasion in complex brain parenchyma and limit the efficiency of anti-integrin therapies in patients. Moreover, compensation by non-integrin glioma cell adhesions systems may compromise therapeutic strategies against invasion, proliferation, chemo- and radio-resistance of glioma cells in the brain.

CONCLUSION

In conclusion, the data presented in this thesis provide a novel view on glioma cell invasion mechanisms: (1) glioma cells occupy the peritumoral brain tissue as multicellular networks (2) within the networks glioma cells are connected with filamentous junctions, which are formed and resolved over time during glioma network migration; (3) p120 catenin

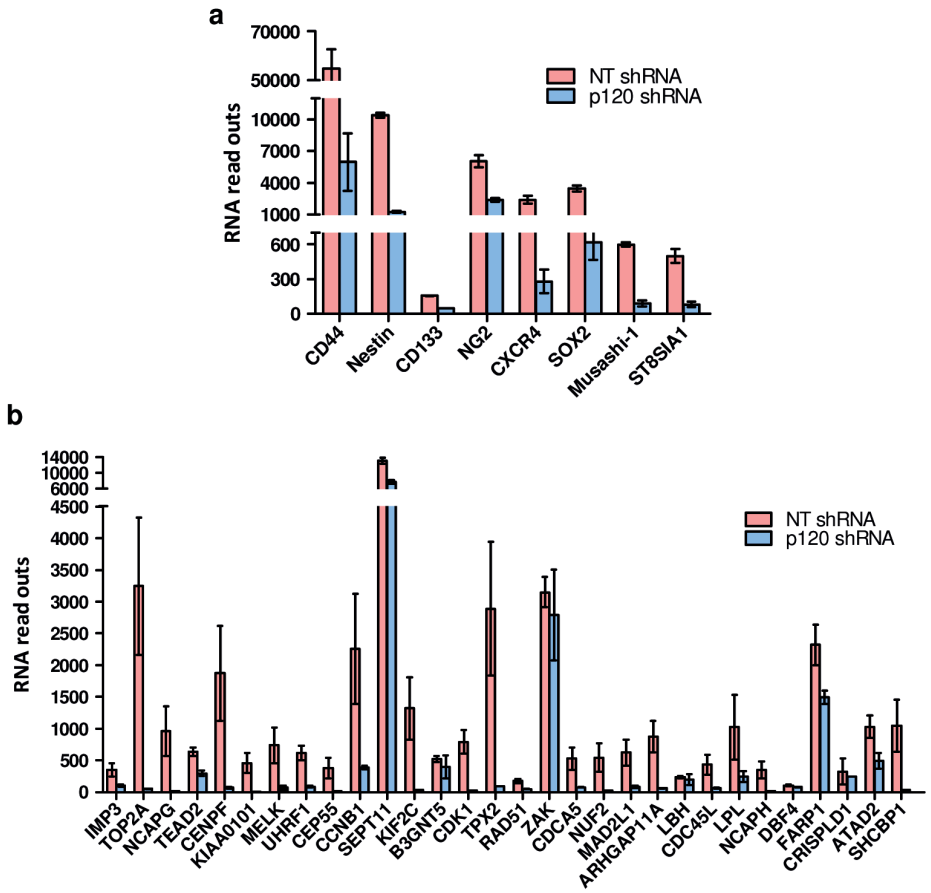

Figure 4. Genes encoding glioma stem-like cell (GSC) markers are down-regulated after p120 catenin knock-down in glioma cells. **a**. Common GSC markers collected from review[4]. **b**. Genes up-regulated in GSC vs neuronal stem cells based on microarray data[58]. RNA sequencing data for patient-derived glioblastoma cell line E-468 (Chapter 4).

plays a crucial role in glioma network expansion, promoting formation of filamentous cell protrusions, intercellular cadherin junctions and proliferation of glioma cells; and (4) β1 integrin - laminin 511 interactions drive glioma cell invasion along basement membranes of brain blood vessels.

Whether targeting of p120 catenin and β1-integrin pathways can improve the efficacy of chemotherapy and irradiation of gliomas requires further investigation.

REFERENCES

1. Brat, D. J. *et al.* Comprehensive, Integrative Genomic Analysis of Diffuse Lower-Grade Gliomas. *N. Engl. J. Med.* **372,** 2481–2498 (2015).
2. Ilkanizadeh, S. *et al.* Glial progenitors as targets for transformation in glioma. *Adv. Cancer Res.* **121,** 1–65 (2014).
3. Patel, A. P. *et al.* Single-cell RNA-seq highlights intratumoral heterogeneity in primary glioblastoma. *Science* **344,** 1396–1401 (2014).
4. Safa, A. R., Saadatzadeh, M. R., Cohen-Gadol, A. A., Pollok, K. E. & Bijangi-Vishehsaraei, K. Glioblastoma stem cells (GSCs) epigenetic plasticity and interconversion between differentiated non-GSCs and GSCs. *Genes Dis.* **2,** 152–163 (2015).
5. Swartling, F. J., Hede, S.-M. & Weiss, W. A. What underlies the diversity of brain tumors? *Cancer Metastasis Rev.* **32,** 5–24 (2013).
6. Zong, H., Verhaak, R. G. W. & Canoll, P. The cellular origin for malignant glioma and prospects for clinical advancements. *Expert Rev. Mol. Diagn.* **12,** 383–394 (2012).
7. Osswald, M. *et al.* Brain tumour cells interconnect to a functional and resistant network. *Nature* **528,** 93–98 (2015).
8. Cayre, M., Canoll, P. & Goldman, J. E. Cell migration in the normal and pathological postnatal mammalian brain. *Prog. Neurobiol.* **88,** 41–63 (2009).
9. Cuddapah, V. A., Robel, S., Watkins, S. & Sontheimer, H. A neurocentric perspective on glioma invasion. *Nat. Rev. Neurosci.* **15,** 455–465 (2014).
10. Canoll, P. & Goldman, J. E. The interface between glial progenitors and gliomas. *Acta Neuropathol* **116,** 465–477 (2008).
11. Suzuki, S. O. & Goldman, J. E. Multiple cell populations in the early postnatal subventricular zone take distinct migratory pathways: a dynamic study of glial and neuronal progenitor migration. *J. Neurosci.* **23,** 4240–4250 (2003).
12. Kawauchi, T. Cellullar insights into cerebral cortical development: focusing on the locomotion mode of neuronal migration. *Front. Cell. Neurosci.* **9,** 394 (2015).
13. Jiang, X. & Nardelli, J. Cellular and molecular introduction to brain development. *Neurobiol. Dis.* **92,** 3–17 (2016).
14. Barry, D. S., Pakan, J. M. P. & McDermott, K. W. Radial glial cells: key organisers in CNS development. *Int. J. Biochem. Cell Biol.* **46,** 76–79 (2014).
15. Gonzalez-Gomez, P., Anselmo, N. P. & Mira, H. BMPs as therapeutic targets and biomarkers in astrocytic glioma. *Biomed Res. Int.* **2014,** 549742 (2014).
16. Swartling, F. J., Cancer, M., Frantz, A., Weishaupt, H. & Persson, A. I. Deregulated proliferation and differentiation in brain tumors. *Cell Tissue Res.* **359,** 225–254 (2015).
17. Osswald, M., Solecki, G., Wick, W. & Winkler, F. A malignant cellular network in gliomas: potential clinical implications. *Neuro. Oncol.* **18,** 479–485 (2016).
18. Jung, E. *et al.* Tweety-homologue 1 drives brain colonization of gliomas. *J. Neurosci.* (2017). doi:10.1523/JNEUROSCI.3532-16.2017
19. Farin, A. *et al.* Transplanted glioma cells migrate and proliferate on host brain vasculature: a dynamic analysis. *Glia* **53,** 799–808 (2006).
20. Gritsenko, P. G., Ilina, O. & Friedl, P. Interstitial guidance of cancer invasion. *J. Pathol.* **226,** 185–199 (2012).
21. Kim, Y. & Kumar, S. CD44-mediated adhesion to hyaluronic acid contributes to mechanosensing and invasive motility. *Mol. Cancer Res.* **12,** 1416–1429 (2014).
22. Sin, W. C. *et al.* Astrocytes promote glioma invasion via the gap junction protein connexin43. *Oncogene* **35,** 1504–1516 (2016).
23. Naus, C. C., Aftab, Q. & Sin, W. C. Common mechanisms linking connexin43 to neural progenitor cell migration and glioma invasion. *Semin. Cell Dev. Biol.* **50,** 59–66 (2016).

24. Elias, L. A. B., Wang, D. D. & Kriegstein, A. R. Gap junction adhesion is necessary for radial migration in the neocortex. *Nature* **448,** 901–907 (2007).
25. Peglion, F. & Etienne-Manneville, S. N-cadherin expression level as a critical indicator of invasion in non-epithelial tumors. *Cell Adh. Migr.* **6,** 327–332 (2012).
26. Cai, D. *et al.* Mechanical feedback through E-cadherin promotes direction sensing during collective cell migration. *Cell* **157,** 1146–1159 (2014).
27. Kardash, E. *et al.* A role for Rho GTPases and cell-cell adhesion in single-cell motility in vivo. *Nat. Cell Biol.* **12,** 11–47 (2010).
28. Beadle, C. *et al.* The role of myosin II in glioma invasion of the brain. *Mol Biol Cell* **19,** 3357–3368 (2008).
29. Paul, C. D., Mistriotis, P. & Konstantopoulos, K. Cancer cell motility: lessons from migration in confined spaces. *Nat. Rev. Cancer* **17,** 131–140 (2017).
30. Thompson, E. G. & Sontheimer, H. A role for ion channels in perivascular glioma invasion. *Eur. Biophys. J.* **45,** 635–648 (2016).
31. Balzer, E. M. *et al.* Physical confinement alters tumor cell adhesion and migration phenotypes. *FASEB J. Off. Publ. Fed. Am. Soc. Exp. Biol.* **26,** 4045–4056 (2012).
32. Katsetos, C. D. *et al.* Emerging microtubule targets in glioma therapy. *Semin. Pediatr. Neurol.* **22,** 49–72 (2015).
33. Panopoulos, A., Howell, M., Fotedar, R. & Margolis, R. L. Glioblastoma motility occurs in the absence of actin polymer. *Mol. Biol. Cell* **22,** 2212–2220 (2011).
34. Schackmann, R. C. J., Tenhagen, M., van de Ven, R. A. H. & Derksen, P. W. B. p120-catenin in cancer - mechanisms, models and opportunities for intervention. *J. Cell Sci.* **126,** 3515–3525 (2013).
35. Kourtidis, A., Ngok, S. P. & Anastasiadis, P. Z. p120 catenin: an essential regulator of cadherin stability, adhesion-induced signaling, and cancer progression. *Prog. Mol. Biol. Transl. Sci.* **116,** 409–432 (2013).
36. Cadwell, C. M., Su, W. & Kowalczyk, A. P. Cadherin tales: Regulation of cadherin function by endocytic membrane trafficking. *Traffic* **17,** 1262–1271 (2016).
37. Anastasiadis, P. Z. *et al.* Inhibition of RhoA by p120 catenin. *Nat. Cell Biol.* **2,** 637–644 (2000).
38. Elia, L. P., Yamamoto, M., Zang, K. & Reichardt, L. F. p120 catenin regulates dendritic spine and synapse development through Rho-family GTPases and cadherins. *Neuron* **51,** 43–56 (2006).
39. Salhia, B. *et al.* Inhibition of Rho-kinase affects astrocytoma morphology, motility, and invasion through activation of Rac1. *Cancer Res.* **65,** 8792–8800 (2005).
40. McCrea, P. D. & Gottardi, C. J. Beyond beta-catenin: prospects for a larger catenin network in the nucleus. *Nat. Rev. Mol. Cell Biol.* **17,** 55–64 (2016).
41. Salinas, P. C. Wnt signaling in the vertebrate central nervous system: from axon guidance to synaptic function. *Cold Spring Harb. Perspect. Biol.* **4,** (2012).
42. Frattini, V. *et al.* The integrated landscape of driver genomic alterations in glioblastoma. *Nat. Genet.* **45,** 1141–1149 (2013).
43. Yuan, L. & Arikkath, J. Functional roles of p120ctn family of proteins in central neurons. *Semin. Cell Dev. Biol.* (2017). doi:10.1016/j.semcdb.2017.05.027
44. Kosik, K. S., Donahue, C. P., Israely, I., Liu, X. & Ochiishi, T. Delta-catenin at the synaptic-adherens junction. *Trends Cell Biol.* **15,** 172–178 (2005).
45. Lu, Q., Aguilar, B. J., Li, M., Jiang, Y. & Chen, Y.-H. Genetic alterations of delta-catenin/NPRAP/Neurojungin (CTNND2): functional implications in complex human diseases. *Hum. Genet.* **135,** 1107–1116 (2016).
46. Yuan, L., Seong, E., Beuscher, J. L. & Arikkath, J. delta-Catenin Regulates Spine Architecture via Cadherin and PDZ-dependent Interactions. *J. Biol. Chem.* **290,** 10947–10957 (2015).
47. Martinez, M. C., Ochiishi, T., Majewski, M. & Kosik, K. S. Dual regulation of neuronal morphogenesis by a delta-catenin-cortactin complex and Rho. *J. Cell Biol.* **162,** 99–111 (2003).
48. Abu-Elneel, K. *et al.* A delta-catenin signaling pathway leading to dendritic protrusions. *J. Biol. Chem.* **283,** 32781–32791 (2008).
49. Gu, D. *et al.* Caspase-3 cleavage links delta-catenin to the novel nuclear protein ZIFCAT. *J. Biol. Chem.* **286,** 23178–23188 (2011).
50. Basu, R., Taylor, M. R. & Williams, M. E. The classic cadherins in synaptic specificity. *Cell Adh. Migr.* **9,** 193–201 (2015).
51. Morin, P., Flors, C. & Olson, M. F. Constitutively active RhoA inhibits proliferation by retarding G(1) to S phase cell cycle progression and impairing cytokinesis. *Eur. J. Cell Biol.* **88,** 495–507 (2009).
52. Goldberg, L. & Kloog, Y. A Ras inhibitor tilts the balance between Rac and Rho and blocks phosphatidylinositol 3-kinase-dependent glioblastoma cell migration. *Cancer Res.* **66,** 11709–11717 (2006).
53. Lee, M., Ji, H., Furuta, Y., Park, J. & McCrea, P. D. p120-catenin regulates REST and CoREST, and modulates mouse embryonic stem cell differentiation. *J. Cell Sci.* **127,** 4037–4051 (2014).
54. McCrea, P. D., Maher, M. T. & Gottardi, C. J. Nuclear signaling from cadherin adhesion complexes. *Curr. Top. Dev. Biol.* **112,** 129–196 (2015).
55. Conti, L. *et al.* REST controls self-renewal and tumorigenic competence of human glioblastoma cells. *PLoS One* **7,** e38486 (2012).
56. Kamal, M. M. *et al.* REST regulates oncogenic properties of glioblastoma stem cells. *Stem Cells* **30,** 405–414 (2012).
57. Marisetty, A. L. *et al.* REST represses miR-124 and miR-203 to regulate distinct oncogenic properties of glioblastoma stem cells. *Neuro. Oncol.* (2016). doi:10.1093/neuonc/now232
58. Sandberg, C. J. *et al.* Comparison of glioma stem cells to neural stem cells from the adult human brain identifies dysregulated Wnt-signaling and a fingerprint associated with clinical outcome. *Exp. Cell Res.* **319,** 2230–2243 (2013).
59. Suwala, A. K., Hanaford, A., Kahlert, U. D. & Maciaczyk, J. Clipping the Wings of Glioblastoma: Modulation of WNT as a Novel Therapeutic Strategy. *J. Neuropathol. Exp. Neurol.* **75,** 388–396 (2016).
60. Kierulf-Vieira, K. S. *et al.* Wnt inhibition is dysregulated in gliomas and its re-establishment inhibits proliferation and tumor sphere formation. *Exp. Cell Res.* **340,** 53–61 (2016).
61. Codrici, E., Enciu, A.-M., Popescu, I.-D., Mihai, S. & Tanase, C. Glioma Stem Cells and Their Microenvironments: Providers of Challenging Therapeutic Targets. *Stem Cells Int.* **2016,** 5728438 (2016).
62. Lathia, J. D. *et al.* Integrin alpha 6 regulates glioblastoma stem cells. *Cell Stem Cell* **6,** 421–432 (2010).
63. Nakada, M. *et al.* Integrin alpha3 is overexpressed in glioma stem-like cells and promotes invasion. *Br. J. Cancer* **108,** 2516–2524 (2013).
64. Carbonell, W. S., DeLay, M., Jahangiri, A., Park, C. C. & Aghi, M. K. beta1 integrin targeting potentiates antiangiogenic therapy and inhibits the growth of bevacizumab-resistant glioblastoma. *Cancer Res.* **73,** 3145–3154 (2013).

APPENDIX &

SUMMARY

Gliomas are a heterogeneous group of primary brain tumors originating from transformed brain cell progenitors which abnormally reproduce brain development programs[1–3]. The high lethality of glioma patients results from diffuse glioma cell dissemination in the brain parenchyma[4]. After surgical resection of the primary lesion, residual glioma cells which have invaded into surrounding tissue beyond the resecting margin give rise to recurrent tumor formation often followed by fatal outcome[5,6]. Glioma cells invade in the brain stroma along the intertwining networks formed by astrocytes, neurons, oligodendrocytes and blood vessels[4,7]. However, due to the anatomic and molecular complexity of these invasion routes, molecular mechanisms of glioma cell invasion in the brain have neither been resolved nor therapeutically exploited.

The aims of this thesis were: (1) to design three-dimensional (3D) invasion assays recapitulating glioma cell dissemination in different anatomical environments of the brain – along blood vessels and in neuronal/astrocytic networks; (2) to perform 3D reconstruction of glioma lesions and characterize glioma invasion patterns in patient brain samples; (3) to identify cell-cell and cell-matrix adhesion strategies involved in glioma cell invasion in the brain.

Chapter 2 describes the brain tissue architecture at cellular and molecular levels and recapitulates the main anatomical structures which guide glioma cell invasion in the brain. Myelinated axons, astrocyte processes and blood vessels create a complex system of microchannels utilized by glioma cells for their disseminations. The extracellular space in the brain parenchyma is filled primarily with a soft matrix composed by hyaluronan-lectican-tenascin molecular complexes, unlike connective tissue where collagen bundles are predominant in extracellular matrix. While integrins are the main adhesion receptors mediating glioma cell migration along basement membranes in perivascular space, the mechanisms of cell-cell and cell-matrix interactions during glioma cell invasion along myelinated axons and astrocyte processes are still not elucidated.

In **Chapter 3** we introduce set of novel 3D in vitro assays reproducing the major routes of glioma cell invasion in the brain parenchyma identified in mouse xenograft and glioma patient brain samples: cohesive cell migration along blood vessels and multicellular glioma networks invading in astrocyte enriched peritumoral stroma. In reconstituted basement membrane (rBM) interface assays (1) glioma cells retained N-cadherin cell-cell junctions and invaded collectively in the interfaces representing in vivo perivascular microchannels formed by basement membranes and brain parenchyma. Similarly, glioma cells invaded cohesively along capillaries and bigger vessels in mouse brain slice organotypic assay (2). In 3D astrocyte scaffolds (3) glioma cells invaded as multicellular networks being interconnected with dendritic-like filaments, a major glioma cell invasion mode identified in patient brain samples[8] (Chapter 4). Each assay thus recapitulates aspects of glioma invasion in distinct brain compartments in vivo and is suitable for high-throughput screening of clinically relevant treatments to inhibit glioma cell invasion and proliferation.

In **Chapter 4** using 3D reconstruction of glioma lesions from mouse brain xenografts and patient samples multicellular glioma networks were identified as a major invasion pattern in different histological subtypes of gliomas. Glioma network invasion in 3D astrocyte scaffolds was enabled by cyclic formation and resolution of dendritic-like interactions between moving glioma cells, which were stabilized by focal adherens junctions. Down-regulation of p120 catenin in glioma cells induced disintegration of the multicellular networks and profound glioma growth deficiency in vitro and in vivo. RNA seq analysis identified significant deregulation of axonogenesis and cell proliferation pathways after p120 catenin shRNA knock-down in patient derived glioma cells, implicating p120 dependent pathways on morphogenesis-like programs.

Chapter 5 describes the role of integrins in engaging with brain-derived matrix molecules to drive glioma cell invasion. Using assays described in Chapter 3, we identified β1 integrin-laminin 511 interactions as a major interaction accounting for glioma cell invasion along blood vessels and in astrocyte enriched stroma. However, these interactions were relatively resistant to adhesion-perturbing anti β1 integrin antibodies combined with cRGD peptide targeting aV and a5 integrins, indicating potential limitations of antibody based therapies targeting glioma cell invasion.

In **Chapter 6** we summarize data presented in the thesis and integrate them with existing concepts, which describe the mechanisms of glioma cell invasion in the brain. We also discuss p120 catenin regulated pathways and β1 integrin-laminin 511 interactions as possible molecular targets to improve anti-glioma therapies.

REFERENCES

1. Brat, D. J. *et al.* Comprehensive, Integrative Genomic Analysis of Diffuse Lower-Grade Gliomas. *N. Engl. J. Med.* **372,** 2481–2498 (2015).
2. Patel, A. P. *et al.* Single-cell RNA-seq highlights intratumoral heterogeneity in primary glioblastoma. **344,** 1396–1401 (2014).
3. Ilkanizadeh, S. *et al.* Glial progenitors as targets for transformation in glioma. *Adv. Cancer Res.* **121,** 1–65 (2014).
4. Cuddapah, V. A., Robel, S., Watkins, S. & Sontheimer, H. A neurocentric perspective on glioma invasion. *Nat. Rev. Neurosci.* **15,** 455–465 (2014).
5. Gilbert, M. R. *et al.* Dose-dense temozolomide for newly diagnosed glioblastoma: a randomized phase III clinical trial. *J. Clin. Oncol.* **31,** 4085–4091 (2013).
6. Stupp, R. *et al.* Effects of radiotherapy with concomitant and adjuvant temozolomide versus radiotherapy alone on survival in glioblastoma in a randomised phase III study: 5-year analysis of the EORTC-NCIC trial. *Lancet. Oncol.* **10,** 459–466 (2009).
7. Gritsenko, P. G., Ilina, O. & Friedl, P. Interstitial guidance of cancer invasion. *J. Pathol.* **226,** 185–199 (2012).
8. Osswald, M. *et al.* Brain tumour cells interconnect to a functional and resistant network. *Nature* **528,** 93–98 (2015).

NEDERLANDSE SAMENVATTING

Gliomas vormen een heterogene groep van primaire breintumoren en zijn afkomstig van getransformeerde voorlopers van hersencellen die op abnormale wijze breinontwikkelingsprogramma's doorlopen[1–3]. De hoge lethaliteit van gliomas wordt veroorzaakt door de diffuse verspreiding van gliomacellen in het parenchym van het brein[4]. Gliomacellen die het omringende weefsel hebben binnengedrongen voorbij de resectiemarges kunnen na chirurgische verwijdering van de primaire tumor zorgen voor terugkeer van de ziekte, vaak met dodelijke afloop[5,6]. Gliomacellen verplaatsen zich door het stroma van het brein via netwerken van astrocyten, neuronen, oligodendrocyten en bloedvaten[4,7]. Echter, vanwege de anatomische en moleculaire complexiteit van deze verspreidingsroutes zijn de moleculaire mechanismen van gliomacelinvasie in het brein nog niet volledig opgehelderd, en zijn er nog geen therapieën die hierin ingrijpen.

De doelen van deze scriptie zijn: (1) het ontwerpen van driedimensionale (3D) kweekmodellen die nabootsen hoe gliomacellen zich verspreiden in verschillende anatomische gebieden van het brein – langs bloedvaten en in neuronale/astrocytische netwerken; (2) het reconstrueren van gliomalaesies in 3D en het karakteriseren van het invasiepatroon van glioma in hersenmateriaal van patiënten; (3) het identificeren van cel-cel en cel-matrix adhesiestrategieën die betrokken zijn bij de verspreiding van gliomacellen in het brein.

Hoofdstuk 2 beschrijft de weefselstructuur van het brein op cellulair en moleculair niveau met betrekking tot de verspreidingsroutes van gliomacellen. Gemyelineerde axonen, uitlopers van astrocyten en bloedvaten vormen een complex systeem van microkanalen waarlangs gliomacellen het brein infiltreren. De extracellulaire ruimte in het parenchym van het brein is voornamelijk gevuld met een zachte matrix van moleculaire complexen van hyaluronan-lectican-tenascin, in tegenstelling tot bindweefsels die voornamelijk uit stijve collageenbundels bestaan. Hoewel bekend is dat gliomacellen tijdens migratie over basale lamina in perivasculaire ruimtes voornamelijk afhankelijk zijn van de integrines voor cel-matrix adhesie, zijn de mechanismen van cel-cel en cel-matrix interactie tijdens gliomacelinvasie langs gemyelineerde axonen en de uitlopers van astrocyten nog niet opgehelderd.

In **Hoofdstuk 3** introduceren we een set van nieuwe 3D kweekmodellen. Deze bootsen de belangrijkste invasiepatronen van gliomacellen na die zijn geïdentificeerd in xenotransplantaatmodellen uit de muis en in humaan patiëntenmateriaal; i.e. collectieve celmigratie langs bloedvaten, en multicellulaire gliomanetwerken die astrocyt-verrijkte peritumorale stroma binnendringen. Perivasculaire microkanalen tussen basale lamina en het breinparenchym uit het eerste invasiepatroon werden gesimuleerd met behulp van grensvlakmodellen met gereconstitueerde basale lamina (1). In deze modellen behielden gliomacellen cel-cel contacten op basis van N-cadherine en migreerden collectief. Gliomacellen migreerden op vergelijkbare wijze langs haarvaten en grotere vaten in een organotypisch breinmodel uit de muis (2). In 3D matrices geproduceerd door astrocyten (3) migreerden gliomacellen als multicellulaire netwerken verbonden met dendrietachtige filamenten. Dit is een belangrijke invasiemodus van gliomacellen die geïdentificeerd is in breinmateriaal van patiënten (Hoofdstuk 4). Elk kweekmodel simuleert dus aspecten van gliomacelinvasie in verschillende breincompartimenten in vivo en is geschikt voor screening met hoge verwerkingscapaciteit van klinisch relevante behandelingsmethoden om gliomacelinvasie en -proliferatie te remmen.

In **Hoofdstuk 4** werden multicellulaire gliomanetwerken geïdentificeerd als belangrijk invasiepatroon in verschillende histologische subtypes van glioma. Hiertoe werden gliomalaesies in xentransplantaten in muisbreinen en patiëntenmateriaal gereconstrueerd in 3D. Het binnendringen van gliomanetwerken in 3D matrices van astrocyten werd gefaciliteerd door cyclische formatie en opheffing van dendrietachtige interacties tussen gliomacellen, die werden gestabiliseerde door focale adherens junctions. Vermindering van expressie van p120 catenine in gliomacellen induceerde desintegratie van de multicellulaire newerken en uitgesproken groeideficiëntie in vitro en in vivo. RNA seq analyse identificeerde significante ontregeling van signaalroutes van axonogenese en celproliferatie na shRNA knock-down van p120 catenine in gliomacellen van patiënten, hetgeen impliceert dat er p120-afhankelijke signaalroutes bestaan in morfogeneseachtige programma's.

Hoofdstuk 5 beschrijft de functie van interacties tussen integrines en matrixmoleculen afkomstig uit het brein in gliomacelinvasie. Met behulp van de kweekmodellen uit Hoofdstuk 3 identificeren we interacties tussen β1 integrine en laminine 511 als belangrijke factor in gliomacelinvasie langs bloedvaten en in astrocyt-verrijkte stroma. Deze interacties waren echter relatief bestendig tegen verstoring met behulp van anti-β1 integrine antilichamen gecombineerd met cRGD peptiden die gericht zijn tegen αV en α5 integrines. Dit geeft de eventuele beperkingen weer van therapieën tegen gliomacelinvasie die zijn gebaseerd op antilichamen.

In **Hoofdstuk 6** vatten we de data samen die gepresenteerd zijn in de thesis en integreren we ze in bestaande concepten die de mechanismen van gliomacelinvasie in het brein beschrijven. Daarnaast bespreken we signaalroutes van p120 catenine en interacties tussen β1 integrine en laminine 511 als mogelijke moleculaire doelwitten om therapieën tegen glioma te verbeteren.

REFERENTIES

1. Brat, D. J. *et al.* Comprehensive, Integrative Genomic Analysis of Diffuse Lower-Grade Gliomas. *N. Engl. J. Med.* **372,** 2481–2498 (2015).
2. Patel, A. P. *et al.* Single-cell RNA-seq highlights intratumoral heterogeneity in primary glioblastoma. **344,** 1396–1401 (2014).
3. Ilkanizadeh, S. *et al.* Glial progenitors as targets for transformation in glioma. *Adv. Cancer Res.* **121,** 1–65 (2014).
4. Cuddapah, V. A., Robel, S., Watkins, S. & Sontheimer, H. A neurocentric perspective on glioma invasion. *Nat. Rev. Neurosci.* **15,** 455–465 (2014).
5. Gilbert, M. R. *et al.* Dose-dense temozolomide for newly diagnosed glioblastoma: a randomized phase III clinical trial. *J. Clin. Oncol.* **31,** 4085–4091 (2013).
6. Stupp, R. *et al.* Effects of radiotherapy with concomitant and adjuvant temozolomide versus radiotherapy alone on survival in glioblastoma in a randomised phase III study: 5-year analysis of the EORTC-NCIC trial. *Lancet. Oncol.* **10,** 459–466 (2009).
7. Gritsenko, P. G., Ilina, O. & Friedl, P. Interstitial guidance of cancer invasion. *J. Pathol.* **226,** 185–199 (2012).
8. Osswald, M. *et al.* Brain tumour cells interconnect to a functional and resistant network. *Nature* **528,** 93–98 (2015).

ACKNOWLEDGEMENTS

I would like to thank all people who accompanied and supported me over the time in Cell Biology department. My PhD is really collective achievement, which would not be possible without your help.

First of all, I am grateful to my supervisor Prof. **Peter Friedl**, who gave me a great opportunity to accomplish my PhD. I learnt a lot and gained unique experience in science thanks to you. I will save this knowledge and use it in the future to help people. We started our glioma project almost from zero, then going slowly but surely, we developed a new concept in glioma field, and your prediction about glioma cell networks was confirmed.

I would like to thank my supervisor Prof. **Pieter Wesseling**. I was very lucky to meet you in my life. Your expertise in neuropathology helped me to validate my experimental data with glioma patient samples. I learnt, how important it is in cancer research to verify in vitro and in vivo results with "real" clinical material, and to be always connected to patients, for whom we work and sacrifice our lives.

I thank **Olga Ilina,** my best friend, wife and co-author who always supported me in science and life.

I would like to acknowledge my collaborators and co-authors: **Nader Altasy, Cindy E.J. Dieteren, Anna C. Navis, Jan-Hendrik Venhuizen, Cornelia Veelken, Dirk Schubert, Amparo Acker-Palmer, Bart A. Westerman, Thomas Würdinger, William Leenders, Pieter Wesseling, Hendrik G. Stunnenberg and Peter Friedl**, as well as my gratitude for **Huib Croes, Esther Wagena, Manon Vullings, Kiek Verrijp, Jeroen Mooren and Bianca Lemmers-Van de Weem** for excellent technical support**.** We were a very productive team!

I am very grateful to **Mirjam Zegers**. I discover p120 catenin in my life thanks to you. Your knowledge was really helpful for my experiments.

I would like to thank **Remco van Horssen, Marieke Willemse, Jan Schepens, Anna Navis, Wiljan Hendricks, William Leenders and Pieter Wesseling**. You introduced me to glioma field and your support and advices were very helpful for my project.

I am thankful for Prof. **Be Wieringa** and Prof. **Alessandra Cambi**, your efforts for government of our department enabled productive work of Cell Biology team.

I would like to thank my colleagues and friends who worked and work in our Nijmegen and Houston labs: **Angela, Anna, Antoine, Bettina, Cindy, Cornelia, Eleonora, Esther,**

Gert-Jan, Harsha, Huib, Jan-Hendrik, Jeroen, Julia, Katarina, Lianne, Lidia, Linda, Lying, Manon, Marina, Mariska, Michael, Mirjam, Olga, Peter, Samuel, Sarah, Sjoerd, Steffi L, Steffi A, Steve, Veronika. Light from your souls excited inspiration and happiness in my life. I hope, I emitted the positive light for you as well.

I am grateful for everyone in Cell Biology, Animal Physiology and Biomolecular Chemistry departments. We created a friendly and sunny work atmosphere. Thank you all!

CURRICULUM VITAE

Pavlo Grytsenko was born on May 13, 1977 in Kiev, Ukrainian Soviet Republic (USSR). He studied biology at Taras Shevchenko National University in Kiev and obtained his Master degree in biochemistry in 1999. After graduation, Pavlo Grytsenko started his PhD research on the mechanisms of fibrin polymerization in the Department of Molecular Immunology, Institute of Biochemistry in Kiev, and in 2003 he defended his PhD (speciality "Biochemistry"). From 2003 till 2009 Pavlo worked as a scientist in the Institute of Biochemistry on the project devoted development of immunodiagnostic test-systems for monitoring of blood coagulation and thrombosis in patients. In 2009 he moved to the Netherlands in the group of Prof. Peter Friedl in Cell Biology Department, at Radboud Institute of Molecular Life Sciences in Nijmegen, and started his PhD project on the mechanisms of glioma cell invasion. The results of Pavlo Grytsenko PhD research are presented in this thesis.

LIST OF PUBLICATIONS

Gritsenko PG, Ilina O, Friedl P. Interstitial guidance of cancer invasion // J Pathol (2012) 226:185-199.

Gritsenko P, Leenders W, Friedl P. Recapitulating in vivo-like plasticity of glioma cell invasion along blood vessels and in astrocyte-rich stroma // Histochem Cell Biol (2017) 148:395-406.

Khalil AA, Ilina O, **Gritsenko P**, Bult P, Span PN, Friedl P. Collective invasion in ductal and lobular breast cancer associates with distant metastasis // Clin Exp Metastasis (2017) Sep 11. doi: 10.1007/s10585-017-9858-6.

Gritsenko PG, Friedl P. Multiple adhesion strategies mediate glioma cell invasion in complex environments // (in preparation).

Gritsenko PG, Altasy N, Dieteren CEJ, Navis AC, Venhuizen JH, Veelken C, Schubert D, Acker-Palmer A, Westerman BA, Wurdinger T, Leenders W, Wesseling P, Stunnenberg HL, Friedl P. p120-catenin dependent collective brain infiltration by glioma-cell networks // (in preparation).